The behaviour of ferromagnetic domains in silicon iron under stress

Mason, J. J.

THE BEHAVIOUR OF FERROMAGNETIC DOMAINS IN SILICON IRON UNDER STRESS

by

J.J. MASON, B.Sc.

Presented in candidature for the degree of Doctor of Philosophy.

October, 1961.

Abstract

Polycrystalline and single crystal specimens of silicon iron were strained up to the yield point by the application of external stresses. A bending technique was found to be the most convenient method for doing this. Domain patterns were observed by means of the Bitter technique.

Tensional stresses were applied along the [110] and [001] directions of (110) surfaced specimens and the resulting structures described in detail. This necessitated an analysis of the effect of stress on Bloch Wall energies for various wall orientations. Domain patterns were also examined on (100) surfaced specimens under the effect of compressive forces in the [110] and [100] directions. In the first case the maze patterns so produced were compared with theoretical considerations while in the second example the nucleation and growth of transverse domains were examined. A new model of fir tree structures, proposed by Spacek, was evaluated using a different expression for the magnetostatic energy and this was then applied to measurements on the effect of stress on fir tree closure domains. The theory did not compare very favourably with experiment.

The work of Chikazumi and Suzuki, in which large stresses were applied to a (100) surfaced specimen by scratching the surface, was extended to (110) surfaces.

CONTENTS

Page

1. INTRODUCTION

1.1. Ferromagnetism 1

1.1.1. Molecular Field Theory 1

1.1.2. The Domain Concept 4

1.2. Domain Energy Contributions 5

1.2.1. Exchange Energy 5

1.2.2. Anisotropy Energy 6

1.2.3. Magnetoelastic Energy 8

1.2.4. Magnetostatic Energy 10

1.3. Bloch Walls 12

1.4. Domain Systems in Iron 15

1.5. Observation of Domains 17

1.6. Previous Work on the Effect of Stress on Domain Structures 20

1.7. Object of the Investigation 22

2. THE PREPARATION OF SPECIMENS

2.1. Introduction 24

2.2. Growth of Single Crystals 24

2.3. Orientation of Crystals 26

2.4. Cutting and Shaping the Crystals 27

2.4.1. Apparatus 28

2.4.2. Working Conditions and Results 29

2.5. Polishing and Annealing 30

2.6. Observation of Domains 33

Page

3. THE EFFECT OF EXTERNAL STRESSES UP TO THE YIELD POINT ON A (110) SURFACE.

3.1. Tensional Stress along the [110] Direction 35

3.1.1. Introduction 35

3.1.1.1. Effect of Stresses on Magnetization Directions 35

3.1.2. Experimental Technique 39

3.1.2.1. Direct Tension Method 39

3.1.2.2. Bending Technique 42

3.1.2.3. Strain Gauge Verification 45

3.1.3. Experimental Results and Discussion . 46

3.1.3.1. Zero Stress Pattern 46

3.1.3.2. Transitional Range 47

3.1.3.3. Stress Pattern I 54

3.1.3.4. Stress Pattern II 63

3.2. Tensional Stresses along the [100] Direction 70

3.2.1. The Surface a (110) Plane to within one degree 70

3.2.2. The Surface a few degrees off a (110) Plane 73

4. THE EFFECT OF EXTERNAL STRESSES UP TO THE YIELD POINT ON (100) SURFACES

4.1. A Compressive Stress applied along the [011] Direction on a (100) Surface 78

Page

4.1.1. Introduction 78

4.1.2. Experimental Details 79

4.1.3. Results 80

4.1.4. Theoretical Considerations 81

4.1.4.1. Variation of Domain Spacing with Stress 81

4.1.4.2. Variation of Zig-Zag Angle with Stress 83

4.2. A Compressive Stress applied in a [011] Direction on a Surface a few degrees off a (100) Plane 87

4.2.1. Experimental Details 87

4.2.2. Results 87

4.2.3. Interpretation 88

4.2.4. Conclusion 90

4.3. A Stress applied along the [001] Surface Direction 91

4.3.1. Introduction 91

4.3.2. Nucleation Processes 92

4.3.3. Experimental Observations 93

4.3.4. Theoretical Considerations 96

4.4. A Stress applied along the [010] Direction on a Surface 3^{o} off a (100) Plane 100

4.4.1. Experimental Details and Results 100

4.4.2. Theoretical Considerations 102

Page

4.5. The Effect of Stress on Fir Tree Structures 105
4.5.1. Introduction 105
4.5.2. Proposed Magnetostatic Model 109
4.5.3. Application to Stress Free Case 112
4.5.3.1. Relationship between α and δ .. 112
4.5.3.2. Variation of a with δ 114
4.5.4. Stress applied to Fir Tree Structure 116
4.5.4.1. Experimental Results 116
4.5.4.2. Theoretical Considerations 117
4.5.4.3. Conclusion 119

5. THE EFFECT OF SCRATCHES ON (100) AND (110) SURFACES
5.1. Scratches on a (100) Surface 120
5.2. Scratches on a (110) Surface 123
5.3. Stress Patterns due to Compressive Surface Stresses 127
5.4. Suggestion for the Variation of ω with Distance from Scratch 129
5.5. Stress Patterns on Scratches 131

6. SUMMARY OF RESULTS 133
ACKNOWLEDGMENTS 137
REFERENCES 138

CHAPTER ONE

CHAPTER ONE

INTRODUCTION

1.1 Ferromagnetism

At the beginning of the century basic experimental knowledge of various ferromagnetic phenomena had been established. It had been noted that there existed a temperature, called the Curie Temperature, below which it was possible to attain magnetic saturation by the application of small magnetic fields. At the same time it was possible for the magnetization of the same specimen to be zero in zero applied field.

In order to account for these observations Weiss (1907) proposed two basic concepts. In the first he postulated a strong molecular field which produces a resultant magnetization by the alignment of magnetic carriers. In the second he assumed that actual ferromagnetic specimens are composed of a number of small regions called domains, each one being magnetically saturated, but with the direction of magnetization in different domains not necessarily parallel.

1.1.1. Molecular Field Theory

Weiss followed the work of Langevin (1905) on paramagnetism, except that he introduced an additional field,

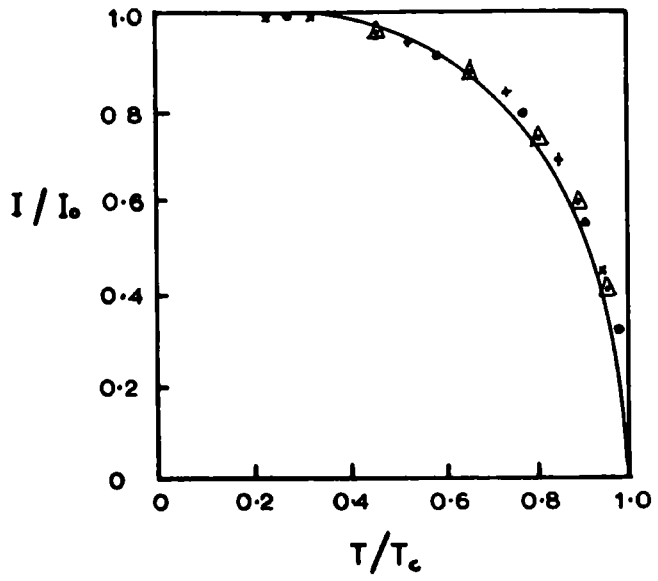

Saturation intensity of magnetization as a function of temperature for

x Iron

△ Nickel

• Cobalt

FIG. 1

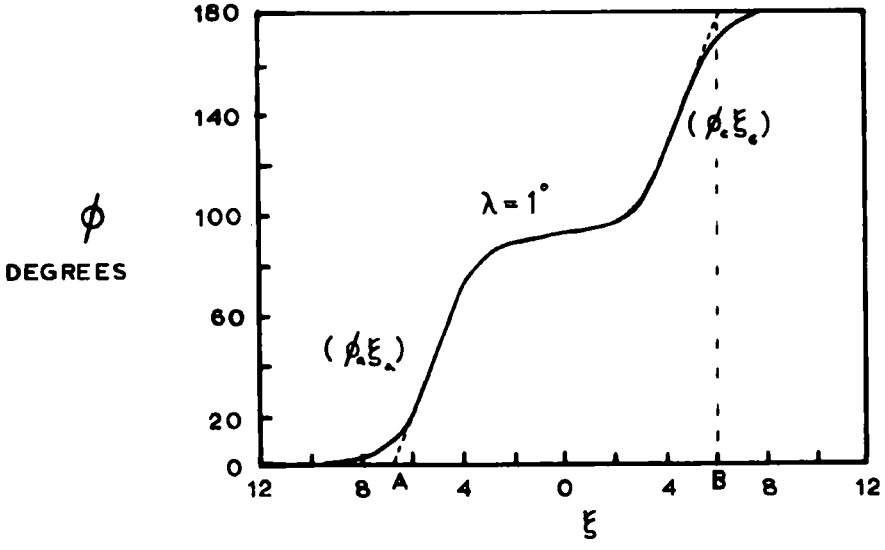

Variation with ξ of ϕ for 180° boundaries in iron

Lilley (1950)

FIG. 3

called the molecular field, acting on the elementary magnets and proportional to the intensity of magnetization. By using the supposition that the dipole orientation is governed by Boltzmann's Distribution Law, he showed that the magnetic susceptibility becomes infinite at a specific temperature and that below this temperature the saturation magnetization is a definite function of temperature. If this variation is plotted in reduced units see Fig. 1 then a curve which is approximately correct for all ferromagnetics is obtained.

Weiss himself did not make any specific predictions about the origin of the molecular field though he did show that its size, about 10^7 oersteds, was far too large to be explained by normal magnetic moment interactions. In 1928 an explanation of the origin of the field was put forward by Heisenberg. He showed, as a result of a quantum mechanical treatment, that the force is due to an electrostatic term arising from overlapping orbital functions. Since there is a correlation, due to the Pauli exclusion principle, between the orbital symmetry and the spin alignment, there is an effective spin-spin coupling. The exchange energy between two atoms i,j is given by

$$E_{ex} = -2 J_{ij} S_i \cdot S_j \qquad (1.1)$$

where S_i is the spin of atom i and J the exchange integral. If J is positive then the minimum energy condition is for the parallel alignment of spins.

It has been shown experimentally, from work on the gyromagnetic ratio, that about 90% of the saturation magnetization is due to electron spins, the rest being due to orbital motion.

Van Vleck (1952) has shown that the spins responsible for ferromagnetism are not those of valence electrons but of unfilled inner electron shells. Thus for a substance to be ferromagnetic, not only must it have an incomplete inner shell but the exchange integral must be positive. Slater (1930) pointed out that this is most likely to occur when a substance with an incomplete inner shell of large radius forms a crystal lattice with a small interatomic spacing.

The non-polar approach by Heisenberg is supplemented in other aspects of ferromagnetism by a band structure model. This is particularly useful in explaining how the number of electron spins per atom participating in the spontaneous magnetization may be non-integral, as is the case in the three common ferromagnetic elements.

1.1.2. The Domain Concept

This was the second hypothesis put forward by Weiss. Since the field needed to increase magnetization from zero to saturation is very small compared with the molecular field it must be assumed that some form of process involving reorientation of domain magnetization directions is taking place rather than an increase in the intrinsic magnetization. Therefore magnetization curves can be analysed in terms of domain wall displacements, irreversible and reversible, and the rotation of the magnetization direction in domains. Even so this does not give any idea of the size and shape of domain structures. Bitter (1931) was the first to take measurements on domain sizes by making the domain walls visible with a magnetic colloid. Unfortunately most of this early work was carried out on mechanically strained surfaces so that the observed structure did not bear any resemblance to the underlying structure. It was not until 1935 that Landau and Lifshitz proposed theoretical domain structures. They pointed out that a domain configuration constituted a system of minimum energy. Each of the forms of energy involved in these considerations will be dealt with, in detail, in the next section.

1.2. Domain Energy Contributions

1.2.1. Exchange Energy

When equation 1.1 is summed over all values ij

$$E_{ex} = -2JS^2 \sum_{i>j} \cos\phi_{ij} \qquad (1.2)$$

is obtained if only nearest neighbour interactions are considered. E_{ex} is the exchange energy and ϕ_{ij} the angle between the spin vectors. In a domain where the spins are parallel the exchange energy is zero but this is not the case when dealing with the region between domains. It is then essential to know the value of $2JS^2$ or more often

$$A = \frac{2JS^2}{a}$$

when considering energy densities, a being the lattice constant.

Of the several determinations of J, Kittel (1949) favours the one relating the experimental value of C in the Bloch Law

$$I = I_0 (1 - CT^{3/2}) \qquad (1.3)$$

for the temperature dependence of saturation magnetization at low temperatures to J by means of

$$C = \frac{\cdot 0587}{25} \left(\frac{k}{2SJ}\right)^{3/2} \qquad (1.4)$$

for a body centred cubic structure. This gives J = 205k, where k is Boltzmann's constant,

and $A = 2.0 \times 10^{-6}$ ergs/cm. Measurements by Fallot (1936) indicate that for 4% silicon iron a value of A of 1.7×10^{-6} ergs/cm should be used. The value of γ_o, the energy per unit area of a 90^o wall with its normal in a [001] direction, is 0.9 ergs/cm^2 for iron and 0.7 ergs/cm^2 for silicon iron, using this value of A. Néel (1944c) using a different method obtained a value of γ_o for iron of 0.7 ergs/cm^2. Stoner (1950) obtained a value of 0.62 ergs/cm^2 for iron from the relationship given in equation (1.17a). However he pointed out the inaccuracies in the evaluation of γ_o due to the many uncertainties in the detailed treatment of exchange interaction effects.

1.2.2. Anisotropy Energy

Upon investigating the magnetization curves of ferromagnetic crystals it can be seen that differing amounts of energy are required to magnetize specimens in different crystallographic directions. The direction requiring the least amount of energy is called the easy direction and is the [100] direction in iron, the [111] direction in nickel and the [0001] direction in cobalt. The energy required to magnetize a specimen can be expressed in terms of the direction cosines α_i of the magnetization vector with respect to the crystallographic

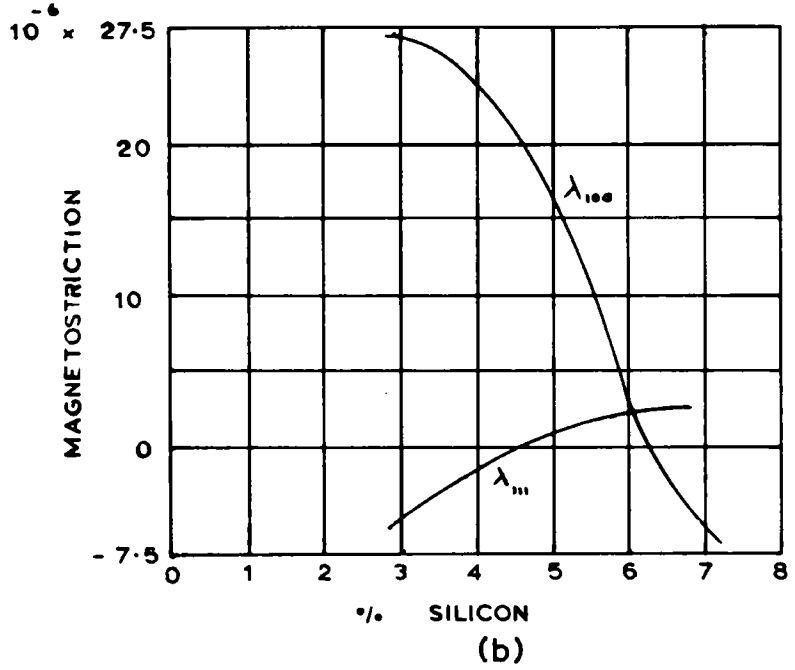
10⁻⁶ x
27·5
20
10
0
- 7·5
MAGNETOSTRICTION
λ100
λ111
0 1 2 3 4 5 6 7 8
% SILICON

(b)

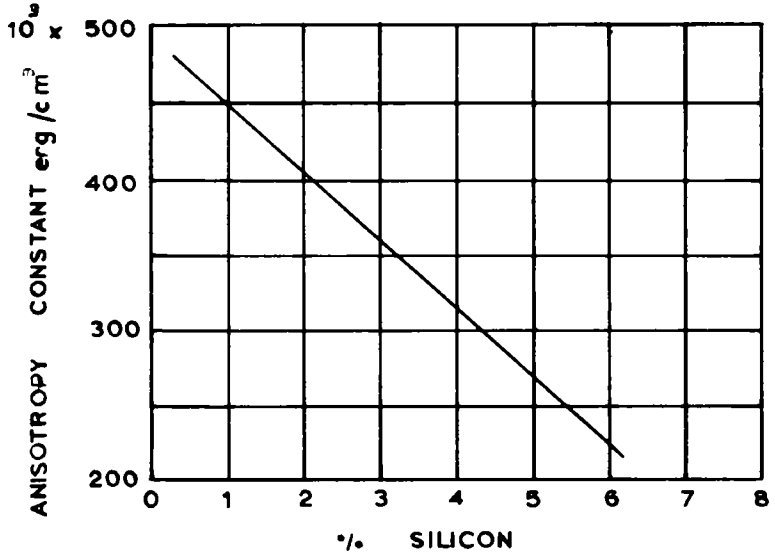
10⁶ x
500
400
300
200
ANISOTROPY CONSTANT erg/cm³
0 1 2 3 4 5 6 7 8
% SILICON

(a)

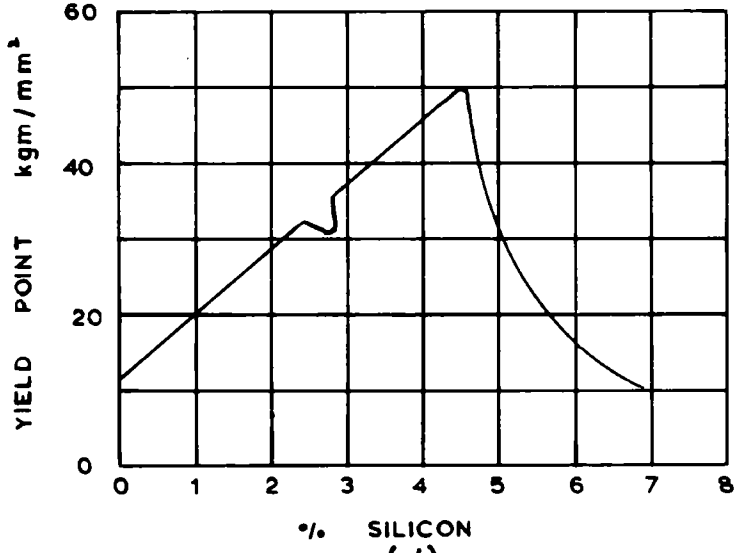
60
40
20
0
YIELD POINT kgm/mm²
0 1 2 3 4 5 6 7 8
% SILICON

(d)

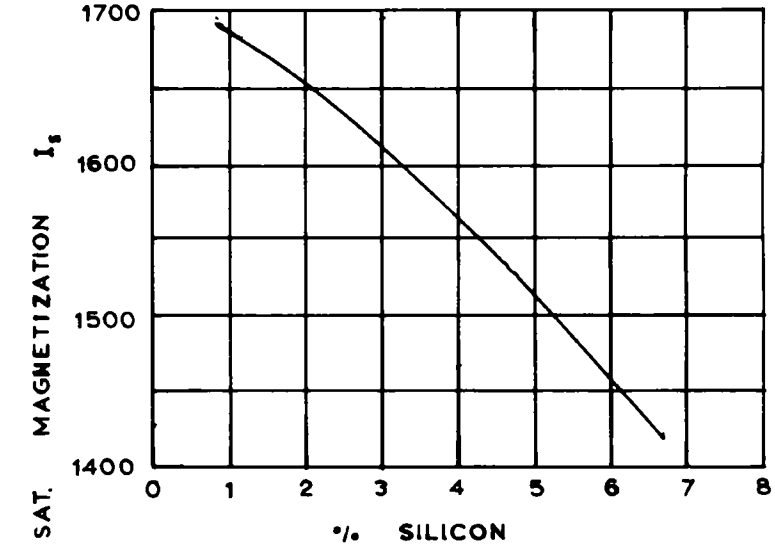
1700
1600
1500
1400
SAT. MAGNETIZATION Is
0 1 2 3 4 5 6 7 8
% SILICON

(c)

FIG 2

axes. For a cubic system only even powers of α_i are consistent with symmetry requirements and a good representation of the energy of magnetization E_{an} per unit volume is given by an expression of the form

$$E_{an} = K_1(\alpha_1^2\alpha_2^2 + \alpha_2^2\alpha_3^2 + \alpha_1^2\alpha_3^2) + K_2\alpha_1^2\alpha_2^2\alpha_3^2 \qquad (1.5)$$

Terms involving higher powers of α_i may also be introduced but the constants K_3, K_4 etc. are usually of rapidly decreasing magnitude. The values of the anisotropy constants for pure iron are $K_1 = 4.2 \times 10^5$ ergs/cm^3 and $K_2 = 1.5 \times 10^5$ ergs/cm^3 at room temperature. Fig. (2a) shows the variation of K_1 for silicon iron with varying amounts of silicon.

The physical origin of anisotropy is rather a difficult problem. Exchange energy, being only a function of the angles between spins, does not lead to anisotropy. A consideration of the interaction of magnetic dipoles localized at lattice points does give rise to small anisotropy effects but these show little agreement with experimental evidence.

The most promising approach so far is to consider that the magnetization, that is the electron spins, interact with the crystal lattice by means of the orbital momenta of the electrons. Recently this has been developed by Fletcher (1955), using the collective electron theory,

for the evaluation of K_1 for nickel at absolute zero. He obtained a value for K_1 of -5×10^7 ergs/cm^3 compared with the experimental value of -8×10^5 ergs/cm^3.

1.2.3. Magnetoelastic Energy

When a crystal undergoes mechanical strain there is an additional energy due to the interaction between the magnetization and the mechanical strain. This is known as the magnetoelastic energy and is equal to zero for an unstrained lattice. It is the reverse effect of magnetostriction, the change in length upon magnetizing a ferromagnetic substance. A formal theory of magnetostriction was developed by Becker and Doring (1939) by minimising the total energy of a crystal i.e. the anisotropy energy, the magnetostrictive energy and the elastic energy. Thus if a state of constant stress is considered, the change in length in a direction specified by direction cosines β_i and by magnetization cosines α_i is

$$\frac{\delta l}{l} = h_1\left(\alpha_1^2\beta_1^2 + \alpha_2^2\beta_2^2 + \alpha_3^2\beta_3^2 - \frac{1}{3}\right) + h_2\left(2\alpha_1\alpha_2\beta_1\beta_2 + 2\alpha_2\alpha_3\beta_2\beta_3 + 2\alpha_3\alpha_1\beta_3\beta_1\right) \qquad (1.6)$$

+ higher terms.

It is more usual to express the constants h_1 and h_2 in terms of the longitudinal magnetostrictions λ_{100} and λ_{111}, the changes in length measured along the directions of magnetization in the [100] direction and the [111] direction

respectively.

Where $\frac{2}{3} h_1 = \lambda_{100}$

and $\frac{2}{3} h_2 = \lambda_{111}$

Fig. (2b) shows the variation of λ_{100} and λ_{111} for various percentages of silicon in silicon iron at room temperature.

In an analogous way to the method of Becker and Doring, mentioned above, an expression can be worked out for the energy arising from the magnetostrictive distortion when a specimen is in a stress field. If the stress is defined by the stress tensor Π_{ik} and the strain by the strain tensor A_{ik} then the energy E_σ is given by

$$E_\sigma = \sum_{ik} \Pi_{ik} A_{ik} \tag{1.7}$$

If A_{ik} is expressed in a power series of α_i up to the second order, this leads to

$$E_\sigma = -\frac{3\lambda_{100}}{2}\left[\Pi_{11}\alpha_1^2 + \Pi_{22}\alpha_2^2 + \Pi_{33}\alpha_3^2\right] - 3\lambda_{111}\left[\alpha_1\alpha_2\Pi_{12} + \alpha_2\alpha_3\Pi_{23} + \alpha_3\alpha_1\Pi_{31}\right] \tag{1.8}$$

In our case the most interesting type of stress is the pure tension σ dynes/cm^2. If this has direction cosines $(\gamma_1\gamma_2\gamma_3)$ then

$$\Pi_{ik} = \sigma\,\gamma_i\gamma_k$$

and

$$E_\sigma = -\frac{3\sigma}{2}\left[\lambda_{100}(\alpha_1^2\gamma_1^2 + \alpha_2^2\gamma_2^2 + \alpha_3^2\gamma_3^2 + 2\lambda_{111}(\alpha_1\alpha_2\gamma_1\gamma_2 + \alpha_2\alpha_3\gamma_2\gamma_3 + \alpha_3\alpha_1\gamma_3\gamma_1)\right] \tag{1.9}$$

A much quoted equation is that obtained from equation (1.9) by putting $\lambda_{100} = \lambda_{111} = \lambda$, and expressing the angles in terms of θ, the angle between the stress and the magnetization. It is

$$E_\sigma = -\frac{3\lambda}{2}\sigma\cos^2\theta \qquad (1.10)$$

This implies that if λ is positive then the stress energy is a minimum when the magnetization is rotated into the stress direction. Note that the magnetostriction in this case is isotropic.

1.2.4. Magnetostatic Energy

The last energy expression to be considered is the energy of a magnetic vector in its own field and is known as the magnetostatic energy. The energy is given by

$$E_{m.s.} = -\frac{1}{2}\int \mathbf{I}.\mathbf{H}\, dv \qquad (1.11)$$

where I is the magnetization and H is the field arising from the magnetization, the integration being carried out over the volume of the specimen. Perhaps the most important situation to be worked out in domain theory is the magnetostatic energy of parallel strips of poles of alternate sign. The method is that due to Kittel (1949).

Let the strips lie in the x,y plane, the y axis being parallel to the axis of the strips. The surface density ρ of magnetic poles is expanded as a Fourier series $\Sigma\rho_n$

and the solution for the potential Φ expressed thus

$$\Phi_{x,z} = \sum A_n \rho_n \exp\left(\frac{-n\pi z}{\ell}\right) \qquad (1.12)$$

A_n is determined from the boundary conditions,

$$\left[\frac{\delta\Phi}{\delta z}\right]_{z=-0} - \left[\frac{\delta\Phi}{\delta z}\right]_{z=+0} = 4\pi\rho \qquad (1.13)$$

As the magnetostatic energy for a two dimensional problem in (x,z) can be written

$$E_{m.s} = \frac{1}{2}\int \rho(x)\Phi(x,0)\,dx \qquad (1.14)$$

$E_{m.s}$ can be found. In the case of magnetization normal to the surface, and strips of width D

$$E_{m.s} = .852\ I^2 D$$

In cases where the magnetization vector makes a small angle δ with the surface of the specimen the alternating pole density is given by I sin δ. Shockley (1948) has shown that in this case the magnetization can move slightly from the easy direction giving an effective permeability μ^+. In the stress free case, this can be shown to be given by

$$\mu^+ = 1 + \frac{2\pi I^2}{K_1} \qquad (1.15)$$

for a (100) surface of a cubic system. This is introduced into a correcting factor $\frac{2}{1+\mu^+}$ for the magnetostatic energy.

1.3. Bloch Walls

A ferromagnetic may be considered to be made up of a system of domains, each one being magnetized along a direction of easy magnetization. The region between two such domains is known as a Bloch Wall after some preliminary work on its energy and thickness by Bloch (1932). Neel (1944) has shown that the component of magnetization normal to the boundary, must not only be the same on both sides of the wall but also in the transition region. Let us consider the energy associated with free poles formed when the wall makes a small angle θ to the zero pole position. The pole density on the wall will be $\sqrt{2}$ I sin θ and the field produced normal to the wall will be $2\pi\sqrt{2}$ I sin θ. The magnetic energy will be $2\pi I^2$ sin θ per unit volume which is 2×10^7 sin θ ergs/cc for iron. Thus the energy of the system would increase greatly if magnetic poles were formed on the boundary wall. With this in mind it is possible to visualize two main types of boundary in iron, a 180° boundary with its normal moving in a (100) plane and a 90° boundary with a normal in a (110) plane.

Since the magnetization vectors rotate from one easy direction to another in the boundary wall, the wall energy must be expressed by

$$E_{TOTAL} = E_{an} + E_{ex}$$

At equilibrium it can be shown that the exchange and anisotropy contributions to the total energy are equal. Let the magnetization vector I be specified by the co-ordinates (θ, ϕ) where θ is the angle between I and the normal to the wall (x direction) and ϕ is the angle between the projection of I on the wall and the y direction. The wall energy can be expressed by

$$\gamma = 2 \int_{\text{limits of wall}} E_{ex}\, dx \qquad (1.16)$$

As the angle between spins in adjacent layers is $\sin\theta d\phi$

$$E_{ex} = \alpha\, a^2 \sin^2\theta \left(\frac{d\phi}{dx}\right)^2$$

Putting $E_{an} = \beta f_{an}$ one obtains

$$\frac{\gamma}{\gamma_0} = 2 \sin\theta \int_{\phi_1}^{\phi_2} f_{an}^{1/2}\, d\phi \qquad (1.17)$$

where $$\gamma_0, (\alpha\, a^2\, \beta)^{\frac{1}{2}} \qquad (1.17b)$$

is a unit for the energy per unit area of boundary wall.

Fig. 3 shows the variation of ϕ with distance through a 180° wall making an angle of 1° with the [100] direction. The effective width of the boundary is the distance AB which can be expressed analytically by

$$\frac{b}{b_0} = \left(\xi_c - \xi_a\right) + \phi_a \left(\frac{d\xi}{d\phi}\right)_a + (\pi - \phi_c)\left(\frac{d\xi}{d\phi}\right)_c \qquad (1.18)$$

where (ϕ_a, ξ_a) (ϕ_c, ξ_c) are the first and third points of inflexion and

$$b_o = \left(\frac{\alpha\, a^2}{\beta}\right)^{\frac{1}{2}}$$

This above treatment is due to Lilley (1950) and deals only with boundaries with normals in the [100], [110] and [111] directions. The results are shown in the table below.

		Values of Energies in γ/γ_o		
Type of Boundary	Normals	[100]	[110]	[111]
Iron	90^o	1.000	1.727	1.185
	180^o	2.000	2.760	

Several workers have dealt with a general expression for the orientation of a 90^o Bloch Wall in iron. Graham (1958) solved the problem graphically, whereas Kaczer and Gemperle (1959) took

$$\frac{\gamma}{\gamma_o} = 4 \sin\theta \int_0^{\phi_2} f_{an}^{\frac{1}{2}}\, d\phi$$

where, once again f_{an} is the reduced dependence of the anisotropy energy and is a polynomial of the fourth degree in cos ϕ. The integral is however one of an elliptic function and so was solved numerically, to an accuracy of about $\frac{1}{2}\%$.

The energy of the wall, expressed as a function of ψ, the angle between the normal of the wall and the [100] direction becomes

$$\frac{\gamma}{\gamma_o} = 1{\cdot}7274 - 1{\cdot}2289\cos\psi + 0{\cdot}5015\cos^2\psi \qquad (1.19)$$

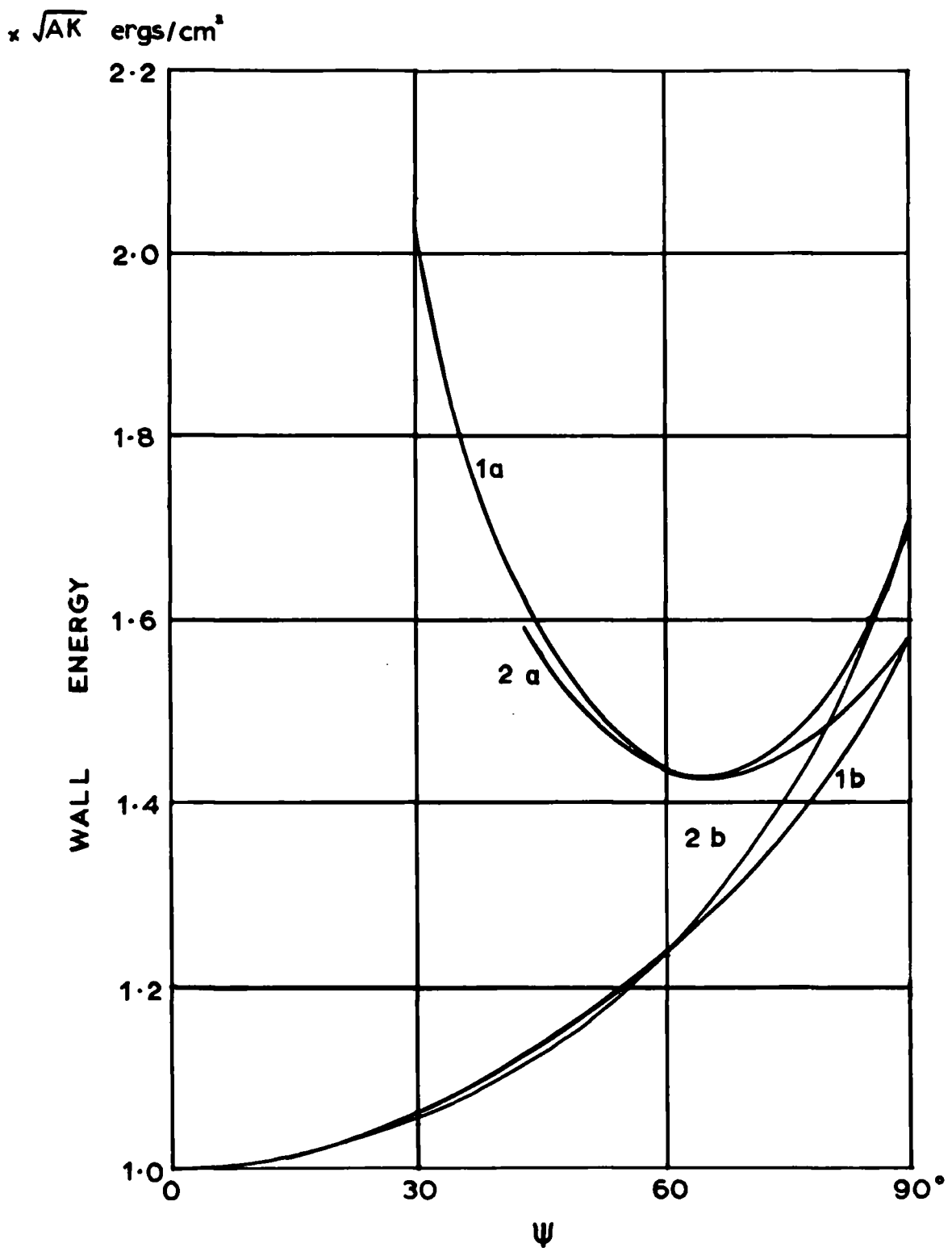

γ Energy of 90° wall as a function of wall orientation 1b, 2b.
1(a, b) Chikazumi and Suzuki (1955)
2(a, b) Kaczer and Gemperle (1959)
γ / sin Ψ 1a, 2a

FIG. 4

This relationship is shown in Fig. 4. Also shown is an approximation to the solution by Chikazumi and Suzuki (1955). Upon obtaining

$$\gamma = 2\sqrt{A}\sin\theta \int_{\phi_1}^{\phi_2} g(\theta,\phi)^{\frac{1}{2}}\, d\phi$$

where $g(\theta,\phi)$ is the anisotropy energy and $A = \frac{2JS^2}{a}$, they express the anisotropy energy by a Fourier series thus

$$g(\theta,\phi) = g_0 + g_1\cos\left(\frac{\pi\phi}{\phi_1}\right) + g_2\cos\left(\frac{2\pi\phi}{\phi_1}\right) + \cdots\cdots \quad (1.20)$$

and then approximately

$$g(\theta,\phi) = 2g_0\cos^2\left(\frac{\pi\phi}{2\phi_1}\right) \quad (1.21)$$

where $g_0 = \frac{g(\theta,0)}{2}$

They obtain the result

$$\gamma = \frac{8}{\pi}\sqrt{g_0 A}\left(\frac{\phi_1}{\sin\phi_1}\right) \quad (1.22)$$

This can be seen to be quite a good approximation in the range ψ 0°-65° to the more exact work of Kaczer and Gemperle. (Fig. 4).

The effect of stress on wall energies will be discussed later.

1.4. Domain Systems in Iron

Domain structures are a function of the shape, size and orientation of any particular crystal. A few simple structures will be considered and it will be shown how they compare with experimental work.

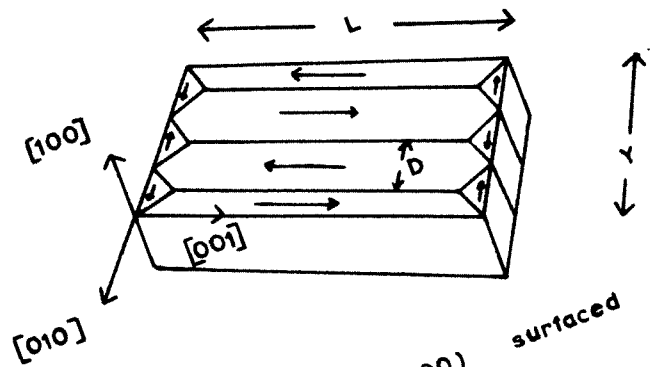

Stress free domain structure for a (100) surfaced iron crystal

FIG. 5

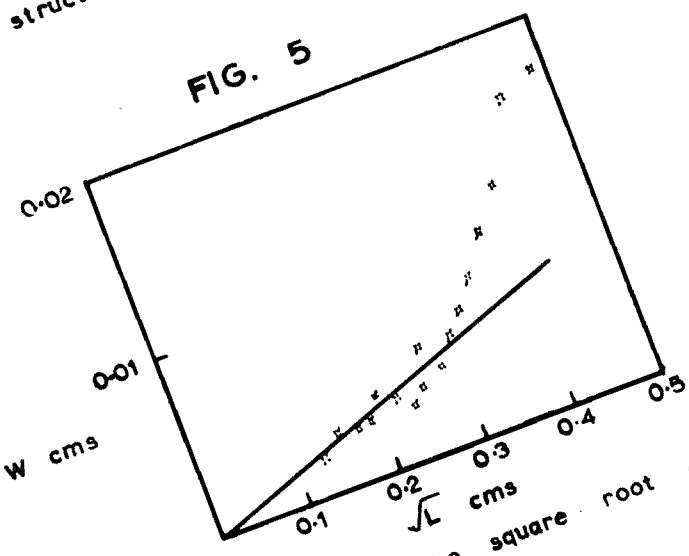

Domain width as a function of the square root of the crystal length
Williams et al. (1949)

FIG. 6

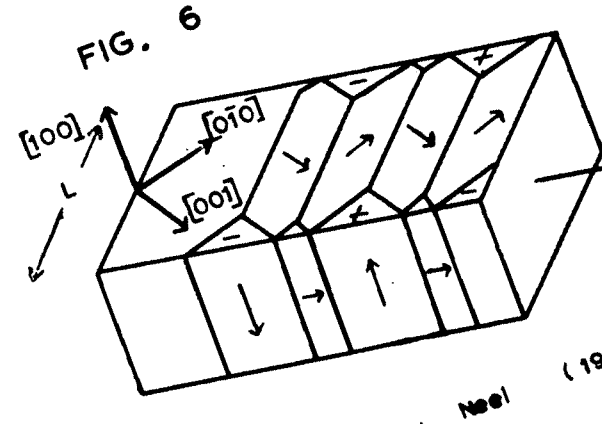

Domain structure proposed by Neel (1944)
Field H applied in [011] direction

FIG. 7

A crystal cut as shown in Fig. 5 has a main (100) surface and is bounded by [100] edges. Evaluating the energy for a surface area L, one obtains

$$\text{Wall energy} = \frac{\gamma L t}{D}$$

and magnetoelastic energy due to closure domains

$$= \tfrac{1}{2} C_{11} \lambda_{100}^2 \quad \frac{Dt}{2}$$

Minimising the sum of these energies with respect to D, one obtains

$$D = \sqrt{\frac{4\gamma L}{C_{11} \lambda_{100}^2}}$$

In a paper by Bozorth, Williams and Shockley (1949), structures similar to this were observed. By taking measurements near the corner of a crystal with a (100) surface and [110] edges, values of D as a function of L were obtained. The measurements did not agree very well with the $D \propto L^{\frac{1}{2}}$ relationship, probably because the edges of the crystal were not in [100] directions. (Fig. 6).

Systems similar to the above except that the main (100) surface is bounded at the ends by (111) planes have been investigated in the range L>1cm by Martin (1957), L 1 - .1 cm by Carey (1960) and L less than .1 cm by Martin and Bloor (1959). The theoretical relationship is

$$D = 1.32 \left(\frac{\gamma}{k} \right)^{\frac{1}{4}} L^{\frac{3}{4}}$$

and the experimental results agree quite well with this.

A similar structure to the one mentioned above is observed on a (110) surface of polycrystalline silicon iron with the magnetization in the surface easy direction separated by 180° walls. There are no closure domains in this case therefore the contributions to the domain energy are the magnetostatic energy and the wall energy. This gives as a minimum energy condition

$$D = \sqrt{\frac{\gamma L}{1.7\ I_s^{\,2}}}$$

for a single crystal with no closure domain. This relationship has not been verified experimentally.

Bates and his co-workers (Bates and Neale (1950), Bates and Mee (1952) and Bates and Hart (1956)) have done much interesting work on a Néel cut specimen (see Fig. 7) with magnetic fields of various sizes along the direction indicated. They have been interested for the main part in the variation of D with the thickness L in the [110] direction and the applied field H. From the later measurements they were able to check some theoretical measurements of Néel (1944a).

1.5 Observation of Domains

The two main methods of domain observation are the Bitter pattern technique introduced by Bitter (1931) and

a much later technique using the Kerr Magneto-Optical Effect, developed by Fowler and Fryer (1954).

The Bitter technique consists of placing a colloidal suspension of iron oxide on the ferromagnetic under investigation. The particles are drawn to regions in which the magnetic field gradient has a local maximum. These regions are usually intersections of a Bloch Wall with the surface of the specimen. Colloid is also attracted to scratches which lie normal to the magnetization direction. This affords a useful technique for the detection of magnetization directions. The main disadvantage of the method is that it is impossible to obtain patterns with specimens of low anisotropy and consequently relatively wide walls, because of the low stray field at the Bloch Walls. Another disadvantage of the method is that the colloidal solution tends to dry and stain the surface of the specimen limiting the maximum time available for investigations to much less than an hour.

The normal Bitter technique has been supplemented by a method of Craik (1956) for observing domains under high magnification. He prepared colloid in a solution of 'Celacol' which when dried formed an undistorted thin film. This was then peeled off the surface and examined under an electron microscope.

The Kerr Magneto-Optical method suffers from neither of these aforementioned disadvantages. The principle of the method is that the rotation of the plane of polarization of reflected light depends upon the amount and direction of magnetization at the surface. In the case where the magnetization vector is parallel to the surface the Kerr rotation is zero at normal incidence and reaches a maximum of about 5' at 60° incidence. It is therefore a very critical technique to set up and a method of reducing the background noise has to be used. This consists of superposing the positive photograph of the magnetically saturated specimen on the negatives of the specimen in varying states of magnetization and printing the combined photographs. The disadvantage of this method, therefore, is its complexity which outweighs those of the Bitter technique for observations on iron and silicon-iron.

In order to use these techniques the specimen must be prepared so as to remove the mechanically deformed layer on the surface caused by polishing. This is done either by annealing or by electropolishing, details of which will be given later.

1.6 Previous Work on the Effect of Stress on Domain Structures

Dijkstra and Martius (1953) investigated the effect of stresses, up to the yield point, applied to a (110) surface of polycrystalline silicon-iron sheet. When a tensional stress was applied along a [100] direction no change of pattern was observed. A similar stress along a [110] direction proved more interesting. At a stress of about 0.1 kgm/mm^2 the domain structure changed to one where the main magnetization directions were the easy directions nearest to the direction of stress. At higher unspecified stresses a second type of structure appeared which was not interpreted. Both of these structures will be considered in more detail later.

Kirenskii, Dylgerov and Savchenko (1957) applied tensional stresses along a [100] direction on a (110) surface of silicon-iron and found that at about 15 kgms/mm^2 a marked change of structure occurred. Domains tended to split up by the formation of new walls between the existing ones. No explanation for this was made. The effect of stresses along a [100] direction of a crystal surface a few degrees off a (110) plane was investigated. The elimination of the dagger closure domains was explained in a quantitative manner as due to the rotation of the easy direction into the surface. Similar work to this

has been carried out by Shur and Zaikova (1958).

The work on (100) surfaces seems to have been mainly limited to investigations of maze patterns produced by strains arising from the mechanically polishing of a surface. In a paper Chikazumi and Suzuki (1955) put forward a model in which the main domains are magnetized normal to the surface. Triangular domains at the surface close the flux, and the walls forming them are zig-zag in nature. They showed how the system varied with stress and predicted a theoretical relationship between this and the zig-zag angle. Bates (1957) has suggested modifications purely on qualitative grounds, for the system when under high stresses.

Maze type patterns were produced on silicon-iron single crystals by Kaczer (1958) by the application of external forces. He applied a uniform compression to the sides of a cylindrical crystal of iron and found that the stress patterns appeared at 10 kgms/mm^2, though no measurements were taken on them. Photographs show them to be highly irregular.

Stephan (1956), (1957) carried out investigations on stress patterns on (100) surfaces obtained by quenching specimens from various temperatures. At fairly high stresses complicated zig-zag structures were formed by the splitting of main zig-zag boundaries. He calculated

the magnitude of the internal stresses by finding the magnetic fields needed to destroy the stress pattern. By this method he obtained stress values up to 70 kgms/mm^2.

External forces have been applied to maze patterns by Suda (1956). He needed to apply a stress of 60 kgms/mm^2 before the structure changed to an effectively stress free pattern of dagger domains. Again the experiment was only qualitative.

The application of tensional stresses to surfaces a few degrees off a (100) plane of silicon-iron was investigated by Bozorth, Williams and Shockley (1949), though again only quantitatively. They showed how fir tree structures changed under such conditions.

1.7 Object of Investigations

Dijkstra and Martius applied stresses to their polycrystalline silicon-iron sheet by stretching with a calibrated spring. This method is inherently inaccurate, unless strain gauges are used, as the strain in the specimen will be determined by the average Young's Modulus of differently orientated grains. By using their work as a starting point, and at the same time explaining the structures more fully with special reference to the transitional period, it was hoped to develop a straining technique which was more suited to work on small single

crystals and also polycrystalline sheet.

It was then hoped to verify Chikazumi and Suzuki's theoretical predictions by applying unidirectional stresses along the [110] direction on a (100) surface.

Further work could be carried out on a (100) surface by applying a stress along a [100] direction and examining the nucleation processes taking place when the bulk of the magnetization changes from one surface easy direction to the other. At the same time quantitative measurements could be made on the effect of stress on fir trees. Recently Spacek (1957), (1958) (1959) has introduced a theory explaining these and it was hoped that this might be used to obtain a theoretical relationship between the size of the fir trees and the applied stress.

The work of Chikazumi and Suzuki could then be extended to a (110) surface. By using a scratch technique very large loads of over 100 kgms/mm^2 can be applied.

It was with these problems in mind that the following work was carried out.

CHAPTER TWO

CHAPTER TWO

PREPARATION OF SPECIMENS

2.1 Introduction

Specimens of Goss type (110) surface silicon iron sheet, 0.37 mms thick, with grain size varying from 1 mm to 10 mms, were obtained from the Steel Company of Wales. A chemical analysis showed the main constituents besides iron to be

3.10%	Silicon
0.014%	Phosphorus
0.005%	Sulphur
0.004%	Carbon

This sheet proved useful for most of the experiments on (110) surfaces but specimens were needed with (100) surfaces. It was therefore decided to grow single crystals of iron, though later (100) cube textured polycrystalline sheet, of similar thickness and grain size to the Goss type sheet, was obtained from the G.E.C. of America.

2.2 Growth of Single Crystals

The raw material for these experiments was obtained from B.I.S.R.A. Sheffield. It was decided to use their pure Swedish iron A.A.K. , even though the yield point

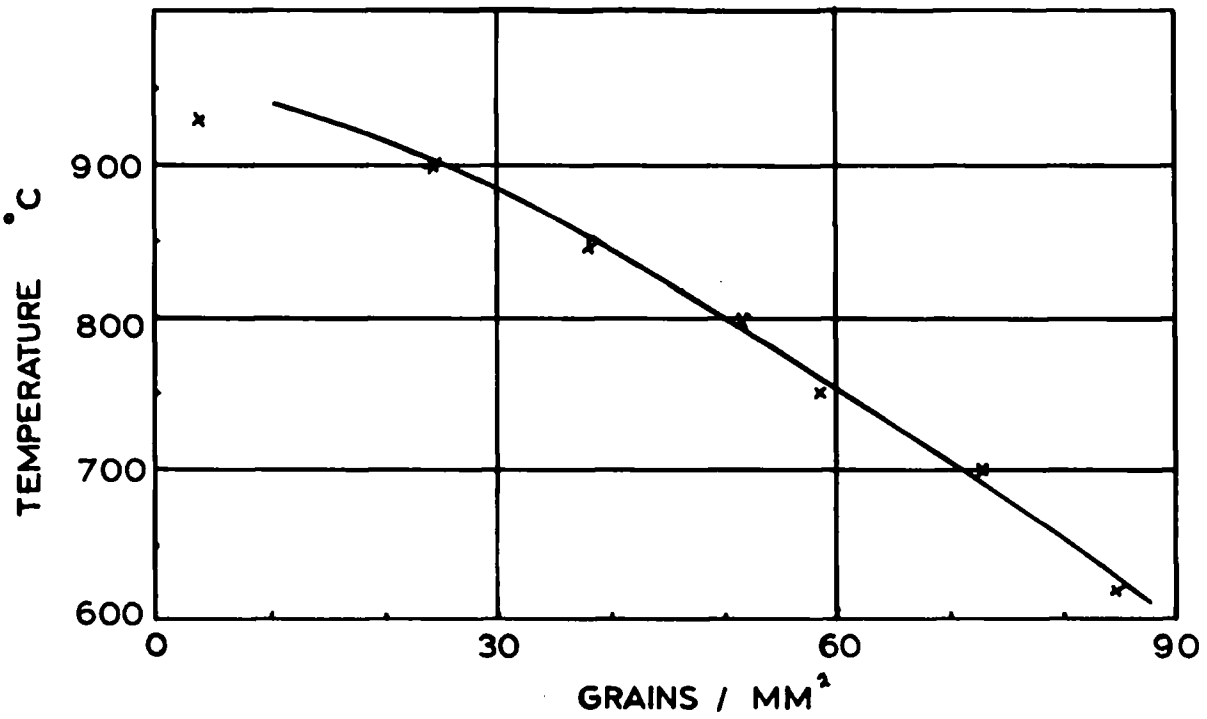

Variation of grain size with temperature of anneal

FIG. 9

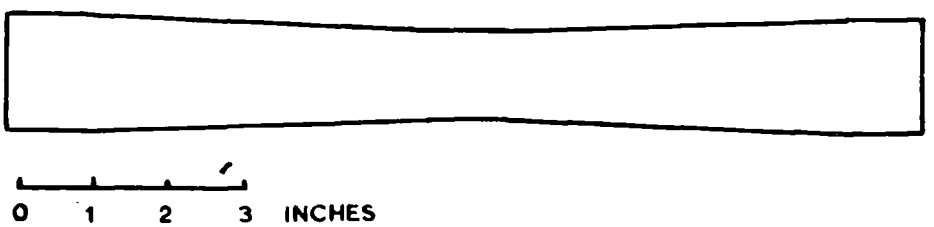

Shape of iron specimen
Thickness = 1/4 inch

FIG. 8

12 kgms/mm^2 is fairly low, in preference to their silicon iron which contains a rather high amount of non-metallic inclusions. The main impurities in the iron are 0.02% carbon and 0.02% silicon.

The crystals were grown by a strain and anneal method following the technique of Holden and Holloman (1949). The specimens are so shaped (see Fig. 8) that recrystallisation is limited to a small volume of critically strained material. Grains formed in this region grow into the lesser strained regions giving finally a large grained product.

Holden and Holloman found that they needed a certain critical grain size, 32 grains/mm^2, before straining the specimen to obtain maximum grain growth. Several small pieces of iron, $\frac{1}{4}$" x $\frac{3}{4}$" x $\frac{1}{2}$", were therefore heated up to various temperatures to find the conditions needed to produce this grain size. The test pieces were held at their maximum temperature for 18 hours then allowed to cool at 60° per hour, in an atmosphere of wet hydrogen. This was obtained by bubbling cylinder hydrogen through water maintained at 62°C. Fig. 9 shows the variation of grain size with the temperature of anneal. A specimen, shaped as in Fig. 8, was machined from the bar of Swedish iron and then heated, under the same conditions as the test pieces, at the critical temperature 860°C.

It was then strained the critical amount, a change in width at the centre of 1.6%. This corresponded to an applied load of 1.4 tons. The strained specimen was then annealed in pure dry hydrogen at 890°C for 72 hours followed by cooling at a rate of 70°C/hour. The hydrogen was purified by passing cylinder hydrogen over platinised asbestos at 300°C - 400°C to remove oxygen and then through a phosphorus pentoxide tube to remove water vapour.

Using this technique crystals up to 4 cms x 1.5 cms x .63 cms were obtained.

2.3 Orientation of Crystals

The crystals were initially orientated to within 3° by reflecting light from etch pits and measuring the angle with an optical goniometer. By using an etchant consisting of 1 part concentrated nitric acid and 4 parts water for 5 minutes, well developed pits with (100) faces were formed.

A more accurate determination was then carried out using a back reflection X-ray technique. The specimen was set at a fixed distance from the film, 3 cms for convenience, and knowing this the angles defining specific zones of the crystal could be worked out. Three intersecting zones were chosen on the film and by plotting these

on a sterogram as a function of ϕ, the angle of the zone axis to the film, and α, the angle between the vertical direction and the axis of the zone, the angles between the zones could be worked out. These angles were then compared with a table of angles between prominent zones for the cubic system, see Barrett (1943). The indices (h,k,l) of a face which is common to the zones (u,v,w) and (u',v',w') can be evaluated from the relationship

$$h = vw' - v'w$$

$$k = wu' - w'u$$

$$l = uv' - u'v$$

This method is capable of determining the orientation of a crystal to within $\pm \frac{1}{2}^{o}$ with the apparatus used.

2.4 Cutting and Shaping the Crystals

Next it was necessary to cut certain crystallographic planes in the orientated crystals and also to cut certain shapes from the polycrystalline sheet. It is essential that this cutting is as strain free as possible since this will reduce the amount of reannealing needed. Also if the specimen is badly strained then it could possibly recrystallise on annealing.

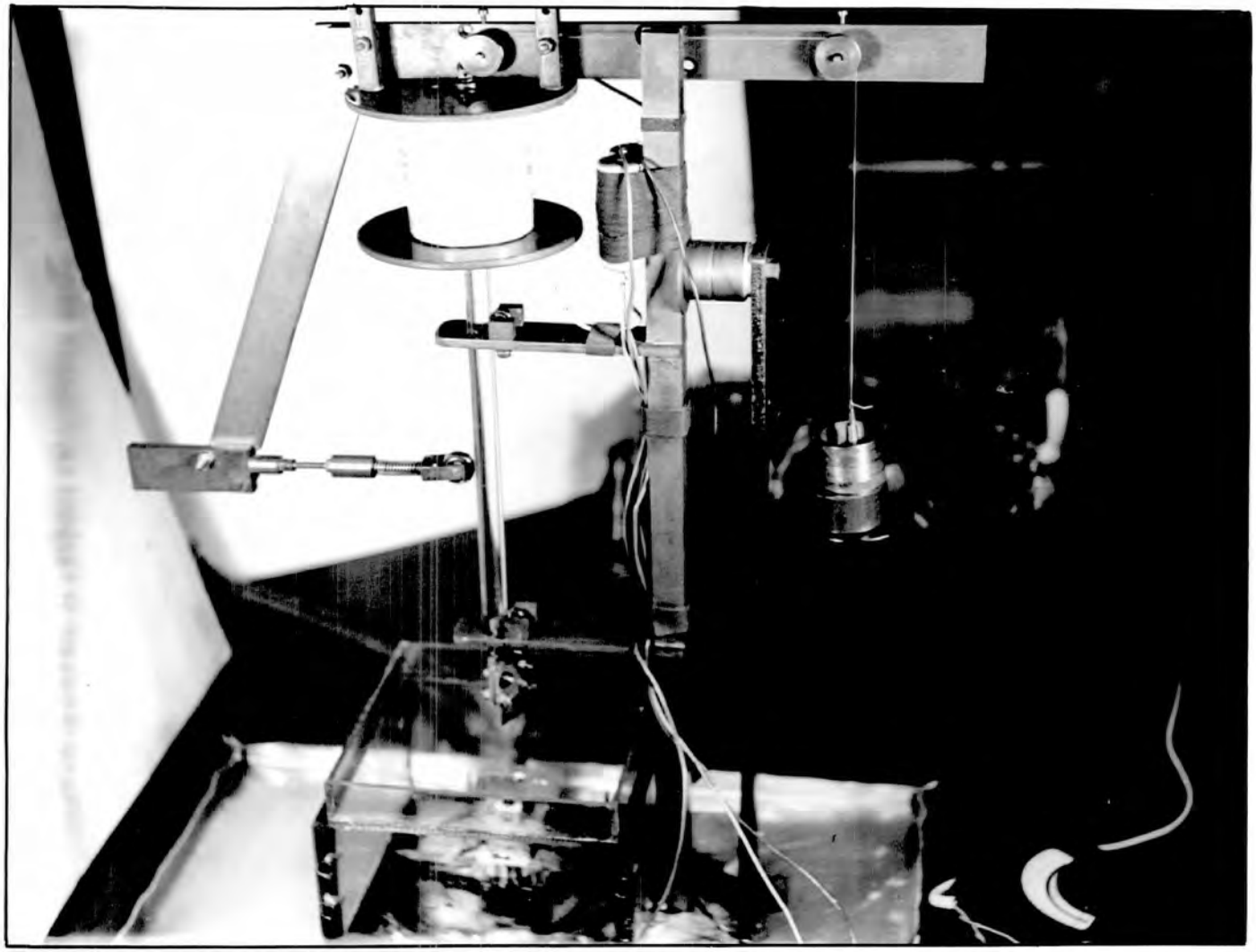

FIG. 10a

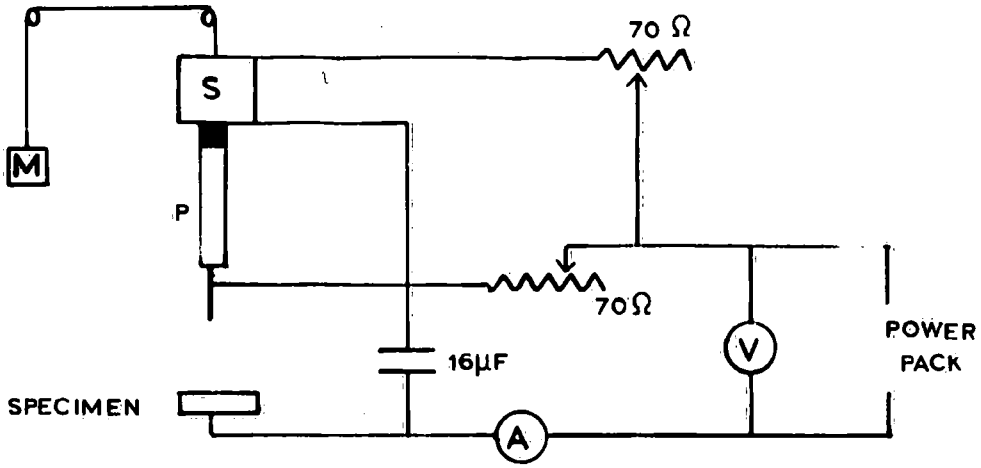

Schematic diagram of the electrospark apparatus

FIG. 10 b

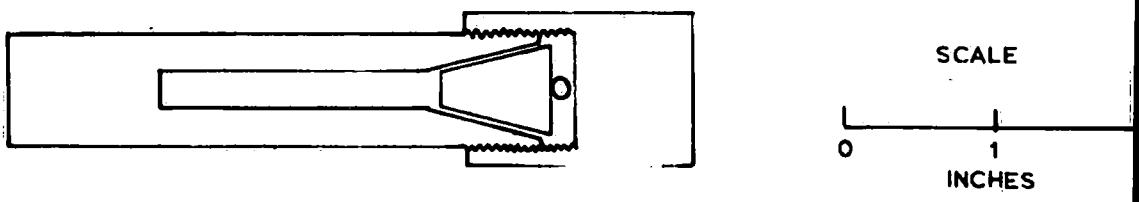

Steel vessel for annealing crystals

FIG. 11

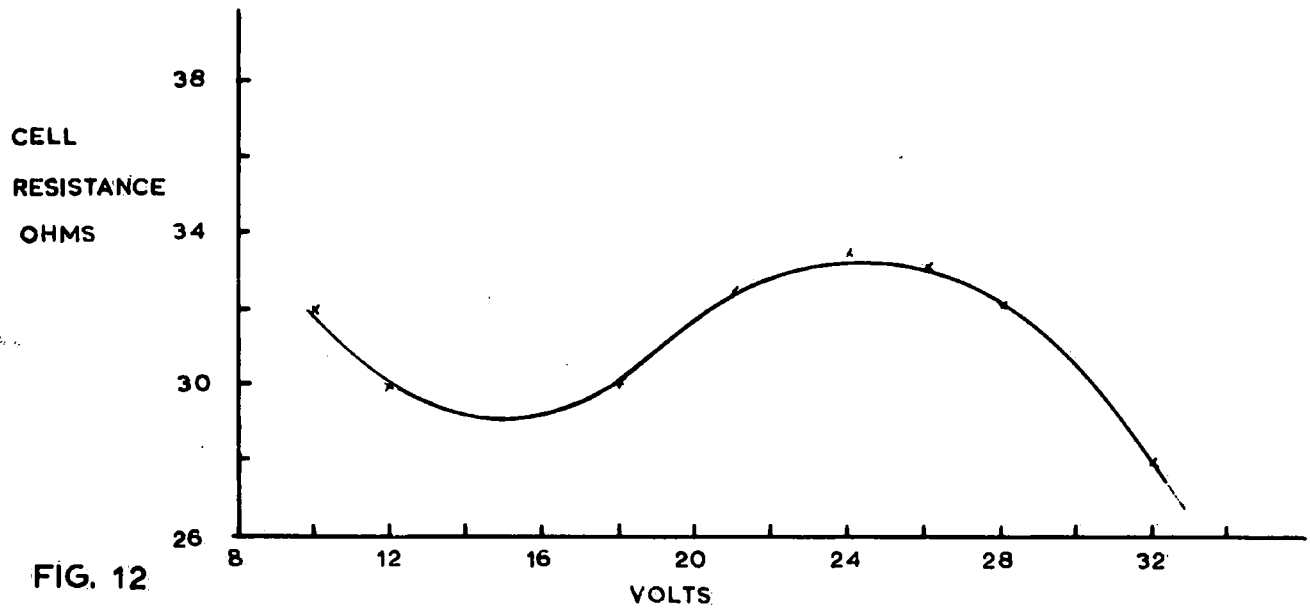

FIG. 12

Voltage resistance relationship for electropolishing silicon iron
Specimen 2·7 cm^2 Current density 0 25 amps/ cm^2

2.4.1. Apparatus

For the above reasons it was decided to carry out the cutting operations using an electrospark technique [Nosov and Bykov (1956) ; Cole, Bucklow and Grigson (1961)]. In this method an electric discharge passes between two electrodes and erodes the contacting areas away. As the specimen is the anode it wears away at a greater rate than the tool, the cathode.

The apparatus used is shown in Fig 10 (a and b). The perspex rod P which carries the cutting tool is located in a vertical plane by means of three roller races, one of which is spring loaded. The cutting arm is counterbalanced by an adjustable weight M. Friction is reduced to a minimum in the system by carrying the load on two pulleys fitted with ball races.

The cutting is controlled electromagnetically by means of a soft iron core fitted into the top of the perspex rod, which moves inside a small solenoid S. This has 3,000 turns of 30 s.w.g. copper wire giving a field of about 500 oersteds/amp. The control works in the following way. When the machine is sparking there is a small current flowing through the solenoid. This is cut off when the distance between the electrodes is too great for a spark to pass and so the tool moves downwards, due to the effective increase in weight, until sparking once

more takes place.

The specimen is mounted on a twin arc goniometer, both arcs being accurate to within 10'. The goniometer itself can rotate about a vertical axis over a scale which can be read to about 15', and can move in a horizontal plane a maximum of 1 cm on two slides at right angles. Thus the specimen can be set up at any desired angle with respect to the cutting tool to an accuracy better than that with which the orientation of the specimen has been determined. The anode is mounted in a perspex tank 15 cms x 15 cms x 10 cms which contains the coolant, transformer oil, which was chosen for its low viscosity and high dielectric constant. This prevents the electrodes melting and fusing. The power is derived from a mains rectifier capable of giving 100 watts.

2.4.2. Working Conditions and Results

Various charging potentials, ranging from 25 volts to 100 volts were tried with a fixed capacitance 16μF. The rate of cutting was directly proportional to the voltage. At maximum voltage this was $\frac{1}{4}$ cu. mm/min/cm. length of electrodes. The surfaces produced were examined under a microscope and found to be pitted to a depth of 10-20 microns. As the depth of the pits seemed independent of applied voltage the apparatus was normally

run at 100 volts.

Several metals were tried as cutting tools. Steel eroded at almost the same rate as the iron and silicon iron crystals, whereas brass and copper wore away at about half the rate. Due to its ease of machining and availability, brass was always used in preference to copper.

The surfaces so prepared showed very little contamination from the decomposition of oil and cathode material.

In some cases the surfaces were found to be a degree or so from that desired. A convenient method for obtaining the desired orientation was by fine grinding. The specimen was fixed by means of a goniometer head to a spring loaded horizontal arm which moved about an accurately vertical arm, across a steel polishing wheel once every minute. The surface of the specimen was first set up parallel to the surface of the wheel by covering the latter with marking blue. The specimen was then rotated by means of the goniometer head, the same one as used in the electrospark apparatus, to the desired orientation. Wet carborundum was used as an abrasive in grades varying from 240 to 3F.

2.5 Polishing and Annealing

The specimens were polished by hand using successive grades of emery paper from 1F to 4/0. They were then polished on a rotating wheel using Hyprez Diamond Compound

of grades 8 micron, 3 micron and $\frac{1}{4}$ micron as abrasives.

The crystals so prepared were then annealed. First annealing in a stream of pure dry hydrogen, purified as described before, at 820°C for 8 hours followed by a 30°C/hour cool was tried. This proved unsuccessful as a thin layer of impurity formed on the surface necessitating further polishing. A method was then tried of placing the specimen in a silica tube inside a steel vessel (see Fig. 11). This was filled with hydrogen, sealed, then annealed as before in a stream of pure hydrogen. Once again a clean surface was not obtained.

However good results were obtained using a vacuum furnace. The vacuum was obtained using an Edwards 2M2 Mercury Diffusion Pump working with a rotary backing pump. The heater was of 0.012 inch diameter tungsten wire wound on a $^{11}/_{16}$" diameter grooved, $^{1}/_{32}$" pitch, silica tube. This was surrounded by a $\frac{3}{4}$" internal diameter mullite tube to reduce heat losses. In order to keep the temperature, which was measured with an iron constantan thermocouple, at 830°C, a satisfactory temperature of anneal, 40 watts were dissipated. Even at this temperature the pressure was kept as low as 0.08 microns. Satisfactory strain free domain structures were obtained after annealing at 830°C for 3 hours and cooling at 300°C/hour.

Even though domain structures could be seen at this stage it was found necessary to remove the slight scratches remaining by a light electropolish. The apparatus used was very similar to that described by Bates and Mee (1950) having a stationary cathode and rotating anode. Stainless steel cathodes were used in sizes varying from 2" diameter to $4\frac{1}{2}$" diameter depending upon the size of the specimen being polished. The specimen was attached to the rotating spindle by means of a small horseshoe magnet. This, and any part of the specimen not needing polishing, were coated with a layer of polystyrene cement. It was found essential for good polishing, that the centre of rotation of the anode should lie outside the specimen. The electrolyte used was made up of 133 ccs glacial acetic acid, 25 grams chromium trioxide and 7 ccs water.

By using a Wheatstone Bridge net, as described by Bates and Mee, the optimum polishing conditions, which correspond to maximum cell resistance, were found. A typical voltage resistance graph is shown in Fig. 12. Using an anode rotation of 70 r.p.m. good results were obtained with a cell voltage of 25 volts for a silicon iron specimen, and 23 volts for a pure iron specimen. The current density was 0.25 amps/cm^2.

When the specimen had been vacuum annealed after mechanical polishing, a 5 minute electropolish was sufficient to produce a smooth surface. However in some cases, when the specimen was too large for the furnace, it had to be electropolished directly after mechanical polishing. In these cases polishing times of up to 30 minutes were necessary, resulting in rather uneven surfaces.

2.6 Observation of Domains

Before observing the domain structure the specimens were demagnetized by exposure to a decreasing alternating magnetic field. A magnetic colloid technique was used for the observation of domains. The colloid recipe used was that of Elmore (1938) with one slight difference. It was made up to a concentration 4 times that described by Elmore. The staining of the surface by the colloid was not a serious problem as this took about $\frac{1}{2}$ an hour. Often the experiment could be carried out in this period, and if this was not possible the surface could be cleaned by soaking in absolute alcohol.

The domains were observed using a Cooke Troughton & Simms reflected light microscope at magnifications varying from 50x to 400x, although the most useful magnification was found to be 100x. Photographs were taken with a Leica

35 mm camera which was coupled to the microscope by means of an adaptor with a focussing eyepiece. The film used was Ilford Pan F, chosen for its high contrast and small grain size and was developed in ID 11. Exposure times between 1 second and 10 seconds were found necessary depending upon lighting conditions.

Measurements on the films were carried out by projecting the negatives onto a ground glass screen at 10x magnification by means of a Durst 609 enlarger. This allowed direct measurements to be made with a ruler and protractor on the ground glass screen.

CHAPTER THREE

CHAPTER THREE

EFFECT OF EXTERNAL STRESSES UP TO THE YIELD POINT ON A (110) SURFACE

3.1 Tensional force along the [110] direction

3.1.1. Introduction

Dykstra and Martius (1953) studied the effect of a tensional stress, applied by means of a calibrated spring, along a [110] direction on a (110) surface of silicon iron polycrystalline sheet. In this section the results obtained by applying tensional stresses by direct loading and by cantilever bending will be compared.

3.1.1.1. Effect of Stresses on Magnetization Directions

It is important in interpreting new domain structures to consider the effect of stress on magnetization directions. In a zero stress system the magnetization direction in a single domain is governed solely by the magnetic anisotropy energy. In a domain under stress a further energy term, given by equation (1.9) must be taken into account.

Consider a compressive stress σ dynes/cm^2 applied along the [001] surface direction of a specimen with a (110) surface. The energy $E_{[001]}$ associated with magnetization along the [001] direction equals $+\frac{3}{2}\sigma\lambda_{100}$ while the energy of magnetization along the [010] and [100]

directions remains zero. It is therefore conceivable that a system originally magnetized along the [001] direction could change under this stress to a system magnetized mainly along the [010] direction.

The energy $E_{[110]}$ for magnetization along the [110] direction is $K_1/4$ and so taking the values of K_1 and λ_{100} for silicon iron, the energy $E_{[110]}$ equals $E_{[001]}$ at a stress of 23 kgms/mm^2. This does not mean that above this stress the magnetization will rotate from the [001] direction to the [110] direction as these two minima are separated by an energy maximum. To find the stress required to do this, it is necessary to consider the general case with the magnetization making an angle α with the [001] direction while still lying in the (110) plane. The total energy is then

$$E_{TOT} = \frac{3}{2}\sigma\lambda_{100}\cos^2\alpha + K_1\cos^2\alpha\sin^2\alpha + \frac{K_1}{4}\sin^4\alpha$$

the first term being due to magnetoelastic energy and the last two due to anisotropy energy.

Minimising this with respect to α, three roots are obtained,

$$\cos\alpha = 0$$

$$\sin\alpha = 0$$

$$\text{and } \cos^2\alpha = \frac{K_1 + 3\sigma\lambda_{100}}{3K_1}$$

The first two are minima up to $\sigma = \frac{2K_1}{3\lambda_{100}} = 91$ kgms/mm^2. The maximum given by the third equation corresponds at zero stress to $\alpha = 55^\circ$. As the stress increases, the angle between the maximum and the [001] direction, the direction of stress, becomes smaller until at $\sigma = 91$ kgms/mm^2 it equals zero. When $\alpha_{max} = 0$ the [001] direction becomes a point of inflexion and so above this critical stress the magnetization will rotate into a [110] direction. It is interesting to note that there is no rotation away from the crystallographic axes before this stress of 91 kgms/mm^2.

It can readily be seen that similar results can be obtained by applying a tensional stress σ dynes/cm^2 along the [110] direction. Once again, taking α to be the angle between the magnetization direction and the [001] direction and differentiating the total energy with respect to α, three turning points are obtained

$$\sin \alpha = 0$$

$$\cos \alpha = 0$$

$$\text{and } \sin^2 \alpha = \frac{2K_1 - \frac{3}{4}\sigma(\lambda_{100} + \lambda_{111})}{3K_1}$$

At a stress given by $\sin^2 \alpha = 0$, the [001] direction again becomes a point of inflexion while the [110] direction still remains a minimum. This stress is given by

$$\sigma = \frac{4K_1}{3(\lambda_{100} + \lambda_{111})}$$

$$= 224 \text{ kgms/mm}^2$$

Fig (2d) shows the variation of yield point for various percentages of silicon in silicon iron due to Yensen (1915). The value of the yield point for the silicon iron used in the following experiments is about 40 kgms/mm^2. Therefore as these experiments are carried out in the elastic range the only favourable direction of magnetization in the surface must be the [001] direction.

This treatment shows that it needs stresses greater than the yield point to make the [110] direction an easy direction and the stresses required to change the magnetization from a [001] direction, given by $E_{[001]} = \frac{3}{2}\sigma\lambda_{100}$, to a [010] direction, $E_{[010]} = 0$, must be greater than zero. In fact the latter change-over stress is very dependent on the specimen shape and therefore the energies of the two domain systems, and factors such as these must be taken into account when working out the change-over stress.

It is interesting to consider the effect of the compressive stress σ dynes/cm^2 along the [110] direction on the two easy direction [100] and [010] which make an angle of 45° to the direction of stress. This will apply to some work in chapter four. If this magnetization vector

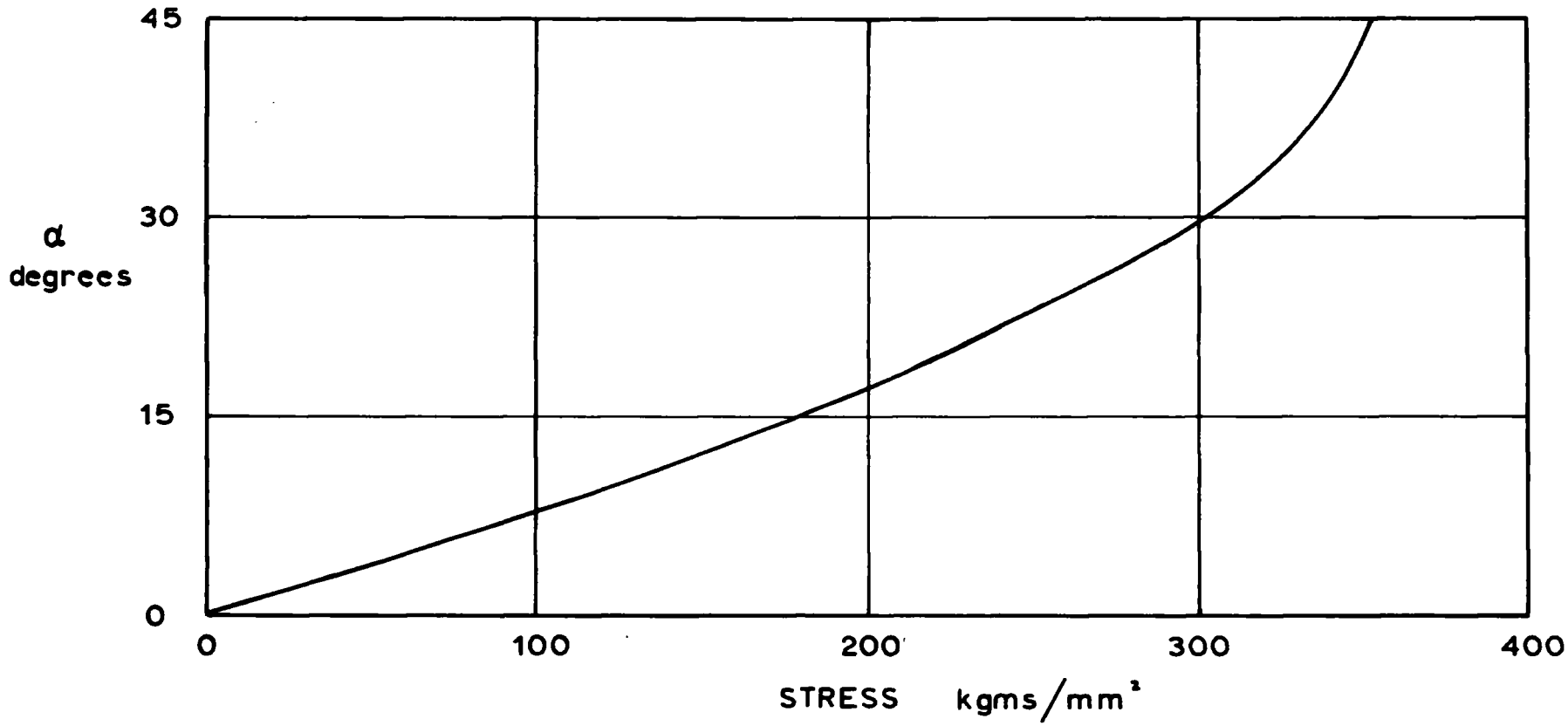

Variation of the easy direction with a compressive stress along a [110] direction

$\alpha = 0$ corresponds to the [100] direction

$\alpha = 45°$ corresponds to the [110] direction

FIG. 13

makes an angle α to the [100] direction in the (001) plane, the total energy can be expressed as

$$E_{TOT} = K_1 \cos^2\alpha \sin^2\alpha + \frac{3}{4}\sigma\lambda_{100} + \frac{3}{2}\sigma\lambda_{111}\cos\alpha\sin\alpha$$

Upon minimising this with respect to α, three roots are obtained

$$\sin\alpha = \cos\alpha = {}^{1}/\sqrt{2}$$

$$\text{and} \quad \sin\alpha\cos\alpha = \frac{-3\sigma\lambda_{111}}{4K}$$

The roots for $\alpha = 45^{\circ}$ give a maximum up to a stress of 351 kgms/mm^2 at which they become points of inflexion. Above this stress the [110] direction is a minimum. The easy directions are given by

$$\cos\alpha\sin\alpha = \frac{-3\sigma\lambda_{111}}{4K_1}$$

Fig. 13 shows the variation of the easy directions with stress. It is very interesting to note that they rotate into the stress direction as the stress is increased due to the fact that λ_{111} is negative. At stresses below the yield point this rotation is almost negligible, the maximum amount being 4°.

3.1.2. Experimental Technique

3.1.2.1. Direct Tension Method

The first attempt to strain polycrystalline specimens was made by directly loading the specimens with weights. One end of the specimen, 5 cms x 1 cm x 0.035 cms, was

clamped by means of screws to a block, fixed on the substage of the microscope, while the other end was similarly fixed in a movable block. This was connected to the weights by means of a steel wire running over a pulley. The height of the pulley was so arranged that while under tension the specimen was horizontal. The disadvantages of this system were the difficulty of applying high stresses and the uncertainty of the exact stress in the grain under investigation. As it was thought unwise to use specimen widths less than 0.75 cms due to spurious edge effects, loads of the order of 40 kgms only produced stresses of about 15 kgms/mm^2. At these loads the specimen tended to slip out of its holders, so that other attempts were made to anchor the specimens more firmly. None of the methods tried were very satisfactory for if they held the specimens securely they tended to create large unmeasureable stresses. The method used by Dijkstra and Martius, one of electrosparking holes in the specimens and applying the load through pins, was tried but found unsuccessful. The pins ripped out of the holes at fairly low stresses.

A micro-temsile test apparatus was kindly loaned by King's College Metallurgy Department. The springs in this machine were calibrated by stretching a uniform mild steel rod of 0.15 cm radius. The distance between two

scratches on the rod, just over 7 cms apart, was measured by means of a travelling microscope to an accuracy of 0.002 cms. By plotting the extension of the springs against the extension of the rod, and knowing the value of Young's modulus (20×10^{11} gynes/cm^2) for mild steel, a mean value of the force applied on stretching the spring a fixed amount could be worked out. This was 677 ± 35 kgms/cm. The specimens were gripped in taper jaws and had to be 20 cms long due to the unwieldly nature of the apparatus. They were cut as wide as possible, 2-3 cms, so as to include as many grains as possible. The grain size was much larger, 5-10 mms in diameter, than in the sheet used by Dijkstra and Martius in which grains were about 1 mm in diameter. The microscope was set up on the tensile machine. A grain was chosen near the centre of the strip with its [110] direction along the axis of tension. This was done by lining up the domain pattern with one part of a crosswire in the eyepiece, the other part having previously been lined up with the axis of tension. An accuracy of $\pm 1^{\circ}$ was obtained.

The sensitivity of the experiment was not very good. The travelling microscope could be read to only 0.005 cms as during the experiment there was not enough time to take a series of readings. This corresponded to 2 kgms

which works out, for the size of specimens mentioned above, to a stress of about 2 kgms/mm^2.

Magnetic fields were applied along the axis of the strip by means of a pair of Helmholtz coils 7 cms in diameter and each containing 300 turns of wire. Although it was not necessary to know the value of the applied field to a very high accuracy, $\pm$ 10 oersteds, the coils were calibrated by means of a fluxmeter and search coil. They gave a linear current/field relationship up to a field of 90 oersteds at 1 amp. A vertical field was applied by means of a small solenoid 3.5 cms in diameter, 1.2 cms deep, containing 300 turns. This was placed on the specimen, and the field on its surface was calculated to be 100 oersteds at 1 amp. The magnetic fields were used to help in the determination of magnetization directions for which purpose values between 10 and 20 oersted were usually necessary.

The results obtained from this method corresponded directly to those obtained by Dijkstra and Martius.

3.1.2.2. Bending Technique

There are two main disadvantages of the technique just described. The need for very long specimens virtually rules out single crystal work. Also the apparatus cannot be used for applying compressive forces. This is

necessary, for instance, when dealing with a single crystal having a (100) surface. The main domains are magnetized along the length of the specimen, the [001] direction, and the only method of rotating the magnetization into the other surface easy direction [100] , is by applying a compressive force, along the [001] direction.

The work on a (110) surface was repeated, using a bending technique to strain the specimens, to see in what way the presence of a stress gradient across the specimen affected the results.

Consider a strip of thickness t, clamped at one end, bent into an arc of radius r. If the central part of the strip is considered to be at zero stress then the change in length at the top surface equals

$$\frac{t}{2r}$$

If the vertical displacement of the end of the specimen is Δ, and the length of the specimen L then

$$\cos \frac{L}{r} = \frac{r-\Delta}{L}$$

As L/r is fairly small, $\cos L/r$ can be taken, to a fairly good approximation, to be

$$1 - \frac{(L/r)^2}{2}$$

And the strain $\frac{\Delta L}{L}$ in the surface layer is given by

$$\frac{\Delta L}{L} = \frac{t\Delta}{L^2} \qquad (3.1)$$

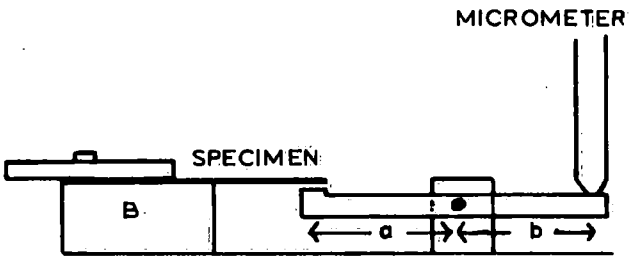

Bending apparatus

FIG. 14

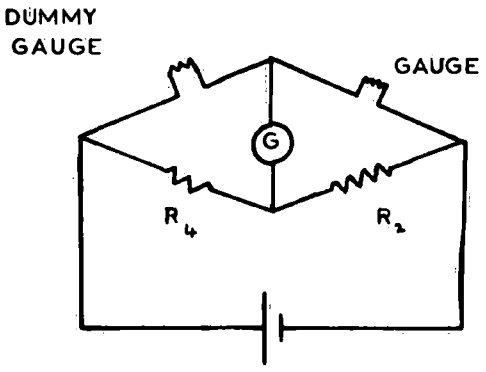

Strain gauge bridge

FIG. 15

As this strain applies to all the surface layer, a knowledge of the value of Young's modulus in any particular grain allows the stress in that grain to be evaluated. Benford (1946) obtained the following values of Young's modulus for various directions in a single crystal of 3.2% silicon iron. The units are dyne cm^{-2}.

$Y_{[100]}$ 1.30×10^{12} $Y_{[110]}$ 2.06×10^{12} $Y_{[111]}$ 2.81×10^{12}

For a specimen of thickness 0.035 cms and bending arm 2 cms, a stress of 30 kgms/mm^2 is produced with Δ = 2 mms. It was found possible to illuminate a specimen with L = 2 cms fairly evenly by adjusting the position of the light source up to values of Δ of 4 mms, so long as a high magnification (about 400x) was not used.

Fig. (14) shows the apparatus used. Specimens were compressed by a lever pivoted at its centre. Δ was calculated directly from tha micrometer deflection of the end of the lever as a = b. The block B, which held the specimen firmly, was movable so that the bending arm could be adjusted from 1.5 cms to 3 cms according to the sensitivity required. For applying extensional forces a lever pivoted at one end was used, with the ratio of the arms a:b=1:1.5. A spring at the end nearest the pivot kept the lever in constant contact with the micrometer.

In calculating the stress produced L was measured to an accuracy of 1 part in 500, while Δ, the micrometer reading, could be read to $^1/100$ mm. which corresponds to $^1/10$ kgm/mm^2 in the above example. The thickness t of the specimen was measured to an accuracy of about 1%. From these considerations the stress applied to the specimen could be obtained to an accuracy of 1-2%.

3.1.2.3. Strain Gauge Verification

The stresses in silicon iron strips, 5 cms x 1 cm x 0.033 cms, were checked with strain gauges. A surface of the specimen was roughened with 2/0 emery paper and a Tinsley Type 6E strain gauge, of 100 ohm resistance was stuck to it with 'Durofix'. The gauge was left for 3 days to dry thoroughly.

The resistance of the gauge was measured in a Wheatstone net, which also contained a dummy gauge to act as a temperature compensator (see Fig. 15). Even so the current was usually switched on half an hour or so before a reading was to be taken. The fixed resistance R_4 was taken as 9,900 ohms and the bridge balanced with R_2 to an accuracy of $^1/10$ ohm.

The relationship between the strain and the change of resistance of the gauge is given by

$$\frac{\Delta L}{L} = \frac{\delta R}{R} \, S$$

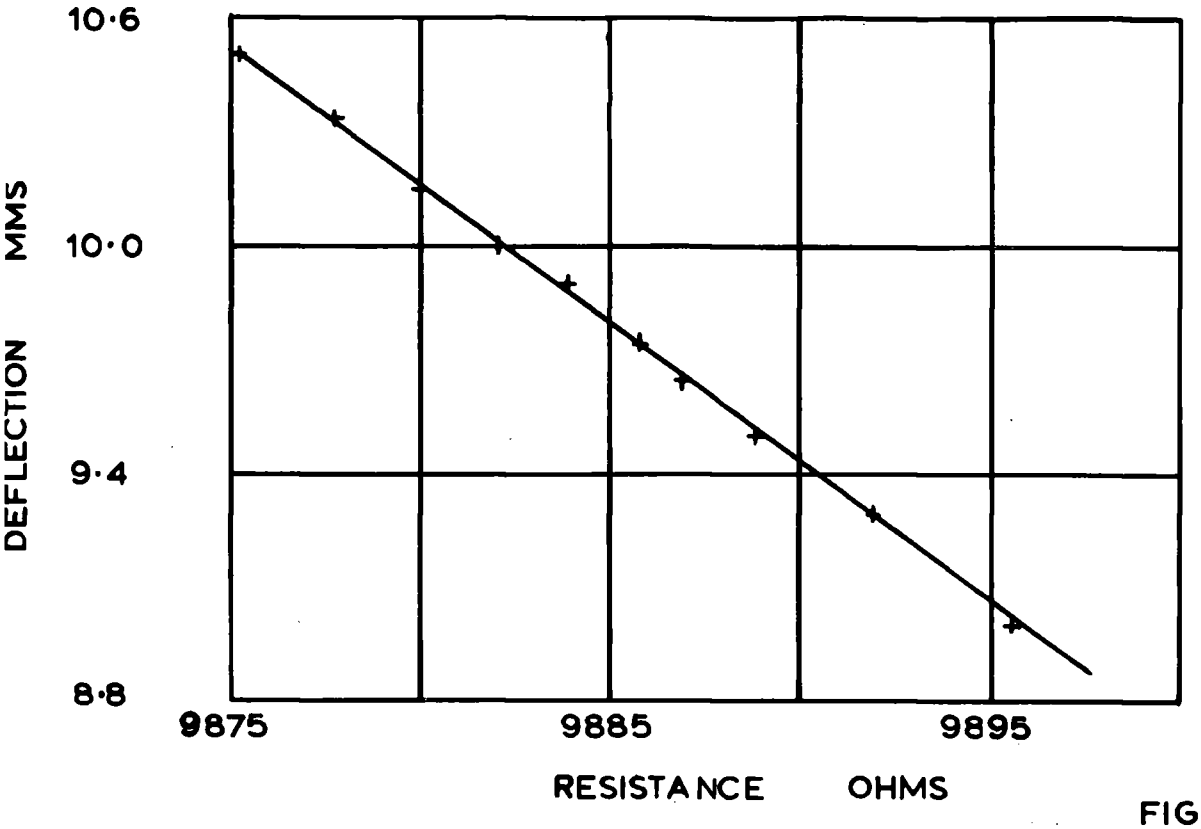

FIG. 16

Typical deflection resistance variation for fixed L

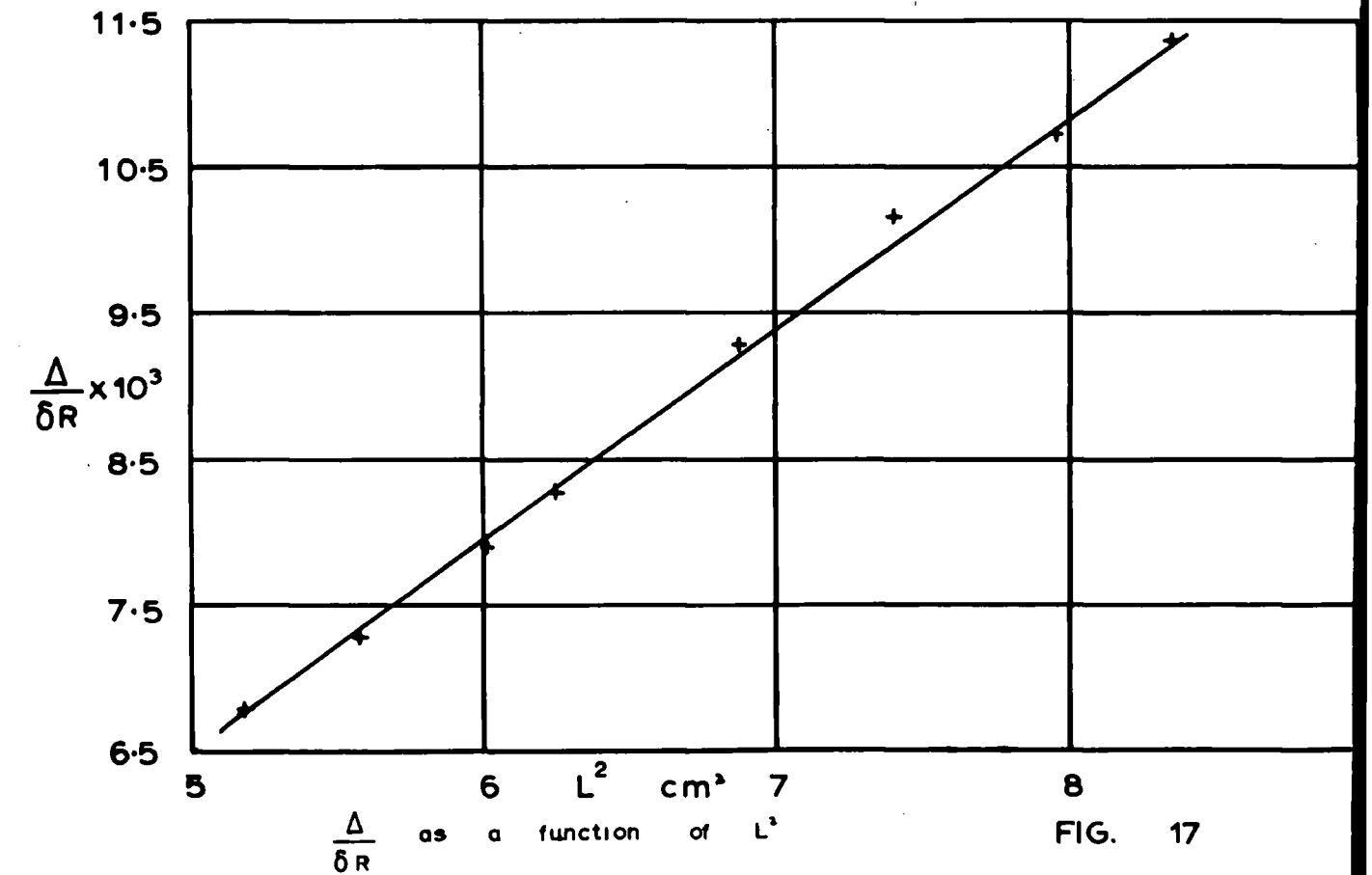

$\frac{\Delta}{\delta R}$ as a function of L^2

FIG. 17

where S is the gauge factor, 2.18 for the gauges used.

Using eq.(3.1), $$\frac{\Delta}{\delta R} = \frac{L^2}{t.R.S.} \qquad (3.2)$$

Fig. (16) shows a typical Δ, δR straight line graph for a specific value of L. Using the gradients of these graphs and plotting them against L^2 should give a straight line with gradient $^1/t.R.S.$ according to equation (3.2). The experimental values are shown in Fig. (17). The experimental value of the gradient is 1.45×10^{-3} while a theoretical value, using R = 9875 ohms, t = 0.033 cms and S = 2.18 gives 1.40×10^{-3}. Allowing for experimental error this shows that the method is quite suitable over the range of Δ's and L's used and that there was probably no sagging at the supports.

3.1.3. Experimental Results and Discussion

3.1.3.1. Zero Stress Pattern

The zero stress structure has been interpreted in section 1.4. The domain spacing is governed by the sum of the Bloch wall energy and the magnetostatic energy.

Graham (1957) considers the orientation of a 180° domain wall in such a system. If γ_o is the energy per unit area of a 180° wall with its normal in a [100] direction, then the total energy for unit surface area

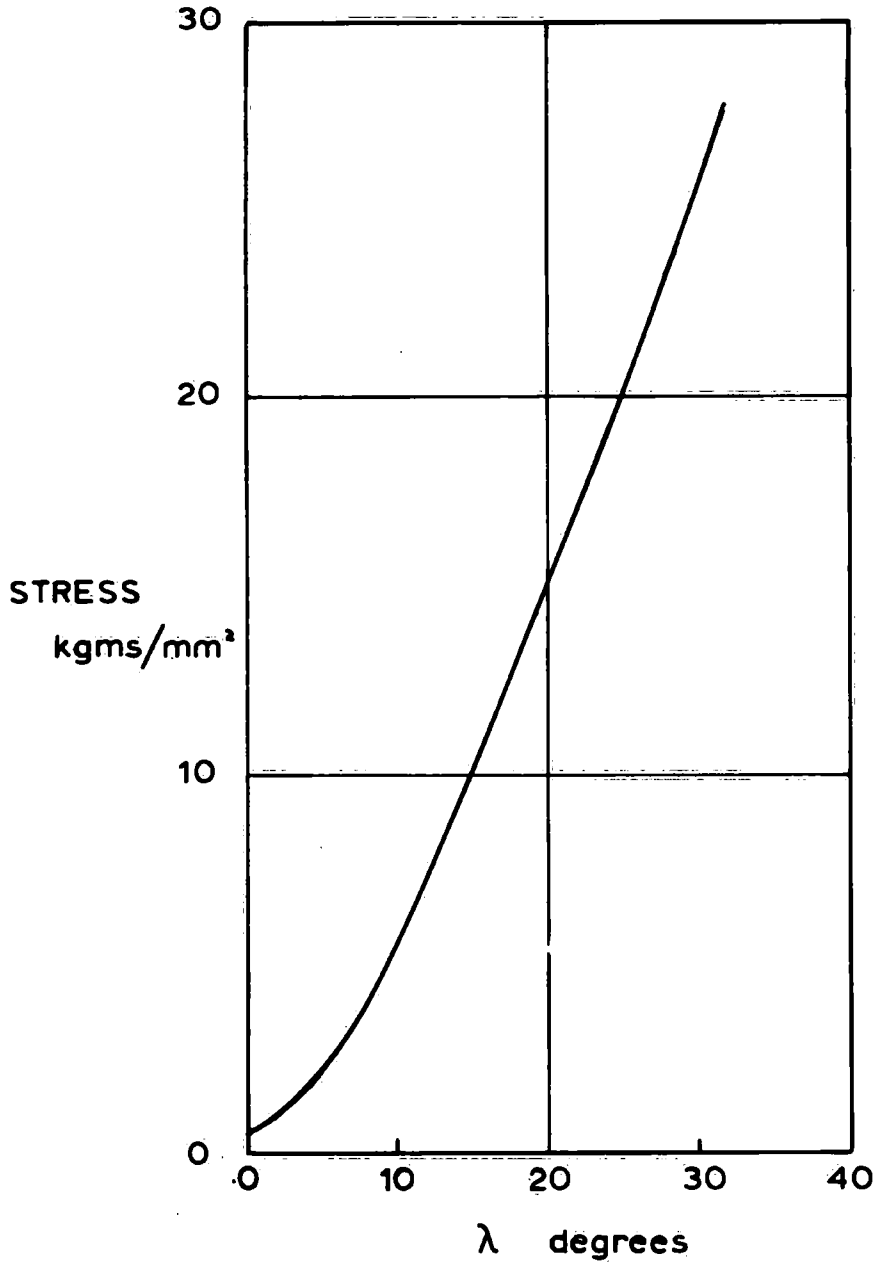

Variation of stress to make wall infinitely wide with λ

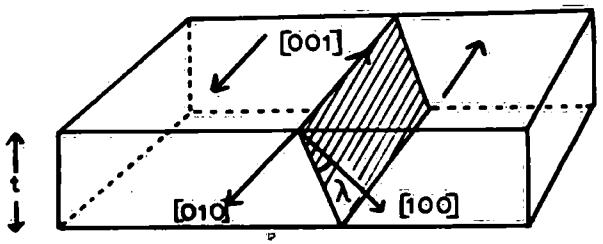

Minimum energy position of 180° wall in a (110) surfaced specimen defined by λ

FIG. 18

of specimen of this wall is $\gamma_o\sqrt{2}t$, where t is the thickness of the specimen. There is an energy minimum between this position and that where the normal to the wall is in a [110] direction and the total energy is $1.38\gamma_o t$. In his calculations, using the expression of Lilley for the wall energy, Graham ignores the terms containing K_2. This is because its value is not known at all accurately, see Tarasov (1939), and if its maximum value of 150×10^3 ergs/cc for pure iron is taken, the energy so produced only accounts for a few percent of the major term. The resulting expression shows a minimum for the Bloch wall energy at $\lambda = 13^o$, where λ is the angle between the wall and the [100] direction (Fig. 18). Graham tried to confirm this theory experimentally by examining two sides of a silicon iron (110) surfaced sheet. The results were not at all conclusive as there was no obvious correlation between the two domain patterns. He explained this by suggesting that the walls could bend from one minimum energy plane to another, giving a range of displacements from 0 to $t. \tan. 32^o$.

3.1.3.2. Transitional Range

When a tensional stress is applied along the [110] direction, the initial pattern starts to break up at

stresses between 0.7 and 1.5 kgms/mm^2. This is a gradual process, the stress at which it starts slightly varying from place to place in a single grain. It is followed by a transitional range, of about 1-2 kgms/mm^2, in which there is no visible domain structure after which stress pattern I starts to form.

The stresses at which the change over took place varied from specimen to specimen though always in the above stated range. Exactly the same range of values were obtained using tensional stresses by both direct pulling and bending.

It is possible that the original domain walls still exist in the transitional period and that the stray field at their intersection with the crystal surface is too weak to attract any magnetic colloid. In order to consider this possibility it is necessary to calculate the effect of stress on domain wall thicknesses.

The effect of stress on Bloch Wall Thickness

The effect of an externally applied stress σ dynes/cm^2 on the Bloch Wall thickness can be calculated by adding the strain components A'_{ij} so produced to those due to magnetostriction A_{ij}. As the effect of stress on domain wall thicknesses is an extension of the effect of magnetostriction we will firstly deal with the treatment

by Lilley of the latter effect.

Equation (1.8) can be written in terms of the strain components A_{ik} thus

$$E_{me} = -\frac{3(c_{11}-c_{12})\lambda_{100}}{2}\left[\alpha_1^2 A_{11} + \alpha_2^2 A_{22} + \alpha_3^2 A_{33}\right] - 3c_{44}2\lambda_{111}\left[\alpha_1\alpha_2 A_{12} + \alpha_1\alpha_3 A_{23} + \alpha_2\alpha_3 A_{31}\right] \quad (3.3)$$

where c_{ij} are the elastic compliances.

To this must be added the elastic part of the energy (Becker and Döring 1939 p. 146).

$$E = \frac{1}{2}C_1(A_{11}+A_{22}+A_{33})^2 + C_2(A_{11}^2+A_{22}^2+A_{33}^2) + 2C_3(A_{12}^2+A_{23}^2+A_{31}^2) \quad (3.4)$$

Under these zero stress conditions the values of A_{ik} can be obtained by minimising the sum of equations (3.3) and (3.4) with respect to A_{ik} giving

$$A_{ik} = \frac{3}{2}\lambda_{111}\alpha_i\alpha_k$$

$$A_{ii} = \frac{3}{2}\lambda_{100}\left[\alpha_i^2 - \frac{c_{12}}{2c_{44}+c_{11}}\right]$$

For a 180° boundary with the adjacent domains magnetized in the [001] and [00$\bar{1}$] directions, the magnetization direction in the wall is given by $(-\sin\lambda \sin\phi, \cos\lambda \sin\phi, \cos\phi)$ where the normal to the boundary is specified by $(-\cos\lambda, -\sin\lambda, 0)$.

Substituting the co-ordinate values for the magnetization in the Bloch wall in equations 3.3 and 3.4 and subtracting from this energy the energy of magnetization in the adjacent domains, the reduced magnetostriction energy term

$$\beta' f_m = \frac{9}{4}(c_{11}-c_{12})\lambda_{100}^2 \sin^2\phi \qquad (3.5)$$

is obtained. This is added to the crystalline anisotropy energy term $f_{an} = \sin^2\phi - \mu\sin^4\phi$

where $\mu = \frac{7+\cos 4\lambda}{8}$

The total anisotropy energy term, taking into account magnetostriction can now be expressed by

$$f_{an} = (1+\tau')(\sin^2\phi - \mu'\sin^4\phi) \qquad (3.6)$$

where $\mu' = \frac{\mu}{1+\tau'}$

and $\tau' = \frac{9}{4K}(c_{11}-c_{12})\lambda_{100}^2$

Using these expressions and equation (1.18) Lilley obtained

$$\frac{b}{b_0} = 2(1+\tau')^{-\frac{1}{2}}\left[\sinh^{-1}\left(\frac{2\mu'-1}{1-\mu'}\right)^{\frac{1}{2}} + 2\mu'^{\frac{1}{2}}\sin^{-1}\left(\frac{1}{2\mu'}\right)^{\frac{1}{2}}\right] \qquad (3.7)$$

In order to add the strain tensors due to the applied stress to those due to magnetostriction it is necessary to express the applied stress in terms of strain tensors A'_{ik}.

The general relationship between the strain components A_{ij} and the stress components $_{ij}$ is given by

$$A_{11} = s_{11}\Pi_{11} + s_{12}\Pi_{22} + s_{13}\Pi_{33} + s_{14}\Pi_{23} + s_{15}\Pi_{31} + s_{16}\Pi_{12}$$
$$A_{22} = s_{21}\Pi_{11} + s_{22}\Pi_{22} + s_{23}\Pi_{33} + s_{24}\Pi_{23} + s_{25}\Pi_{31} + s_{26}\Pi_{12}$$
$$A_{31} = s_{51}\Pi_{11} + s_{52}\Pi_{22} + s_{53}\Pi_{33} + s_{54}\Pi_{23} + s_{55}\Pi_{31} + s_{56}\Pi_{12}$$

Where S_{ij} are the stiffness constants.

For a cubic system the above expression reduces to the following matrix

$$S_{ij} = \begin{vmatrix} S_{11} & S_{12} & S_{12} & 0 & 0 & 0 \\ S_{12} & S_{11} & S_{12} & 0 & 0 & 0 \\ S_{12} & S_{12} & S_{11} & 0 & 0 & 0 \\ 0 & 0 & 0 & S_{44} & 0 & 0 \\ 0 & 0 & 0 & 0 & S_{44} & 0 \\ 0 & 0 & 0 & 0 & 0 & S_{44} \end{vmatrix}$$

For a tensional stress σ dynes/cm^2 in a direction specified by direction cosines $(\gamma_1, \gamma_2, \gamma_3)$ the strain components are given by

$$\begin{aligned} A'_{11} &= \sigma\left[s_{11}\gamma_1^2 + s_{12}(\gamma_2^2 + \gamma_3^2)\right] \\ A'_{22} &= \sigma\left[s_{11}\gamma_2^2 + s_{12}(\gamma_1^2 + \gamma_3^2)\right] \\ A'_{33} &= \sigma\left[s_{11}\gamma_3^2 + s_{12}(\gamma_2^2 + \gamma_1^2)\right] \\ A'_{12} &= \sigma\gamma_1\gamma_2 s_{44} \\ A'_{13} &= \sigma\gamma_1\gamma_3 s_{44} \\ A'_{23} &= \sigma\gamma_2\gamma_3 s_{44} \end{aligned} \qquad (3.8)$$

For cubic crystals the elastic constants c_{ij} are related to the stiffness constants S_{ij} by

$$S_{11} = \frac{c_{11} + c_{12}}{(c_{11} - c_{12})(c_{11} + 2c_{12})}$$

$$S_{12} = \frac{-c_{12}}{(c_{11} - c_{12})(c_{11} + 2c_{12})}$$

$$S_{44} = \frac{1}{c_{44}}$$

Now consider what effect an applied tensional force σ dynes/cm^2 along the [110] direction has on the domain walls in a [001] direction. The resulting strain components are

$$A_{11}' = A_{22}' = \frac{\sigma c_{11}}{2(c_{11} - c_{12})(c_{11} + 2c_{12})}$$

$$A_{33}' = \frac{-\sigma c_{12}}{(c_{11} - c_{12})(c_{12} + 2c_{12})}$$

$$A_{12}' = \frac{\sigma}{2c_{44}} \qquad A_{23}' = A_{31}' = 0$$

The strain components due to magnetostriction according to Lilley are

$$\begin{aligned} A_{12} &= A_{23} = A_{31} = 0 \\ A_{11} &= A_{22} = -\frac{3\lambda_{100} c_{12}}{2(2c_{12} + c_{11})} \\ A_{33} &= \frac{3\lambda_{100}(c_{12} + c_{11})}{2(2c_{12} + c_{11})} \end{aligned} \qquad (3.9)$$

Adding both strain components, the reduced anisotropy energy term becomes

$$f_m = \frac{\sin^2\phi}{K}\left[-\frac{3}{4}\lambda_{100}\left(\sigma - 3\lambda_{100}(c_{11} - c_{12})\right) + 3\sigma\lambda_{111}\sin\lambda\cos\lambda\right]$$

Therefore the effective wall thickness b/b_o can be calculated for various stresses and various wall orientations specified by λ. It is rather complex mathematically to evaluate the stress required to produce a given finite wall width for a given λ. Therefore consider the requirements for the wall to become infinitely thick. These are either

$$1 - \mu' = 0 \quad \text{or}$$

$$\tau' = -1$$

As the stresses needed to satisfy $\tau' = -1$ are much higher than those for $1 - \mu' = 0$, we shall deal with this latter relationship.

It becomes $\tau' = \mu - 1$, (3.10)

By solving equation (3.10) for various values of λ, a series of values of stress which make the wall infinitely wide are obtained. These values are shown in Fig. (19). It can be seen that this stress is 8 kgms/mm^2 for the equilibrium value, at zero stress, of the wall ($\lambda = 13^o$). The stress value only falls in the range 0.7 - 1.5 kgms/mm^2 for values of λ 0-3^o.

The minimum position of the wall has been worked out at a stress of 1 kgm/mm^2 and was found to lie at $\lambda = 12^o$. It therefore seems unlikely that this sort of mechanism can explain the disappearance of the Bloch wall in the

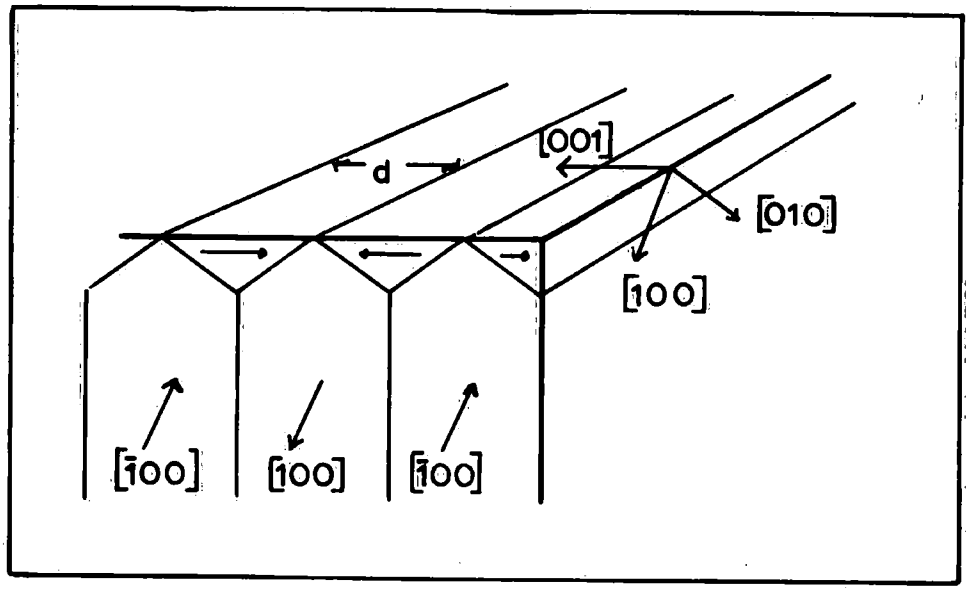

Block diagram of stress pattern I formed on a (110) surface

FIG. 20

transition range. Further information might be found out about this region by using a magneto-optical method for observing the domain structure.

3.1.3.3. Stress Pattern I

Similar observations to those of Dijkstra and Martius were recorded. A series of photographs (Plate I) show the development of these domains and also of the more complex pattern II. The previous workers showed that the surface structure is a closure structure magnetized in the [001] direction, with the main domains magnetized in the [100] directions (Fig. 20). This can be deduced from the fact that a vertical magnetic field of about 10 oersted polarizes the magnetic colloid and causes it to collect on alternate Bloch walls. As the stress is increased the wall spacing d decreases while the concentration of colloid at these walls increases. This latter fact was explained by Dijkstra and Martius as due to an opening up of the closure domains and consequently the appearance on the surface of strips of the main domains. This is probably not true. A similar occurrence on a (100) surface was explained by Chikazumi and Suzuki. They proposed that an increasing stress decreases the depth of the closure domains causing the normal component of the magnetization vector to vary across the wall. The pole density so

formed is proportional to the applied stress. Therefore the stray field at the wall increases with increasing stress.

Theoretical Considerations of Domain Structure

Dijkstra and Martius considered the effect of a tensional stress σ dynes/cm^2 on their proposed domain structure.

The energy per unit surface area of the zero stress structure can be expressed as

$$E'd_o + \frac{t\gamma}{d_o} \qquad (3.11)$$

Where $E'd_o$ is the magnetostatic energy term. A tensional stress along a [110] direction has no effect on the above terms.

The energy of the stress pattern I per unit surface area is

$$\left(\frac{t}{d} - \frac{1}{\sqrt{2}} + \sqrt{6}\right)\gamma + \frac{3}{4}\lambda_{100}\sigma\left(t - \frac{d}{2\sqrt{2}}\right) + E'd \qquad (3.12)$$

The magnetostatic energy term $E' = \left(\frac{1.7I^2\sin^2\delta 2}{1 + \mu^+}\right)$ is the same in equations (3.11) and (3.12) because the surface magnetizations in both cases are in the same direction, and consequently the deviation of the [001] direction from the surface, δ, is the same.

If equations (3.11) and (3.12) are each differentiated with respect to d_o and d respectively, both equilibrium spacings can be calculated as a function of stress. The zero stress pattern spacing is given by

$$d_o = \left(\frac{t\gamma}{E'}\right)^{\frac{1}{2}}$$

and is independent of stress.

The spacing in stress pattern I is given by

$$d = \sqrt{\frac{t\gamma}{E' + \frac{3}{8\sqrt{2}}\lambda_{100}\sigma}} \qquad (3.13)$$

If the values of d and d_o are substituted back into equation (3.11) and (3.12), and the two energies equated, the following relationship for the transitional stress σ_{crit} is obtained.

$$2[E't\gamma]^{\frac{1}{2}} = \left[\sqrt{6} - \frac{1}{\sqrt{2}}\right]\gamma - \frac{3}{4}\lambda_{100}t\sigma_{crit} + 2(t\gamma)^{\frac{1}{2}}\left[E' + \frac{3}{8\sqrt{2}}\lambda_{100}\sigma_{crit}\right]^{\frac{1}{2}}$$

Taking experimental values of t = 0.035 cms

I = 1608

γ = 1.3 dynes/cm

one obtains σ_{crit} = 0.05 kgms/mm^2 for $\delta = \frac{1}{2}^o$

and σ_{crit} = 0.04 kgms/mm^2 for $\delta = 1^o$.

The latter value compares directly with a theoretical value of 0.2 kgms/mm^2 derived by Dijkstra and Martius. The experimental values obtained are 10 times larger than the theoretical values.

If $1/d^2$ is plotted against σ (from equation 3.13) a linear relationship should be obtained, if γ is independent of stress, with a gradient given by $\frac{3}{8\sqrt{2}} \frac{\gamma_{100}}{t\gamma}$. The intercept on the σ axis is given by $\frac{-E' 8\sqrt{2}}{3\lambda_{100}}$.

The effect of a compressive stress σ dynes/cm^2 applied along the [001] direction gives similar results to the case studied above. Once again a stress pattern takes over from the zero stress pattern as the stress is increased. The energy of the first system is given by

$$E'd_0 + \frac{t\gamma}{d_0} + \frac{3}{2} t\sigma\lambda_{100}$$

and that of the second by

$$E'd + \left(\frac{t}{d} - \frac{1}{\sqrt{2}} + \sqrt{6}\right)\gamma + \frac{3}{2}\sigma\lambda_{100}\frac{d}{2\sqrt{2}}$$

The relationship obtained for the equilibrium spacing of the stress pattern I is

$$d = \sqrt{\frac{t\gamma}{E' + 3\lambda_{100}\sigma/4\sqrt{2}}} \qquad (3.14)$$

This differs from equation (3.13) by only a factor of 2 in the stress term.

Effect of stress on the main domain walls

Consider the effect of a tensional force σ dynes/cm^2 acting along the [101] direction on the main Bloch wall of stress pattern I. If the adjacent domains are considered to be magnetized along the [001], [00$\bar{1}$] directions then the normal to the wall is in a [010] direction.

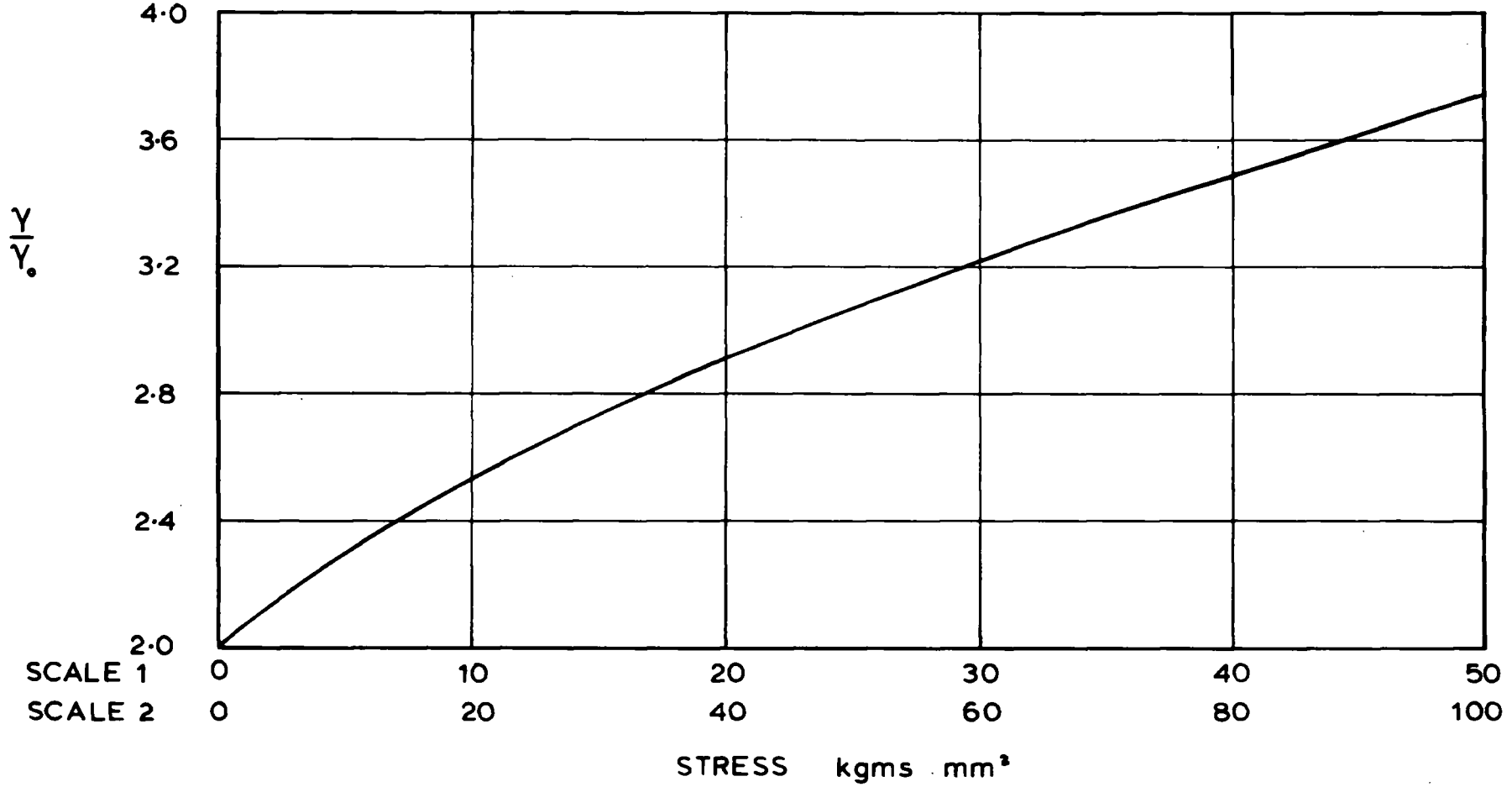

Scale 1 corresponds to a reduced anisotropy energy for the wall energy of $\frac{3}{4}\lambda_{100}\sin^2\phi\left[3\lambda_{100}(c_{11}-c_{12})+2\sigma\right]$

and scale 2 to $\frac{3}{4}\lambda_{100}\sin^2\phi\left[3\lambda\ (c_{11}-c_{12})+\sigma\right]$.

FIG. 21

The strain tensors are given by

$$A_{11}' = A_{33}' = \frac{\sigma c_{11}}{2(c_{11}-c_{12})(c_{11}+2c_{12})}$$

$$A_{22}' = \frac{-\sigma c_{12}}{(c_{11}-c_{12})(c_{11}+2c_{12})} \qquad A_{13}' = \frac{\sigma}{2c_{44}}$$

and $$A_{21}' = A_{23}' = 0$$

Using the same method as described before, the reduced anisotropy energy becomes

$$\beta' f_m = +\frac{3}{4}\lambda_{100}\sin^2\phi\left[\sigma + 3\lambda_{100}(c_{11}-c_{12})\right]$$

As $\lambda = 0$ for the wall under consideration, the wall energy is given by (Lilley 1950)

$$\frac{\gamma}{\gamma_0} = 2\left[(1+\tau')^{\frac{1}{2}} + \tau'\sinh^{-1}(\tau'^{-\frac{1}{2}})\right]$$

where γ_0 is the energy of a 90° wall with its normal in a [001] direction. The relationship between γ/γ_0 and σ is shown in Fig. (21). A similar relationship can be calculated when is a compressive stress acting in a [010] direction. In this case the strain components are

$$A_{11}' = \frac{c_{12}\sigma}{(c_{11}-c_{12})(c_{11}+2c_{12})}$$

$$A_{22}' = \frac{-\sigma(c_{11}+c_{12})}{(c_{11}-c_{12})(c_{11}+2c_{12})}$$

$$A_{33}' = \frac{c_{12}\sigma}{(c_{11}-c_{12})(c_{11}+2c_{12})}$$

$$A_{12}' = A_{13}' = A_{23}' = 0$$

This gives $$\beta' f_m = +\frac{3}{4}\lambda_{100}\sin^2\phi\left[3\lambda_{100}(c_{11}-c_{12}) + 2\sigma\right]$$

The $\gamma/\gamma_0, \sigma$ relationship obtained from this is also shown in Fig. (21).

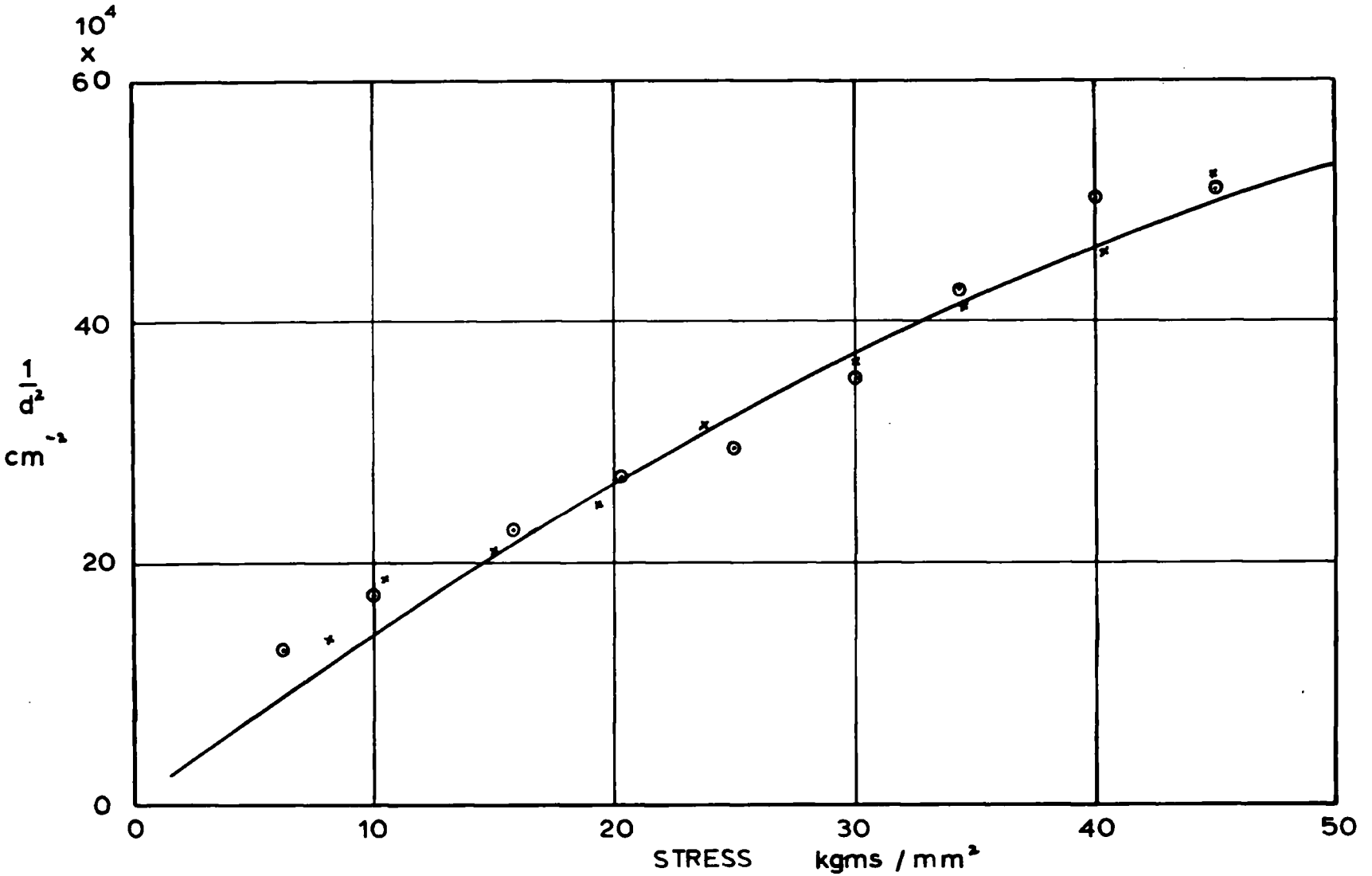

Variation of pattern I spacing with a tensional stress in a [100] direction

⊙ Tensional pull

x Tension applied by bending

FIG. 22

Results

Dijkstra and Martius fitted their experimental results with a straight line graph of gradient 1.5×10^{-4} (See Fig. 23). They did not state the thickness of the specimen, except as an order of magnitude, but by taking $\delta = 0.032$ cms $\gamma = 1.35$ ergs/cm^2 and substituting in equation (3.13) the value of the gradient becomes 1.66×10^{-4}. Their experimental points did not fit the straight line relationship very well as there appeared a marked kink in the graph at about 30 kgms/mm^2. The intercept on the stress axis is +16 kgms/mm^2. The theoretical intercept is given by $\sigma = \frac{-E' 8\sqrt{2}}{3\lambda_{100}}$, which for an angle of 1° degree between the [001] direction and the surface works out to -0.08 kgms/mm^2 and for an angle of $\frac{1}{2}^\circ$ to -0.02 kgms/mm^2. From their stress free pattern it can be seen that the inclination must be of this order of size as the surface is free from closure domains.

The variation of +16 kgm/mm^2 and -0.1 kgms/mm^2 between experiment and theory suggests some inaccuracies in their experiment. Fig. (22) shows a typical $^1/d^2$ σ relationship obtained by applying a tensional stress along the [110] direction. The points seem to fit quite well the curve drawn with a gradient

$$\frac{3\lambda_{100}}{8\sqrt{2}t\gamma_{\sigma=0}}$$

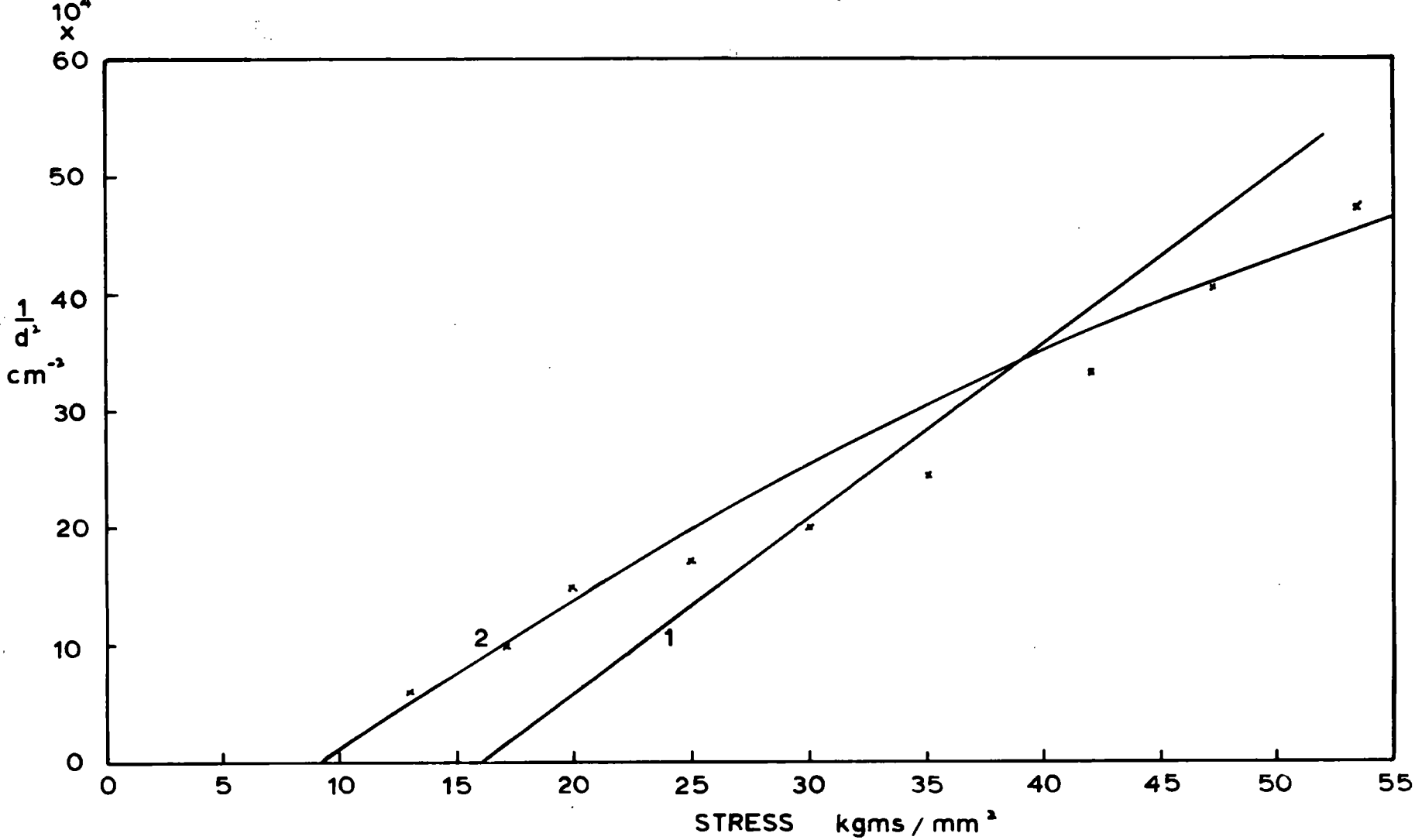

Change in line spacing d with stress.

x Experimental results } Dijkstra and Martius (1953) 2 Present calculations

1 Theoretical curve }

FIG. 23

where c is a multiplying factor for the wall energy and is a function of stress. $\gamma_{\sigma=0}$ is the value of the wall energy at zero stress. The experimental values for this particular curve are t = 0.032 cms $\lambda = 27 \times 10^{-6}$ and $\gamma_{\sigma=0} = 1.35$ ergs/cm^2. If E' is a function of stress, which will be discussed later, it will have a negligible effect on the shape of the curve. It had been hoped to correlate the intercept on the stress axis, which is proportional to E', with d_o, the stress free domain spacing but the error involved in extrapolating the curved graph, and the very small values of intercepts, made the errors far too large. A fairly large range of intercepts for different specimens was found, varying from -3 kgms/mm^2 to +5 kgms/mm^2. This was probably due to differing amounts of residual stress in the specimens.

For comparison a theoretical graph, taking into account the variation of wall energy with stress, is superimposed on the experimental points of Dijkstra and Martius (see Fig. 23). By taking the same zero stress gradient, and an intercept of +9 kgms/mm^2 a better fit is obtained than with the straight line relationship.

Also shown on Fig. (22) are the experimental points obtained by applying a tensional stress along the [110] direction by bending the specimen. They give the same $1/d^2$, σ relationship as obtained with a tensional pull,

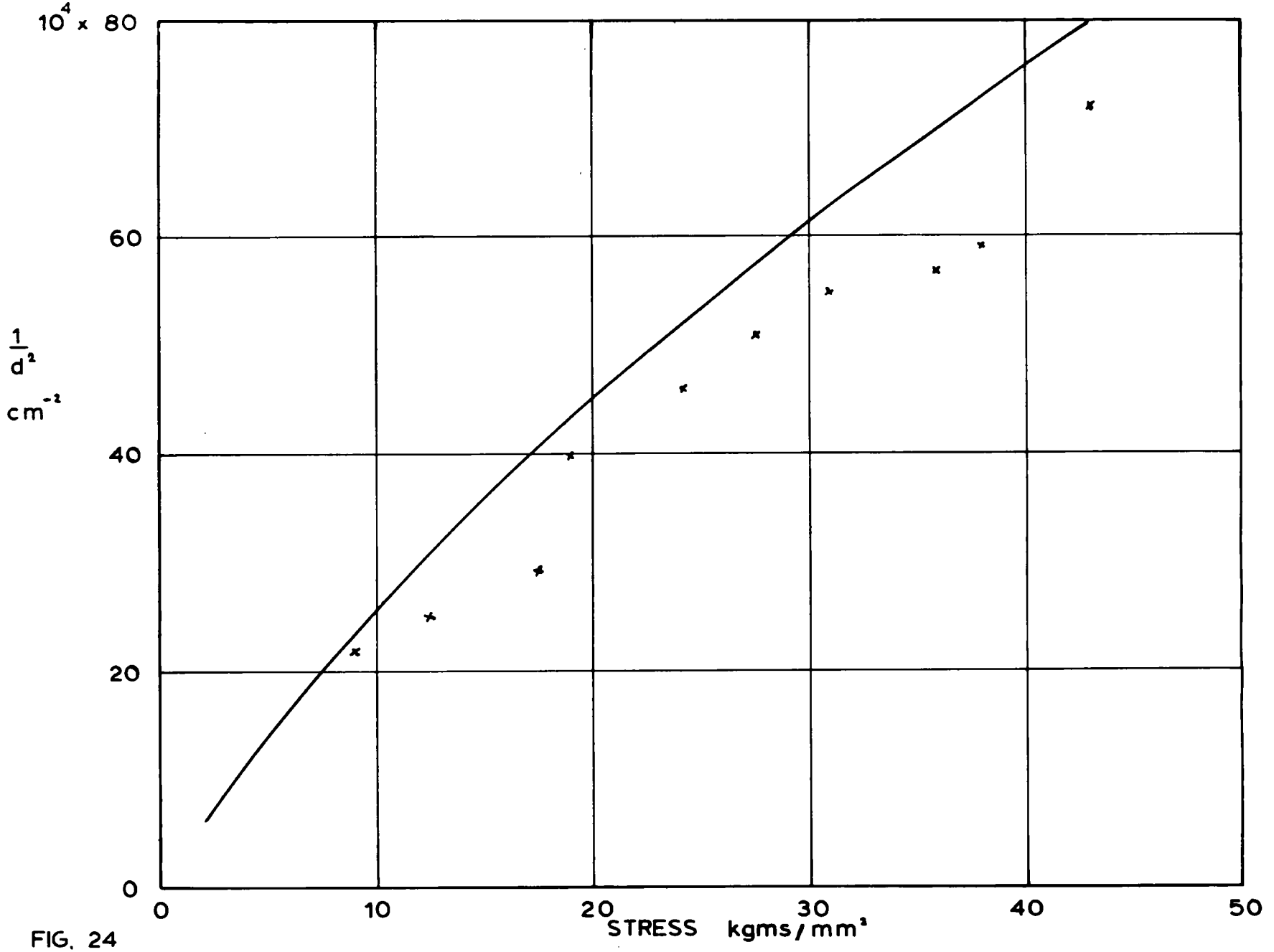

FIG. 24

Variation of pattern I spacing d with a compressive stress σ along the [001] direction. The theoretical line shown has an intercept of 0 kgms/mm².

allowing for experimental errors. As the results on stress pattern I are identical in both cases it seems that this bending technique will give useful results when applied to other specimens.

Fig. (24) shows results obtained by compressing the specimen, by bending, along a [001] direction. In the example shown, the points are fitted with a curve of gradient $3\lambda_{100}/4\sqrt{2}tc\gamma_{\sigma=0}$ and intercept $\sigma=0$ kgms/mm^2. The fit would have been much better had the points been fitted with a curve of intercept $\sigma = 3$ kgms/mm^2. Again intercepts in the range -1 to +3 kgms/mm^2 were obtained with different specimens.

Chain structure

A fact not observed by Dijkstra and Martius was the growth of a chain structure on the surface of the specimen along the walls of stress pattern I. Photographs of this structure are shown in Plate 2. A typical growth sequence is described below.

Stress 28 kgms/mm^2:- Small elliptically shaped domains, length $\sim 1/10$d, formed, seemingly at random, along the walls by the splitting of the wall.

Stress 31 kgms/mm^2:- These have grown to a length of about d with a corresponding increase in width.

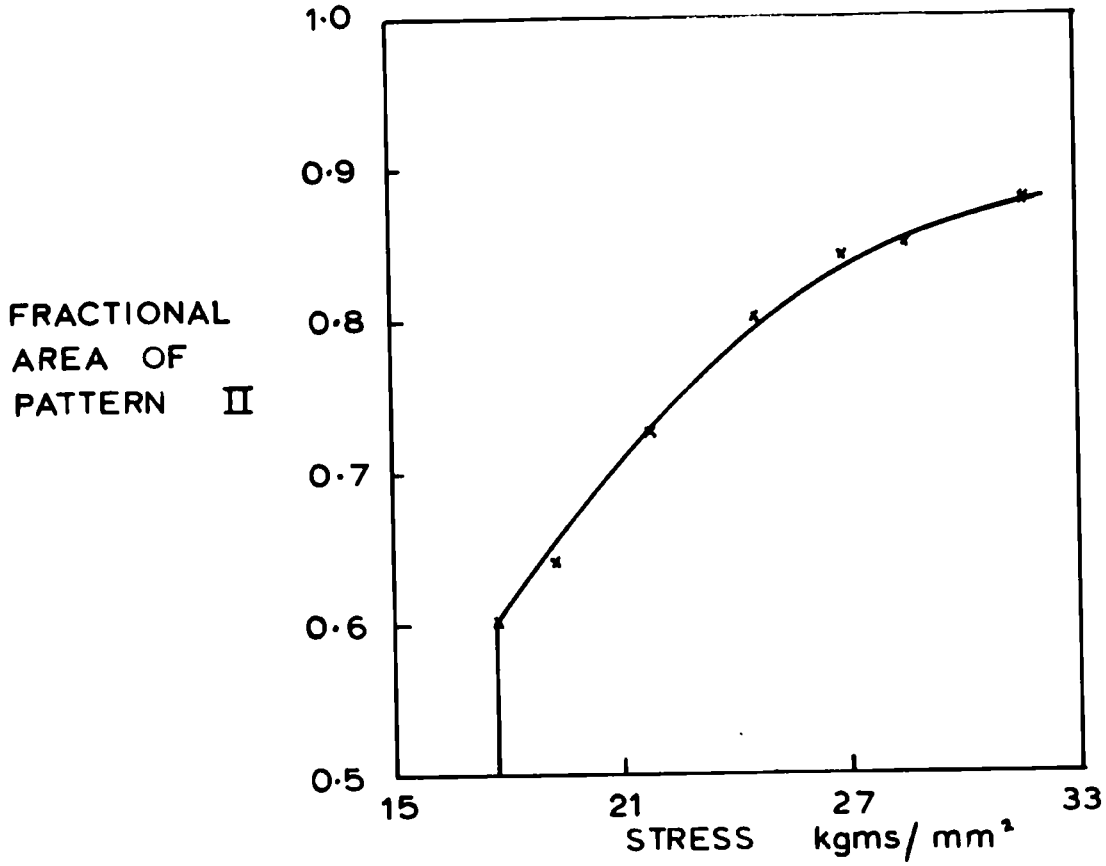

Variation of area of pattern II with stress

FIG. 26

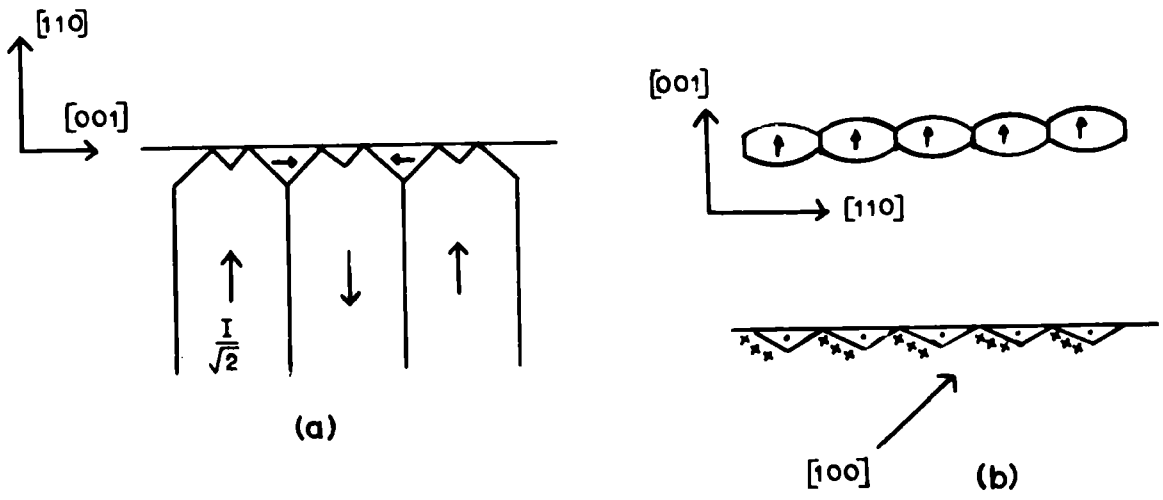

Suggested chain structure on strained (110) surface

FIG. 25

Stress 35 kgms/mm^2:- The number of links has increased until there is no straight wall left, just a continuous chain structure. At this stress, each link is still elliptically shaped.

Stress 37 kgms/mm^2:- up to the yield point:- the links have become barrel shaped, being up to $d/4$ in width and d-2d in length.

If a vertical field was applied, alternate chains disappeared indicating that Fig. (25a) is probably a reasonably good representation of the facts. As no colloid was polarized over the surface of the chain under the influence of a vertical field, the direction of magnetization must lie in the surface of the specimen. An attempt to discover the magnetization direction using the scratch technique proved unsatisfactory. Colloid was not attracted to scratches running in either the [001] or [110] direction. The conclusion that they are small demagnetized regions must be excluded from simple energy considerations. It seems probable that they are regions magnetized in [001] and [00$\bar{1}$] directions, the reduction in closure domain volume energy being sufficient to compensate the formation of free poles on their undersurface (Fig. 25b). These structures did not form on all examples of stress pattern I.

It is interesting to compare this structure with the one observed by Bates and Hart (1956) on a (110) surface of silicon iron. A structure the same as stress pattern I was observed on a single crystal of silicon iron, measuring 1.25 cms x 0.58 cms x 0.025 cms with a field of 10 oersteds applied along the [110] surface direction. This field favours the [100] and [010] easy directions. At a field of about 30 oersteds the domain walls at the surface broadened and assumed a chain like appearance. A further increase in field caused the chains to become wider and at this stage they appear, from photographs, to be the same as those observed on the strained specimen.

However Bates and Hart suggested that the chain structure was formed by the shrinking of the closure domains, due to an increase in the magnetic field, and therefore the appearance of strips of free poles between the closure domains. This indicates that the chains are in fact magnetized along the [100] direction, which is not the case for those observed on the strained specimens.

3.1.3.4. Stress Pattern II

At tensional stresses in the range 20-30 kgms/mm^2 and compressive stresses between 13-20 kgms/mm^2 a second type of domain structure developed. This was called

stress pattern II. Once formed it grew at the expense of pattern I with increasing stress, until at stresses nearing the yield point it covered nearly the whole of the surface, Fig. (26) shows the percentage area of pattern II as a function of stress for a typical specimen.

The structure consists of main zig-zag walls, with a spacing between 1.5 and 2 times that of stress pattern I, running in a [001] direction. A vertical field caused alternate main walls to disappear (see plate 3) while a field in a [110] direction caused alternate areas between these walls to increase and decrease in size. This suggests that the main underlying domains are magnetized in the [100] and [$\bar{1}$00] directions, as in stress pattern I, but separated by 180^{o} walls with normals in the [010] direction.

Between these main walls lies a complicated surface structure. Under a high magnification this was seen to consist of alternately wide and narrow domains at an angle β. to the [110] direction. The spacing of these subsidiary domains varied across the main domains. A vertical field caused alternate walls to disappear indicating that they are probably small closure domains underneath which is a domain structure alternately magnetized up and down.

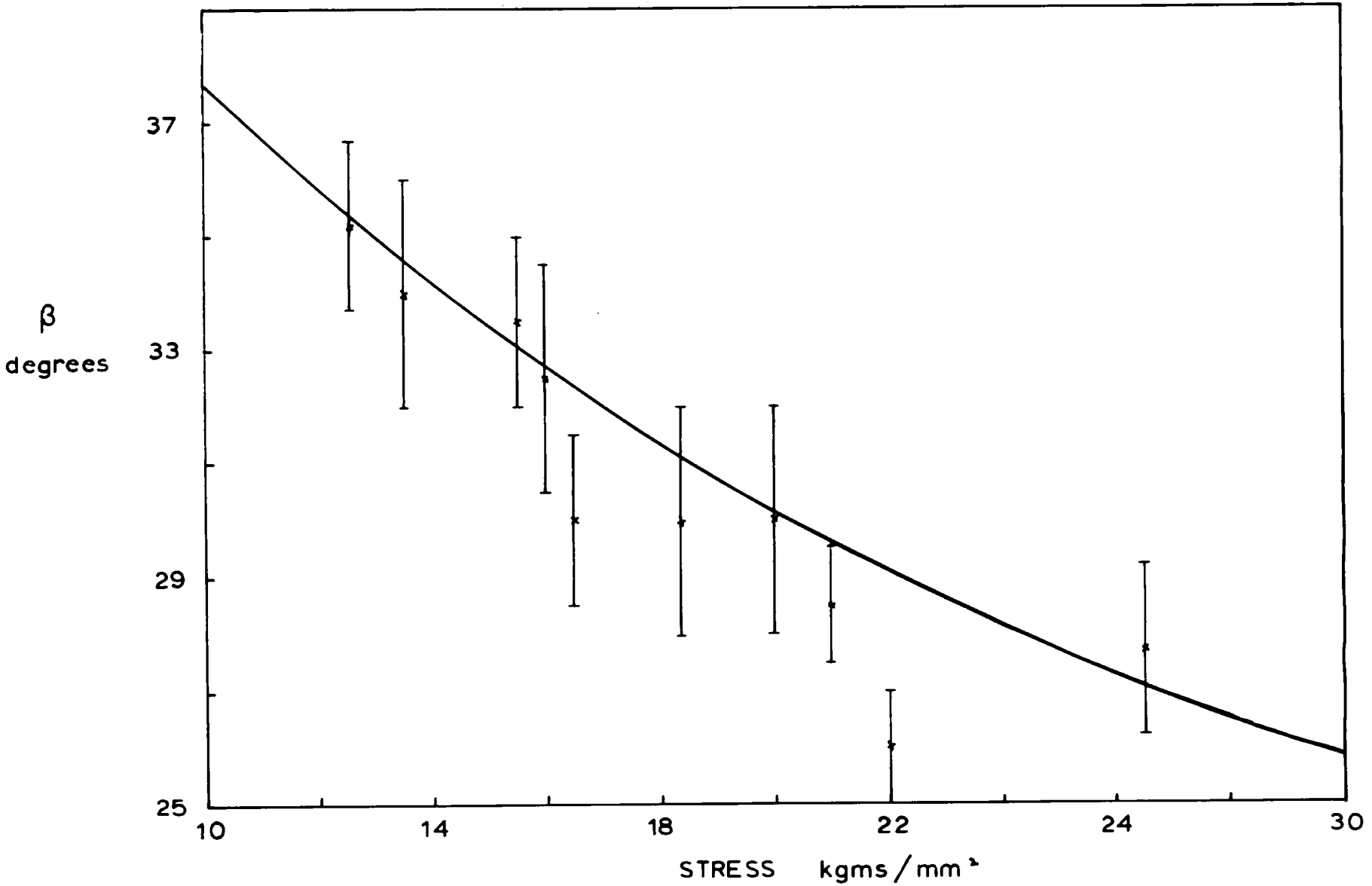

Stress pattern II, variation of β with stress. The full line is the theoretical relationship. Also shown is the standard deviation on each point.

FIG. 27

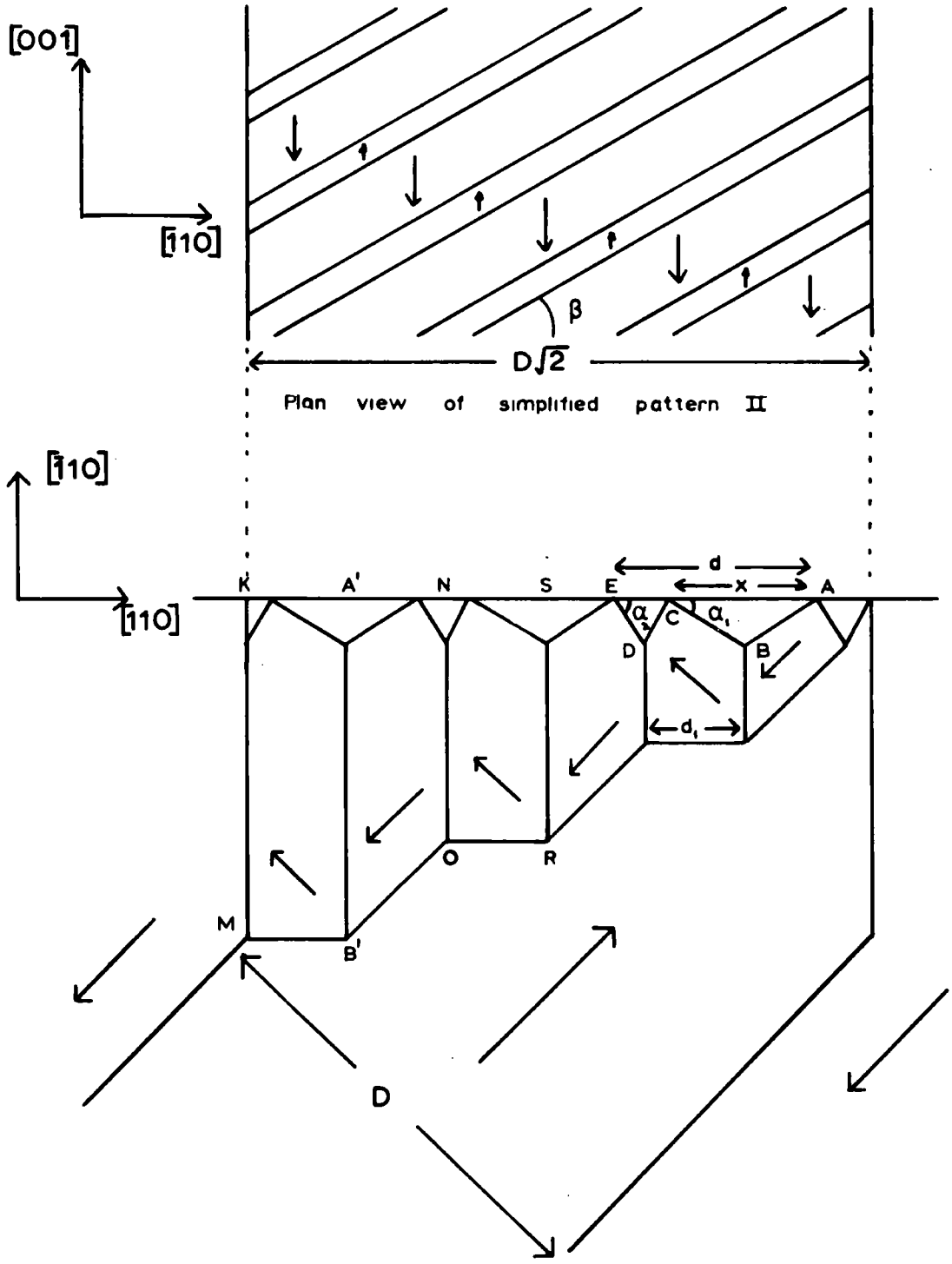
[001]
[110]
β
D√2
Plan view of simplified pattern II
[1̄10]
[110]
K
A'
N
S
E
d
x
A
α
C
α1
D
B
d1
O
R
M
B'
D
Section normal to the surface in a [110] direction

FIG. 28

Upon increasing the stress β was found to decrease as shown in Fig. (27).

Proposed Closure Structure

The proposed structure for the closure domains is shown in Fig. (28). It is similar to that described by Martin (1957). He examined the surface structure on a (100) surface of silicon iron in the form of a flat disc. The edges of the disc were of the (0,k,) family. By this means he was able to observe directly the structure beneath a (111) face. He found that near the edge of the disc the main 180° wall structure branched into what he called an echelon structure, which nearer the surface subdivided again. The similarity between the two systems, one where there is no easy direction in the surface, and the other where the easy surface direction is made unfavourable by applied stresses is obvious.

As a model for the theoretical analysis of this type of structure a simplified echelon system will be considered in which the spacing of the secondary structure is constant in width across the main domain and the angle to the [110] direction is only β and not β and 90°-β.

In order that there are no free poles on the wall ABCD the values of α_1 and α_2 must be related to β by

$$\tan \alpha_2 = \frac{\sin \beta}{\sqrt{2} \cos \beta - \sin \beta}$$

and $$\tan \alpha_1 = \frac{\sin \beta}{\sqrt{2} \cos \beta + \sin \beta}$$

The volume of the closure domains, for unit width of domain is $\frac{x^2}{4} \tan \alpha_1 + \left(\frac{d-x}{4}\right)^2 \tan \alpha_2$

If this is minimised with respect to x, one obtains

$$\frac{x}{d-x} = \frac{\tan \alpha_2}{\tan \alpha_1}$$

which becomes in terms of β

$$\frac{x}{d-x} = \frac{\sin \beta + \sqrt{2} \cos \beta}{\sqrt{2} \cos \beta - \sin \beta}$$

If an experimentally observed value of $\beta = 30^\circ$ is taken, the ratio $\frac{x}{d-x}$ becomes 2.5. This agrees well with a measured value of 3.

A further simplification, the assumption that the wall energy γ is independent of stress is made in a consideration of the energy of the system.

The total energy is made up of the Bloch wall energy and the magnetoelastic energy, the magnetostatic energy being zero.

The total length of walls KM + $\dot{A}\dot{B}$ + NO for the system is given by $L = 2 \sum_{i=1}^{i=n/2} i$

$$= \frac{D}{\sqrt{2}} \left(\frac{D}{2d_1} + 1 \right)$$

And the wall energy of KM, AB etc per unit surface area is

$$\frac{\gamma}{2 \sin \beta} \left(\frac{a}{2d_1} + 1 \right) \qquad (3.15)$$

The length of walls ABCDE can be approximately expressed by

$$\frac{3\gamma}{2 \sin \beta}$$

Domains like KA'MB', NSOR, ... magnetized at right angles to the bulk magnetization, therefore contribute an amount of elastic energy given by $\frac{1}{2} C_{11} \lambda_{100}^2$ per unit volume

$$\text{Volume} = d_1^2 \sum_{i=1}^{i=n/2} i$$

$$\text{and the energy} = \frac{1}{2} c_{11} \lambda_{100}^2 \frac{D d_1}{2\sqrt{2}} \left[\frac{D}{\sqrt{2} d_1} + 1\right] \qquad (3.16)$$

A compressive stress σ dynes/cm^2 in the [001] direction acts on the surface closure domains.

$$\text{The volume of these} = \frac{d}{4} \frac{\tan\alpha_1 \tan\alpha_2}{\tan\alpha_1 + \tan\alpha_2}$$

Therefore the stress energy

$$= \frac{3d}{16\sqrt{2}} \lambda_{100} \sigma \tan \beta$$

Substituting $2d_1 = d$ and $a = D\sqrt{2}$ in equation (3.15) and (3.16) the total energy of the system becomes

$$E = \frac{3d}{16\sqrt{2}} \lambda_{100} \sigma \tan\beta + \frac{1}{\sin\beta}\left[\frac{3\gamma}{2} + \frac{\gamma}{2}\left(\frac{a}{d} + 1\right)\right] + \frac{1}{2} c_{11} \lambda_{100}^2 \frac{a}{8}\left[\frac{a}{d} + 1\right] \qquad (3.17)$$

Minimising the total energy with respect to β gives

$$\frac{\sin^2\beta}{\cos^3\beta} = \frac{16\sqrt{2}}{3 d \lambda_{100} \sigma}\left[\frac{3\gamma}{2} + \frac{\gamma}{2}\left(\frac{a}{d} + 1\right)\right] \qquad (3.18)$$

By substituting experimental values of d and a/d into equation (3.18) a theoretical curve is obtained relating β and σ, see Fig. (27). Even though the a/d is taken as

a mean value, the curve agrees quite well with the experimental points.

If the total energy is minimised with respect to d another relationship is obtained

$$\frac{3}{16\sqrt{2}}\lambda_{100}\sigma\tan\beta = \frac{1}{d^2}\left[\frac{1}{16}c_{44}\lambda_{100}^2 a^3 + \frac{\gamma a}{2\sin\beta}\right] \qquad (3.19)$$

As it is extremely difficult to eliminate β between these equations, the result may be tested numerically by substituting

$$\beta = 30^{\circ}$$

$$\sigma = 20 \text{ kgms/mm}^2$$

$$\text{and } a = 6 \times 10^{-3} \text{ cms.}$$

in equation (3.19). This gives a value of $d = 6.2 \times 10^{-4}$ cms, therefore $a/d = 10$. The observed value was $a/d = 5$.

Change-Over from Pattern I to Pattern II

Although this closure structure fits the experimental results well, it does not explain why it should be more favourable at high stresses than the stress model I.

Section 3.1.3.3. shows how the main domain wall energies in the stress model I increase with tensional and compressive stresses. Now consider the effect of stress on the main domain walls of stress pattern II.

If the domains are considered to be magnetized in [001], [00$\bar{1}$] directions, the wall normal will be in the [010] direction and the stress co-ordinates for an exten-

sional stress σ dynes/cm^2 will be [011] .

The reduced anisotropy energy for this system is

$$\beta' f_m = \frac{9}{4}(c_{11}-c_{12})\lambda_{100}^2 \sin^2\phi - 3|\lambda_m|\sigma \sin\phi\cos\phi$$

Unfortunately the sin ϕ cos ϕ term makes the integration, necessary to obtain the wall energy, too difficult. Nevertheless it can be seen that this energy will decrease with increasing stress. If it is supposed that the change over between the two patterns depends only on the energies of the main wall structures then this critical energy would be expressed by $\sqrt{2}\gamma_{II} = \gamma_I$. If the energy of wall II is taken as constant this corresponds to a stress of 38 kgms/mm^2 (Fig. 21). The value is probably less than this as the energy of wall II decreases and so compares favourably with the experimental values of 20-30 kgms/mm^2.

Using this supposition the changeover stress when the the system is under a compressive stress σ dynes/cm^2 in a [100] direction can be evaluated. The strain components in wall II are

$$A_{11}' = -\frac{\sigma(c_{11}+c_{12})}{(c_{11}-c_{12})(c_{11}+2c_{12})}$$

$$A_{22}' = A_{33}' = \frac{c_{12}\sigma}{(c_{11}-c_{12})(c_{11}+2c_{12})}$$

$$A_{31}' = A_{23}' = A_{31}' = 0$$

This gives a value of the reduced anisotropy of

$$\beta' f_m = \frac{9}{4}(c_{11}-c_{12})\lambda_{100}^2 \sin^2\phi$$

which is independent of stress.

A more exact value of the change-over stress can now be calculated. From Fig. (21) a value of 19 kgms/mm^2 is obtained. As the experimental values lay between 13-20 kgms/mm^2 it seems likely that this mechanism contributes a major term in the evaluation of the change-over stress.

3.2. Tensional Stresses along the [100] direction

3.2.1. The surface a (110) plane to within one degree

Introduction

The strain free surface is characterised by 180° Bloch walls in a [100] direction. A tensional stress is applied along the magnetization direction making it more energetically favourable than the other easy directions.

Dijkstra, Martius, Chalmers and Cavanagh (1954) applied such stresses up to the yield point on polycrystalline silicon iron and found no change in structure whereas Shur and Zaikova (1958) found that stresses greater than 10 kgms/mm^2 caused a reduction in the domain spacing. They did not make any measurements of domain width against stress.

Results

This work was repeated using a bending technique for applying the tensional stresses. Stresses up to the yield point appeared to have no effect on the domain

structure. Slight changes of structure occurred near inclusions and other surface imperfections but the main spacing remained unchanged.

Theoretical Considerations

The domain spacing d is given by

$$d = \left(\frac{t\gamma}{E'}\right)^{\frac{1}{2}} \qquad (3.20)$$

where $E' = 1.7I^2\sin^2\delta \frac{2}{1+\mu^+}$

The effect of stress on the components of equation (3.20) will be considered.

Wall Energy

As the surface of the specimen makes an angle of one degree or less with the [001] direction the stress will be considered to act along the [001] direction.

The strain tensors produced by a stress of σ dynes/cm^2 are

$$A'_{11} = A'_{22} = \frac{-c_{12}\sigma}{(c_{11}-c_{12})(c_{11}+2c_{12})}$$

$$A'_{33} = \frac{\sigma(c_{11}+c_{12})}{(c_{11}-c_{12})(c_{11}+2c_{12})}$$

$$A'_{12} = A'_{23} = A'_{31} = 0$$

This gives an expression for the reduced anisotropy of

$$\tau' = \frac{3\lambda_{100}}{4K_1}\left[3\lambda_{100}(c_{11}-c_{12}) + 2\sigma\right]$$

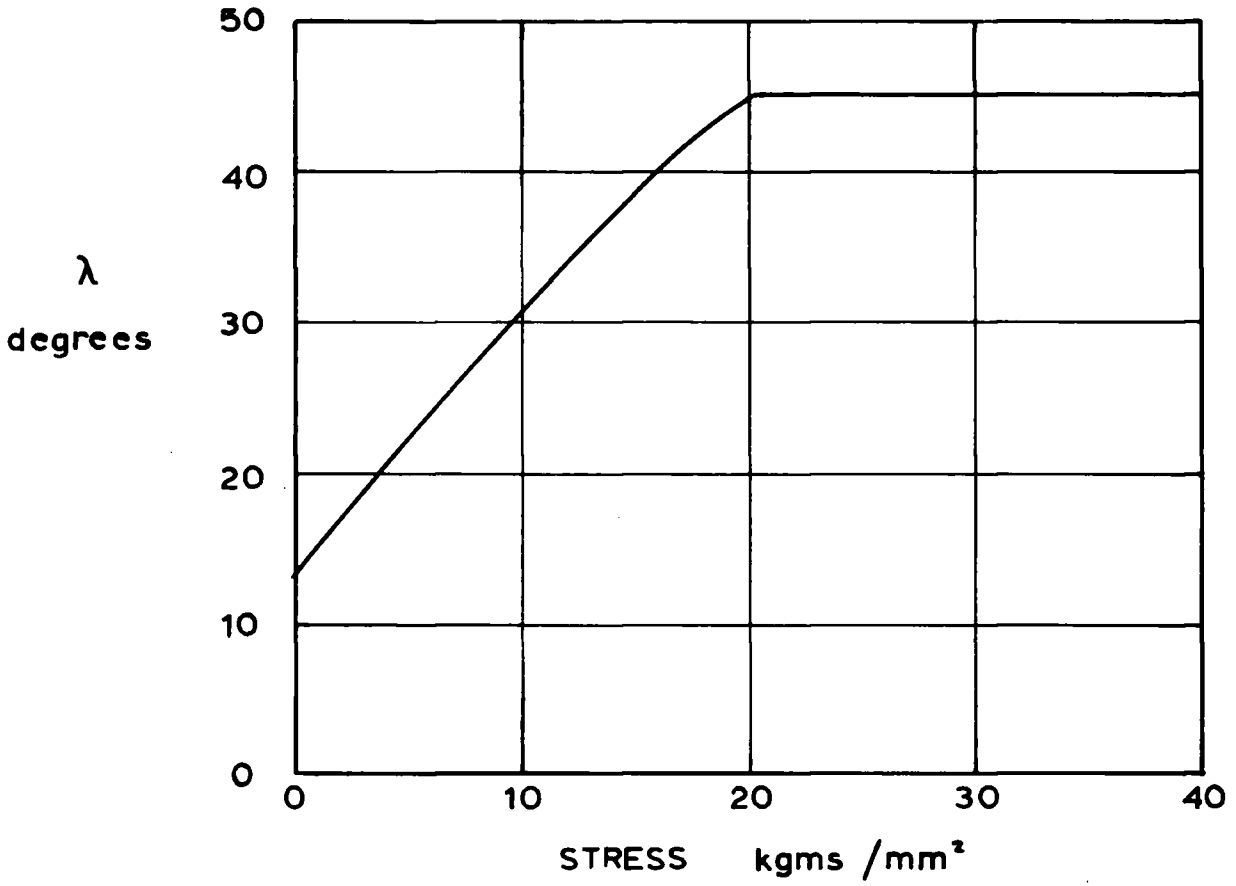

Effect of stress on λ, the minimum energy position of a 180° wall

FIG. 29

A graph of the variation of wall energy with stress for $\lambda=0$ is shown in Fig. (21). If this is approximated by a straight line through the origin, the wall energy γ at a stress of σ kgms/mm^2 can be related to the energy $\gamma_{\sigma=0}$ at zero stress by

$$\gamma = \gamma_{\sigma=0} \left[1 + 0.018\sigma\right]$$

If the wall energy is calculated for various stresses and various values of λ, using equation (1.17) and then multiplied by a factor $\frac{1}{\cos(45-\lambda)}$, to take into account the thickness of the wall, the value of λ corresponding to the minimum effective wall energy can be calculated as a function of stress. This is shown in Fig. (29). With increasing stress the wall rotates away from the (100) plane until at a stress of 20 kgms/mm^2 it lies in the (110) plane. Therefore the increase in effective wall energy will not be as large as shown in Fig. (21).

For example at zero stress $\lambda = 13^\circ$ and

$$\frac{\gamma_{eff}}{\gamma_{\sigma=0}} = 2.634$$

while at 10 kgms/mm^2 $\lambda = 31^\circ$ and

$$\frac{\gamma_{eff}}{\gamma_{\sigma=0}} = 3.125$$

If the change in d was dependent on the wall energy alone then

$$\frac{d_{\sigma=10}}{d_{\sigma=0}} = \sqrt{\frac{3.125}{2.634}}$$
$$= 1.09$$

At $\sigma = 40$ kgms/mm^2 this fraction is 1.21.

One would therefore expect the wall energy to increase by the amount shown above.

Magnetostatic Energy

As δ, the angle between the [001] direction and the surface, has been considered to tend to zero, the stress cannot have any effect on the effective permeability or δ. One would therefore expect the domain spacing to increase slightly with stress due to the increase in wall energy.

However in this case, when δ tends to zero, the magnetostatic energy probably depends upon free poles formed at the grain boundary. Therefore the orientation of the surrounding grains and the effect of stress on them may well be important.

In order that the domain spacing remains constant the magnetostatic energy must increase at the same rate.

3.2.2. Surface a few degress off a (110) plane

Introduction

When the [001] direction makes an angle of between 3 and 4 degrees with the surface a system of closure domains are formed on the surface to reduce magnetostatic energy. This closure structure consists of dagger like domains magnetized along the $[00\bar{1}]$ direction in a main domain magnetized in a [001] direction. In order that there are no free poles on the main part of the dagger

structure, the walls should lie at equal angles to the [110] direction and therefore intersect along a [001] line. The angle λ which these walls make with the [100] and [010] directions will be governed by the minimum energy orientation of a 180^{o} wall. This has been shown at zero stress to be 13^{o}.

A series of photographs (plate 4) shows the effect of stress on this structure. As the stress increases the daggers become smaller in both length and width and the main 180^{o} walls become more distinct. At a stress of about 20 kgms/cm^2 the dagger structure disappears altogether. A small vertical field, applied at this stress, polarizes the colloid over alternate domains showing that the magnetization vectors still make an angle with the surface.

Shur and Zaikova (1958) observed these changes and on purely qualitative grounds, as they did not apply vertical fields to ascertain the magnetization direction, suggested that the disappearance of closure domains was due to the rotation of the magnetization vectors into the surface.

Theoretical Considerations

Equation 1.10 shows that for isotropic magnetostriction the stress energy is given by

$$E_{\sigma} = -\frac{3}{2}\,\sigma\lambda\,\cos^{2}\theta$$

where θ is the angle between the stress and magnetization directions. If this is minimised with respect to θ, it gives the limiting direction into which the magnetization direction rotates when the stress energy is much larger than the anisotropy energy. This is $\theta=0$.

The more general case when $\lambda_{111} \neq \lambda_{100}$ will now be considered. The magnetization direction cosines are $\left(\cos\alpha, \frac{\sin\alpha}{\sqrt{2}}, \frac{\sin\alpha}{\sqrt{2}}\right)$ and the direction cosines of the stress are $\left(\cos\gamma, \frac{\sin\gamma}{\sqrt{2}}, \frac{\sin\gamma}{\sqrt{2}}\right)$.

The differential of the energy with respect to α gives

$$\sin\alpha\cos\alpha\sin^2\gamma(\lambda_{100}+\lambda_{111}) - 2\cos\alpha\sin\alpha\cos^2\gamma\lambda_{100} + 2\lambda_{111}\cos\gamma\sin\gamma(\cos^2\alpha-\sin^2\alpha) = 0$$

If the $\sin^2\gamma$ term is neglected the equation becomes

$$\frac{1}{2}\lambda_{100}\cos\gamma\sin 2\alpha = \lambda_{111}\sin\gamma\cos 2\alpha$$

$$\text{and} \qquad \tan 2\alpha = \tan\gamma \frac{2\lambda_{111}}{\lambda_{100}} \qquad (3.21)$$

This equation corresponds to a position of minimum energy. Substituting into equation 3.21

$$\lambda_{111} = -5 \times 10^{-6}$$

$$\lambda_{100} = +27 \times 10^{-6}$$

$$\text{and} \quad \gamma = 5^{\circ}$$

gives the result $\alpha = -1^{\circ}\ 50'$

The limit to which the magnetization tends at high stresses is $1^{\circ}\ 50'$ away from the easy direction, and the surface direction.

Effect of Stress on effective permeability

The method used is that due to Kittel (1949). If the magnetization vector makes an angle ϕ with the [001] direction the anisotropy energy can be written

$$E_{an} = K\phi^2$$

Similarly, neglecting the effect of λ_{111}, the magneto-elastic energy is given by

$$E_{\sigma} = -\frac{3}{2}\sigma\ \lambda_{100}(1 + \alpha^2\phi^2)$$

where α is direction of stress.

The energy due to a small field H, applied normal to the surface

$$E_H = HI\phi$$

Minimising the total energy with respect to ϕ gives

$$\phi = \frac{HIs}{2K - 3\lambda_{100}\sigma\alpha^2}$$

This gives a susceptibility

$$\psi = \frac{Is^2}{2K - 3\lambda_{100}\sigma\alpha^2}$$

and an effective permeability

$$\mu = 1 + \frac{4\Pi Is^2}{2K - 3\lambda_{100}\sigma\alpha^2}$$

For the stress term to have any effect on the anisotropy term σ must be about 10^4 kgms/mm^2.

Therefore up to 20 kgms/mm^2 the stress has a negligible effect on the effective permeability.

Conclusion

It has therefore been shown that the cause of the disappearance of the dagger structure is not due to a reduction of the magnetostatic energy by either the rotation of the magnetization vector into the surface or by an increase in the effective permeability.

The important factor must be the rotation of the position of minimum energy of the 180^{o} wall, specified by λ, as shown in Fig. 29. At zero stress the reduction of magnetostatic energy, due to the formation of daggers must be balanced by the wall energy of these structures. As the stress increases the value of λ increases, thus increasing the area of Bloch wall for a specific surface area of dagger. Also the energy of the wall per unit area increases. The wall energy will now be greater than the reduction of magnetostatic energy and so the size of the dagger must decrease to restore the energy balance.

At a stress of 20 $kgms/mm^2$ the dagger walls should be normal to the surface, and therefore would not contribute any reduction in the magnetostatic energy. Therefore one would expect the daggers to disappear at this stress. This agrees very well with the observed value.

CHAPTER FOUR

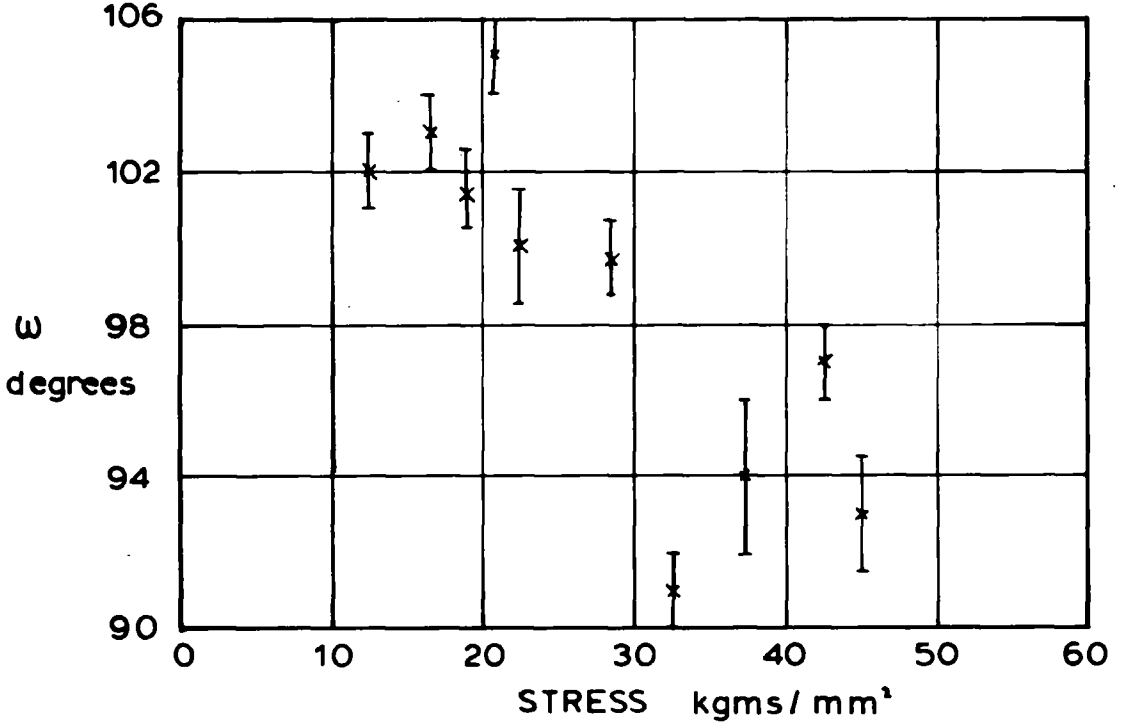

Variation of zig zag angle with stress in a [011] direction

FIG. 32

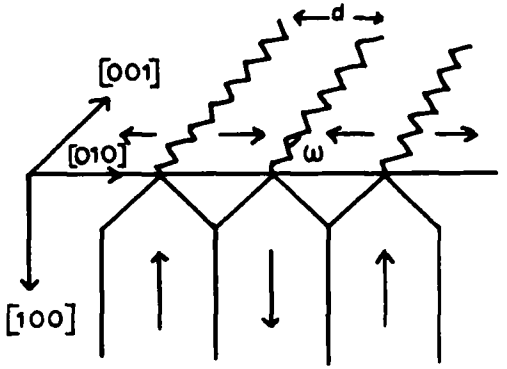

Block diagram of zig zag structure

FIG. 30

CHAPTER FOUR

THE EFFECT OF EXTERNAL STRESSES UP TO THE YIELD POINT ON (100) SURFACES

4.1. A compressive stress applied along the [011] direction on a (100) surface.

4.1.1. Introduction

A compressive force applied in the [011] surface direction, as shown in section 3.1.1.1. will make the easy [100] direction normal to the surface more favourable energetically than the two easy directions lying in the surface. It is therefore equivalent, in these respects, to a tensional force in the [100] direction. This system has been considered by Chikazumi and Suzuki (1955). The structure formed under this stress consists of main domains magnetized normal to the surface, the flux being closed by triangular domains magnetized in one of the surface easy directions, see Fig. 30. The Bloch wall of the closure domains is shown to be zig-zag in nature. This is because the only requirement for no free poles to form on the wall is that the normal to the wall should lie in the (110) plane. As the wall energy is a function of orientation the wall will lie in its minimum energy position. This position corresponds to an angle of $\psi = 62^{\circ}$ (Fig. 4), where 2ψ is the angle between adjacent strips of zig-zag surface. The minimum $\psi = 62^{\circ}$ is equiva-

lent to $\omega = 106^{\circ}$, ω being the observed zig-zag angle at the surface.

Chikazumi and Suzuki applied this model and its variation with changing stress to the maze structure formed on a mechanically polished surface and to the strain pattern produced by a deep scratch in a [001] direction on a (100) surface. In neither case were they able to verify quantitatively their experimental considerations.

4.1.2. Experimental Details

Single crystals of silicon iron were prepared in strips 4 cm x 1 cm x 0.032 cm with the main (100) surface plane bounded by edges in the [011] directions. This is known as the Néel cut. The specimens were compressed along the [011] direction, or the [$0\bar{1}1$] direction using the bending technique. It was possible to repeat this work on polycrystalline material as a piece of 3% silicon iron cube textured sheet, with average grain diameter of about 5 mms and thickness 0.032 cms, was obtained from the General Electric Company, U.S.A. This was cut into specimens of approximately the same size and shape as the single crystals.

4.1.3. Results

The results obtained from the single crystal work were rather disappointing. The zero stress structure was not the same as that described by Néel, being much more complex, probably due to the presence of random stresses in the material. Upon applying a compressional force along the [011] direction this pattern disappeared at about 15 kgms/mm^2 and after a short transitional range of stress the strain pattern as described by Chikazumi and Suzuki appeared. Unfortunately the structure was not at all regular and relationships between $^1/d^2$ (d being the domain spacing) and stress or between ω and stress could not be obtained. The patterns appeared very much like those obtained by Kaczer (1958) by applying a compressive force of cylindrical symmetry to a single crystal of 4% silicon iron cut in a cylindrical shape 1 cm long and 8 mms in diameter. He found that the zig-zag structure appeared at about 10 kgms/mm^2, which must be multiplied by $\sqrt{2}$ to compare directly with the result obtained in the above experiment i.e. 17 kgms/mm^2.

However very good results were obtained upon straining the polycrystalline silicon iron specimens. Plate 5 shows a typical series of photographs taken at various stages of stress.

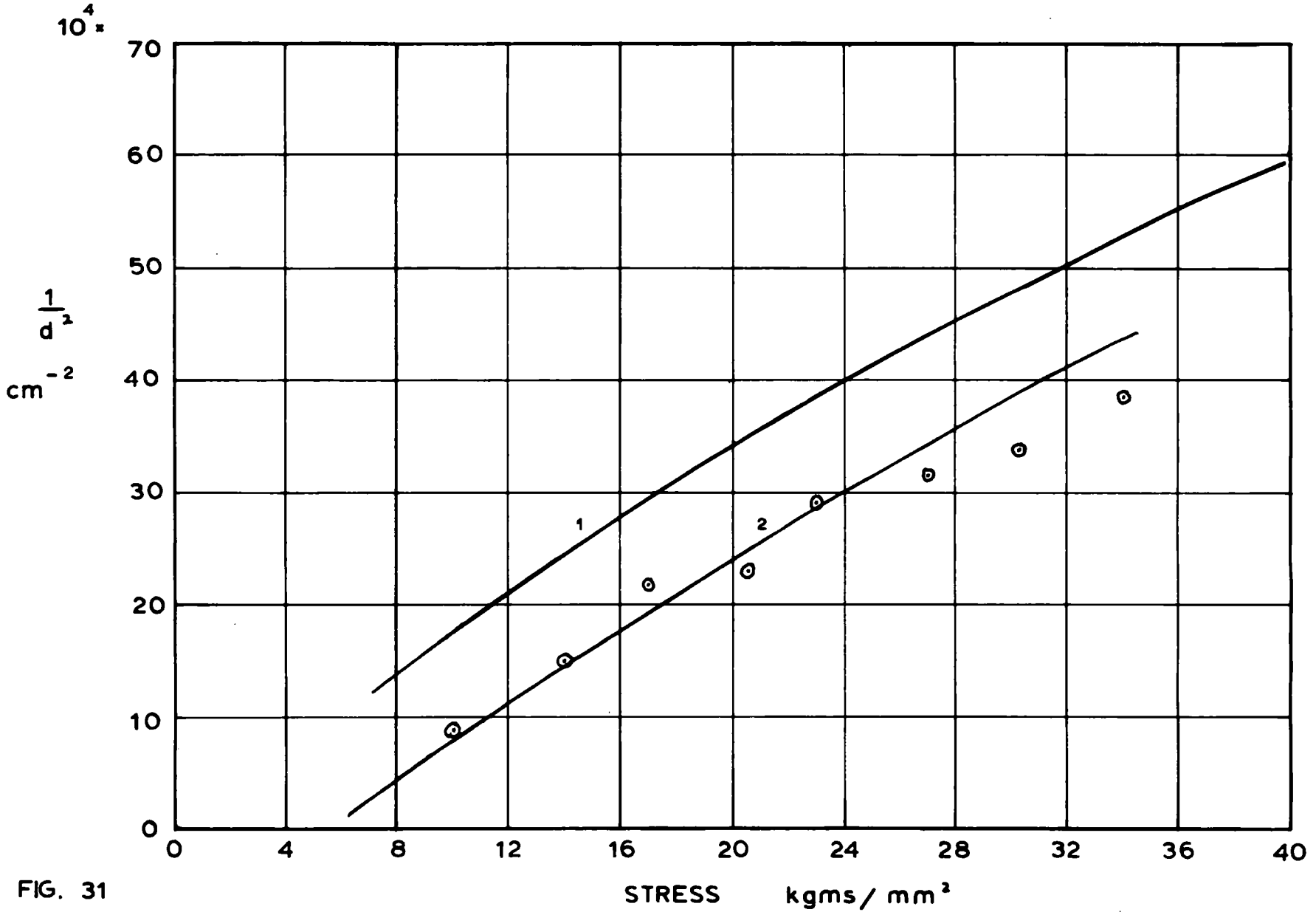

FIG. 31

Theoretical and experimental variations of the domain spacing with stress on a (100) surface. The gradient of the theoretical curve 1, with intecept 0 kgm/mm^2, is virtually the same as that of a line 2 through the experimental points.

At a stress of about 1 kgm/mm^2 the initial structure began to break up and disappear. After a transitional range of about 3 kgms/mm^2 with no apparent domain structure, the stress pattern appeared with zig-zag walls running along the [001] direction. A vertical magnetic field caused alternate walls to disappear, showing the presence of a vertical component of magnetization. As the stress was increased the domain spacing decreased. Fig. 31 shows a typical $^1/d^2$, σ graph. The same patterns were also photographed at a magnification of 400x, so that measurements could be taken on the zig-zag angles. Even so, the error involved in measuring these proved fairly high and in order to obtain satisfactory results 50 measurements had to be taken at each value of stress. These results are plotted in Fig. 32.

This type of stress pattern remained on the surface of the specimens up to the limit of the experiments, i.e. 45 kgms/mm^2, and no other structure was formed.

4.1.4. Theoretical Considerations

4.1.4.1. Variation of domain spacing with stress

The polycrystalline case only will be considered in an attempt to interpret the observations made under these stress conditions. The initial structure consists of 180^o walls in a [001] direction. The energy for unit

surface area of this system, under the influence of a compressive stress σ dynes /cm^2 acting in the [011] direction, can be written as the sum of the magnetostatic, magnetoelastic, and domain wall energies thus

$$\frac{\gamma t}{d_0} + \frac{3}{4}\sigma\lambda_{100} t + A' d_0 \qquad (4.1)$$

t being the thickness of the specimen.

Assuming $2\gamma_{90} = \gamma_{180} = \gamma$, and assuming that γ is independent of orientation, the energy of the stress pattern for unit surface area becomes

$$\gamma\left[\frac{t}{d} - 1 + \sqrt{2}\right] + \frac{3}{4}\sigma\lambda_{100}\frac{d}{2} + A'd \qquad (4.2)$$

The equilibrium spacings of the two systems can be found by minimising expressions (4.2) and (4.1) with respect to d and d_0. The stress pattern spacing thus obtained is given by

$$\frac{\gamma t}{d^2} = \frac{3}{8}\sigma\lambda_{100} + A' \qquad (4.3)$$

where γ is the energy of the main vertical wall.

If the magnetization on either side of the main wall is considered to be in [001] and [00$\bar{1}$] directions, then the stress σ dynes/cm^2 is applied in the [110] direction and the reduced anisotropy energy in the wall is

$$\beta' f_m = + \frac{3}{4}\sin^2\phi\,\lambda_{100}\left[3\lambda_{100}(c_{11}-c_{12}) + \sigma\right]$$

As $\lambda=0$, the variation of wall energy with stress has previously been evaluated and is shown in Fig. 21.

Upon substituting values of t = 0.032 cms, λ_{100} = 26 x 10^{-6}, γ = 1.35 ergs/cm^2 and A = 50 (corresponding to $\delta = 1^o$) into equation (4.3), a value for the intercept on the stress axis at $^1/d^2 = 0$ of $-\frac{1}{4}$ kgm/mm^2 is obtained.

A theoretical graph, taking into account the variation of wall energy with stress is shown in Fig. 31. It has an intercept of $^1/d^2 = 0$ of 0 and a gradient given by $\frac{3}{8}\frac{\lambda_{100}}{\gamma t}$. The experimental points would be fitted more closely by taking an intercept of about 7 kgms/mm^2. A range of intercepts between -1 and +8 kgms/mm^2 was obtained for different specimens. As explained before this is probably due to random stresses in the material.

The cut-off value, that is the stress at which the energies of the two systems are equal, was calculated in the same way as described in section 3.1.3.3. for the (110) surface. For a value of $\delta = 1^o$ i.e. A = 50 this becomes 0.02 kgms/mm^2 which is about 20 times smaller than the observed value.

4.1.4.2. Variation of zig-zag angle with stress

In their treatment of the variation of zig-zag angle with stress, Chikazumi and Suzuki did not consider the

effect of stress on the Bloch wall energy of the closure domains. They assumed that the only effect of stress was to vary the magnetic pole density formed on these walls.

The effect of stress on the wall energy will now be considered. Chikazumi and Suzuki calculated the variation of the energy per unit area of the average plane of the zig-zag wall $\gamma/\sin\psi$ by approximating the anisotropy energy $g(\theta,\phi)$ with $2g_o \cos^2\left(\frac{\Pi\phi}{2\phi_1}\right)$ where $g_o = \frac{g(\theta,0)}{2}$. The direction cosines $(\theta,\phi=0)$ can be written in terms of the angles θ and ψ thus $\left(\frac{1}{\sqrt{2}}\sin(\theta+\psi), \frac{1}{\sqrt{2}}\sin(\theta+\psi), -\cos(\theta+\psi)\right)$

Therefore $$g_o = \frac{K_1}{8}\sin^2(\theta+\psi)[1+3\cos^2(\theta+\psi)]$$

By substituting the magnetization direction cosines and the stress direction cosines $(0, \frac{1}{\sqrt{2}}, \frac{1}{\sqrt{2}})$ into equation (1.9), the magnetoelastic energy E_σ becomes

$$E_\sigma = +\frac{3\sigma}{2}\left\{\frac{\lambda_{100}}{2}\left(\cos^2(\theta+\psi)+\frac{\sin^2(\theta+\psi)}{2}\right)+\frac{|\lambda_{111}|}{\sqrt{2}}\cos(\theta+\psi)\sin(\theta+\psi)\right\}$$

If the zig-zags are symmetrical about the [011] direction then the above energy expression represents the effect of stress on one part of the zig-zag wall and

$$E'_\sigma = +\frac{3\sigma}{2}\left\{\frac{\lambda_{100}}{2}\left(\cos^2(\theta+\psi)+\frac{\sin^2(\theta+\psi)}{2}\right)-\frac{|\lambda_{111}|}{\sqrt{2}}\cos(\theta+\psi)\sin(\theta+\psi)\right\}$$

represents the energy of the other part of the wall.

At a first approximation let the stress energy of the total wall be given by

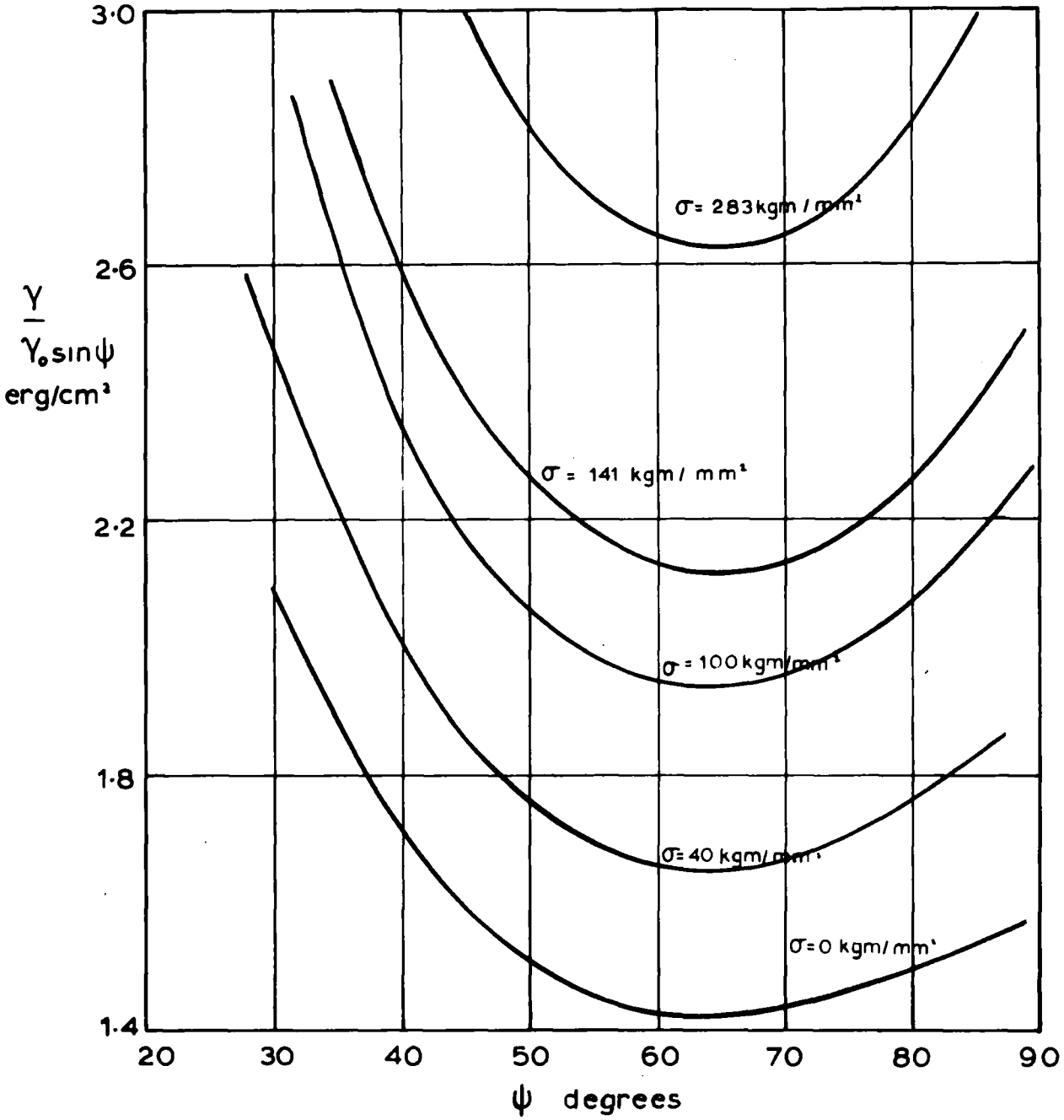

Graphs for various compressive stresses in [011] direction. They show the variation of wall energy with orientation.

FIG. 33

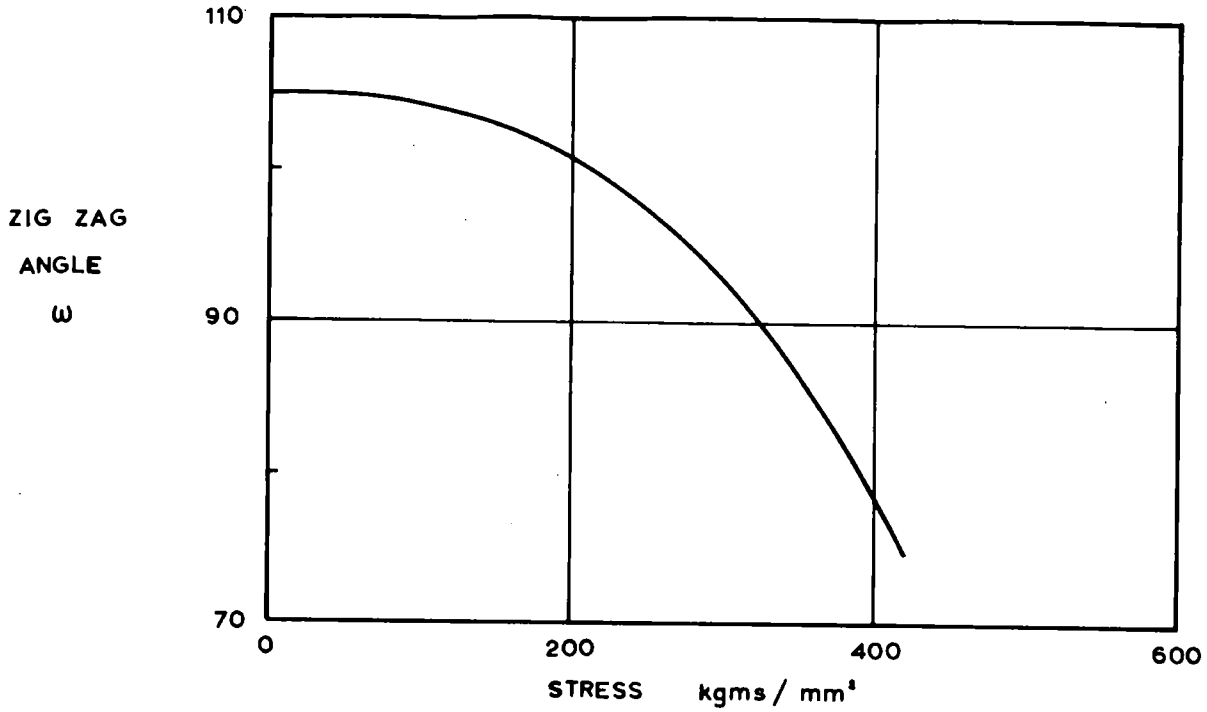

Variation of ω with a compressive stress in the [011] direction

FIG. 35

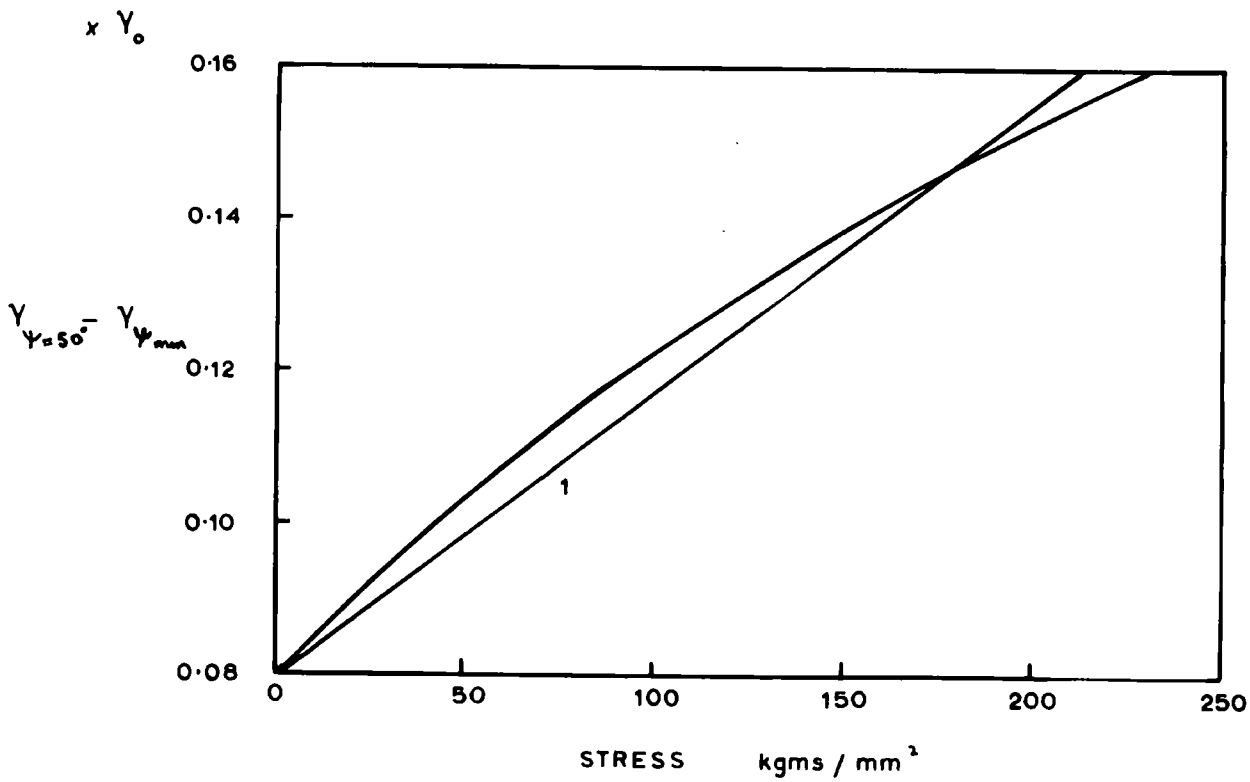

Measurements on the shape of $\gamma / \sin\gamma$ against ψ curves for various stress values. The curves show a steeper profile as the stress increases. Graph 1 is a linear approximation to the curve.

FIG. 34

$$E_\sigma = + \frac{3\sigma}{2}\left[\frac{\lambda_{100}}{2}\left(\cos^2(\theta+\psi) + \frac{\sin^2(\theta+\psi)}{2}\right)\right]$$

as the second term in each expression is smaller than the first. The total anisotropy energy now becomes

$$g_o' = K_1\left\{\sin^2(\theta+\psi)\left[\frac{3\cos^2(\theta+\psi)+1}{8}\right] + \frac{3\sigma\lambda_{100}}{8K_1}\left[\cos^2(\theta+\psi) + \frac{\sin^2(\theta+\psi)}{2}\right]\right\} \qquad (4.4)$$

Fig. 33 shows a series of curves of $\gamma/\sin\psi$ against ψ for various values of the compressive stress. Up to about 200 kgms/mm^2 it can be seen that ψ_{min} remains effectively constant while the value of wall energy at ψ_{min} increases with stress. Chikazumi and Suzuki approximated their zero stress curve using a $(\psi-\psi_{min})^2$ relationship thus

$$\gamma = C + 6.73 \times 10^{-4} (\psi-\psi_{min})^2\sqrt{AK}$$

where ψ is expressed in degrees. As this is differentiated with respect to ψ to find the variation of ψ with stress, the value of C is not important. However upon taking measurements on the graphs it was found that the multiplying constant of $(\psi-\psi_{min})^2$ varied with stress and this is shown in Fig. 34. This variation may be represented approximately by a linear relationship of the form

$$\gamma = C + 6.73 \times 10^{-4}(1 + 3.92 \times 10^{-3}\sigma)(\psi-\psi_{min})^2\sqrt{AK}$$

where σ is expressed in kgms/mm^2

Chikazumi and Suzuki minimised the wall energy term with the free pole energy term

$$E_{m.s} = \text{const} + 1.23 \times 10^{-4}\, m^2 c\psi^2$$

where c is the amplitude of the zig-zag and m the pole density is given by

$$m = \frac{0.18\lambda_{100}T_{xx}}{I}$$

T_{xx} is a tensional force normal to the surface. When dealing with a compressive force σ along the [011] direction this becomes

$$m = \frac{0.18}{2}\,\frac{\lambda_{100}\sigma}{I}$$

Experimental values of c were found to vary between 2.8×10^{-4} cms and 3.7×10^{-4} cms. However by taking the value used in the calculations of Chikazumi and Suzuki of 4×10^{-4} cms, the variation of zig-zag angle ω with σ becomes

$$\sigma\ (\text{kgms/mm}^2) = 2 \times 429\ \ 1 + 3.92 \times 10^{-3}\sigma\,\frac{\omega_{min} - \omega}{\omega + 25}$$

This is shown in Fig. 35. The variation of ω with σ is much less than that derived by Chikazumi and Suzuki and in the experimental range 0-50 kgms/mm^2 is effectively constant. The experimentally measured value of ω at 45 kgms/mm^2 is $90^\circ \pm 3^\circ$ which is 14° less than the value at 5 kgms/mm^2.

Section 3.1.1.1. shows how the easy directions deviate from the crystallographic axes under the influence

of a compressive force in a [011] direction. At about 50 kgms/mm^2 this deviation is only 5^o and it is difficult to see how this would affect the value of the zig-zag angle.

4.2. A compressive stress applied in a [011] direction on a surface a few degrees off a (100) plane.

4.2.1. Experimental Details

Specimens of polycrystalline cube textured sheet were cut into strips 4 cms x 1 cm x 0.032 cms with edges in [110] and [1$\bar{1}$0] directions and compressed along the [011] surface direction. Grains with a zero stress structure consisting of fir tree closure domains were examined. These grains are orientated so that the [001] direction makes an angle of between .5^o and 1.3^o with the surface see Bozorth, Williams and Shockley (1949). Plate 6 shows the variation of the domain structure with stress.

4.2.2. Results

At a stress of between 1 and 2 kgms/mm^2 the fir tree structure broke up and in its place appeared, after a 2 kgm/mm^2 transition range, a zig-zag structure with the zig-zag walls lying in the [010] direction. Between the zig-zag walls were arrowhead closure structures with the arrowhead pointing in the [001] direction. A small vertical field caused alternate zig-zag walls to disappear and colloid to collect over alternate areas between the zig-

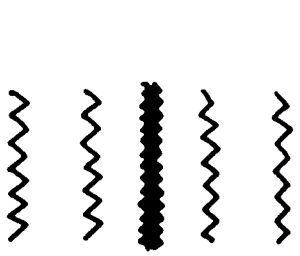

Observed structure, according to model, when vertical field applied.

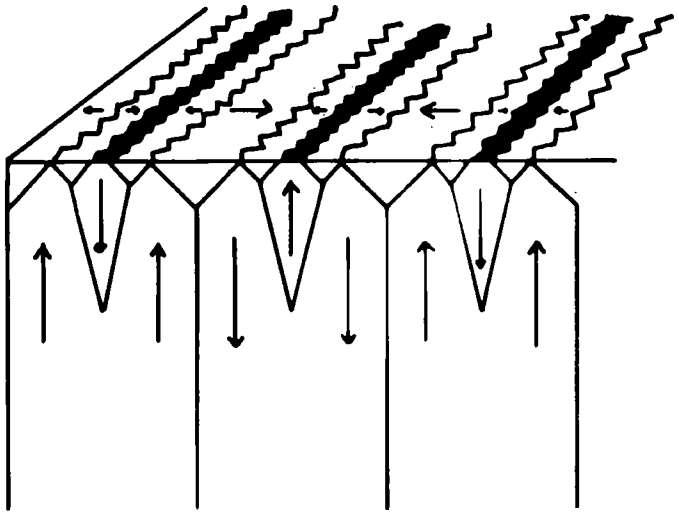

Line and zig zag structure proposed by Bates (1957)

FIG. 37

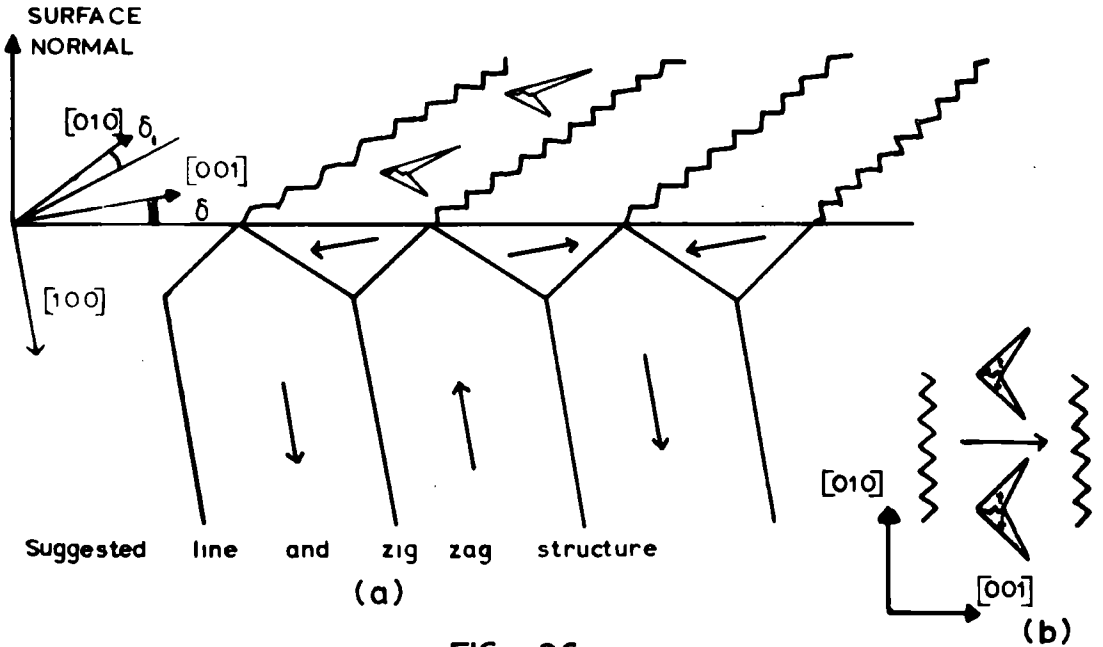

Suggested line and zig zag structure

(a)

FIG. 36

zags. In most cases no colloid collected on the arrowheads though in a few cases it collected over one side of each structure.

As the stress increased the zig-zag spacing decreased as did the size of the arrowheads. At a stress of between 10 and 15 kgms/mm^2 the arrowheads disappeared altogether. As soon as this happened the colloid on the surface of the closure domains was concentrated into a line running in a [010] direction along the centre of each domain. At this stage a vertical field showed an alternating straight line and zig-zag structure with the line deposit much closer to one zig-zag than the other.

This type of structure persisted up to the yield point.

4.2.3. Interpretation

The application of a stress causes the formation of a domain structure with main domains magnetized nearly normal to the surface and with closure domains magnetized in the [001] direction. As the magnetization in the closure domain is not parallel to the surface a free pole density I sin δ is formed on each domain (Fig. 36a). This is demonstrated by the polarisation of colloid on alternate domains upon the application of a vertical field. The magnetostatic energy due to these poles is reduced by the

formation of arrowhead closure domains which must be magnetized in the [010] and [0$\bar{1}$0] directions. Thus if this direction is parallel to the surface no colloid is deposited on the arrowheads. However if the [010] direction makes an angle δ_1 with the surface, colloid will be collected over the arrowhead and, as it is collected over half of each arrowhead in turn, each half must be magnetized in opposite directions (Fig. 36b). As the stress is increased the magnetization direction in the arrowheads becomes more and more unfavourable, thus causing them to decrease in size.

Upon the disappearance of the arrowheads the stray field at the surface becomes much simplified. It consists of a pole strength I cos δ at the zig-zag walls with I sin δ between them. Consider the effect of this type of pole distribution on the concentration of magnetic colloid. If the width of the zig-zag wall is 10^{-6} cms then the pole density at the wall is I x 10^{-6} gauss/sq cm. The distance from the wall at which this field equals that on the surface I sin δ is given by r where

$$\frac{I \times 10^{-6}}{r^2} = I \sin \delta$$

Taking $\delta \sim 1^{\circ}$ r = 10^{-2}cms. This is a very approximate value. The separation of the zig-zag walls is 0.05 mm, then if r~

2×10^{-3}cms, any colloid closer to the wall than this value of r would be drawn towards the wall. This type of mechanism would therefore cause the colloid to be concentrated in a narrow strip 10^{-3} cms wide at the centre of each closure domain. The application of a vertical field would cause alternate pairs of lines and zig-zag walls to disappear as is seen experimentally.

4.2.4. Conclusion

This type of strain structure has been observed previously. In a recent paper, Bates and Carey (1960) described this structure which they called a band structure. It had formed on grains in a sheet of cube textured polycrystalline silicon iron material, but was mainly removed by annealing. Bates (1957) proposed a model for the formation of this type of line and zig-zag structure. In this model the lines at the surface are due to the appearance of the [100] domains at the surface caused by branching Fig. (37). This type of branching is similar to that described by Lifshitz (1944). Bates suggested that this type of branching only occurred at high stress differences between the closure domains and the main underlying domains. Unfortunately this does not agree with the experimental results which have been obtained. Firstly, on the basis of his model, a vertical field would produce a domain structure at variance with that observed.

Secondly this type of structure was observed on specimens under relatively small stresses and is obviously dependent on the orientation of the surface and not on the size of the strain.

4.3. A stress applied along the [001] surface direction

4.3.1. Introduction

Theoretically a single crystal of iron with a (100) surface, bounded by [001] and [010] edges has a domain structure consisting of main domains magnetized along the length of the specimen (Fig. 5). Flux closure is completed at the ends of the specimen by means of triangular domains. If a compressive stress is applied along the length of the specimen, the direction of magnetization of the main domains will become less favourable than the other easy directions. Therefore if the thickness of the specimen is much less than the width, it seems likely from energy considerations that the stress pattern will consist of main domains magnetized in the [010] direction separated by 180° Bloch walls.

In the previous cases, the change over from the stress free pattern to the stressed pattern has been separated by a range of stress in which there has been no visible structure. In this case, as there are domains in the stress free case magnetized in the transverse

direction e.g. spikes and fir trees, it seems likely that growth processes will be revealed. These can be observed as well as the value of the stress at which the change-over occurs.

4.3.2. Nucleation Processes

Nucleation processes, which take place when a domain structure changes from one mode to another characterised by a larger number of phases, have been studied by many workers notably Bates and Martin (1956) and Goodenough (1954). In the main they have been concerned with the formation of domains of reverse and transverse magnetization, which are created in going from a single phase, magnetically saturated state, to a six phase demagnetized state. Their results differed by the order of 100 from theoretical estimates by Kittel (1949) which give the lower limit for the critical reverse field to initiate nucleation to be $^{2K_1}/_{I}$. This is probably due to the existence of high fields in the vicinity of non-magnetic inclusions.

The processes involved in nucleation are rather interesting. Bates and Martin showed that firstly transverse domains were formed at non-magnetic inclusions. The formation of domains of reverse magnetization took place at lower fields and was more difficult to observe.

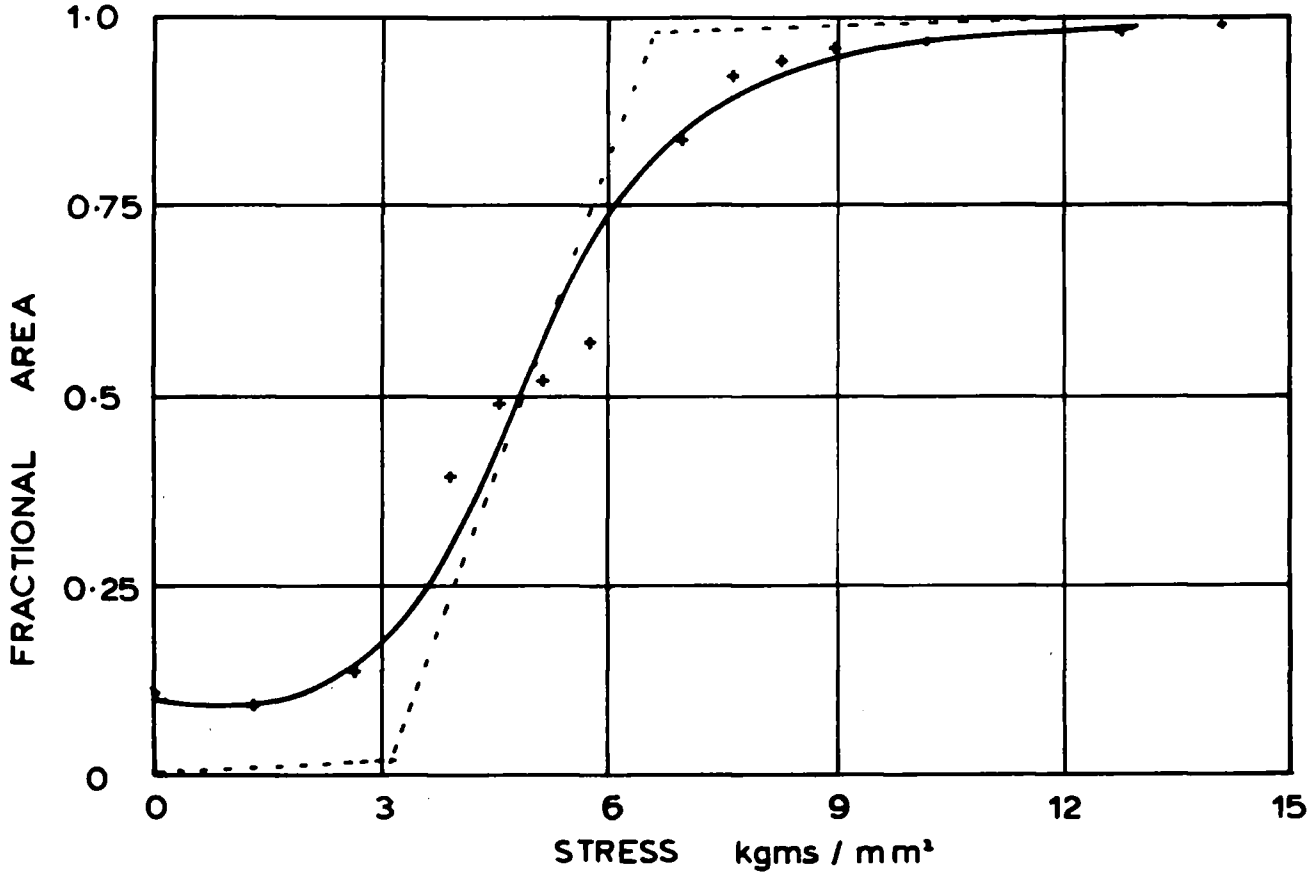

Ratio of areas of magnetization on a (100) surface as a function of stress

FIG. 38

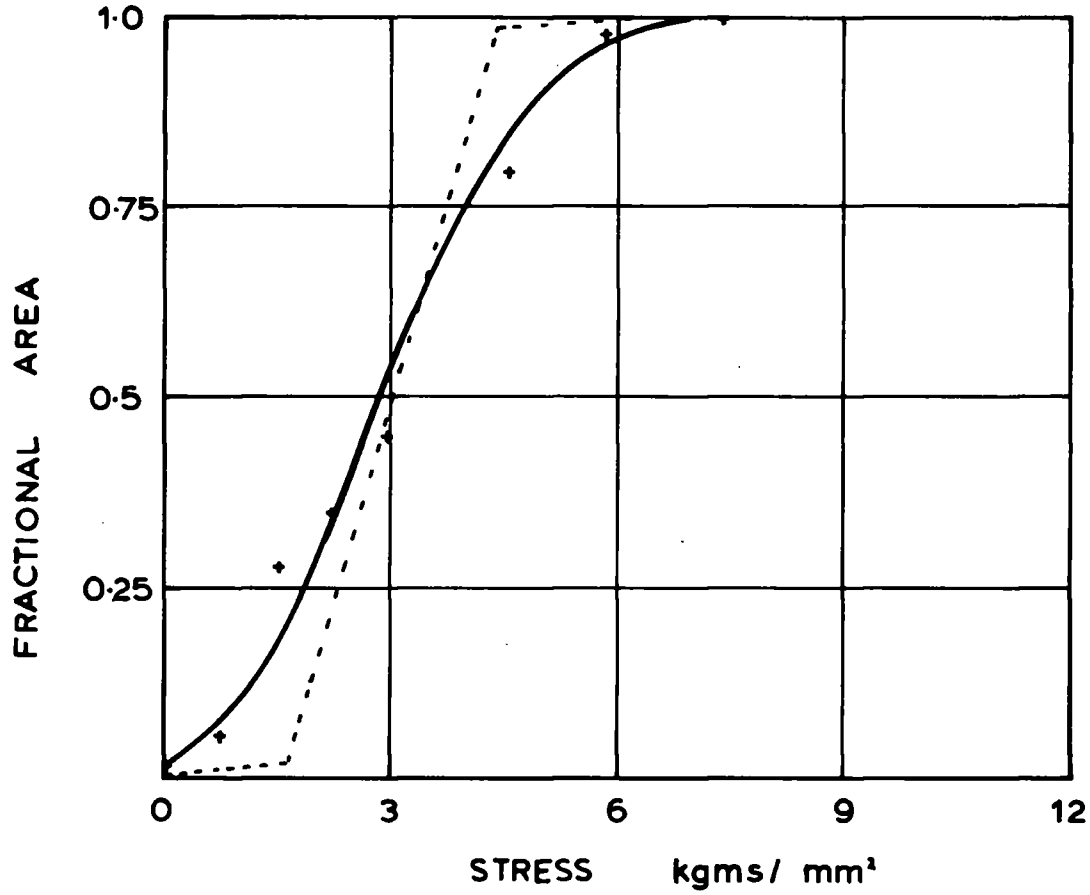

Ratio of areas of magnetization on a (100) surface as a function of stress

FIG. 39

They suggested that these were produced by encounters between 90^{o} walls and large surface pits.

We shall be concerned with two cases. One where the zero stress case is a four phase system, which under the influence of stress, changes to a two phase system. This is in fact the reverse of a nucleation process. In the second case the stress free system is a two phase mode which, under the influence of stress, changes to a different two phase mode via a four phase mode.

4.3.3. Experimental Observations

Single crystals of iron 3.5 cm x 1 cm x 0.03 cms, with the magnetization of the main domains directed along the length of the specimen, the [001] direction, were compressed in this direction using the bending technique. Also similarly shaped specimens of polycrystalline silicon iron sheet were compressively stressed along the direction of main magnetization in suitably orientated grains, i.e. those with the surface not more than 1^{o} away from a (100) plane.

Measurements of the ratio of the surface areas of magnetization in the two easy surface directions were made for varying stress conditions. Two typical graphs of experimental results are shown in Fig. 38 and Fig. 39. In all cases, independent of the mode of growth, the bulk

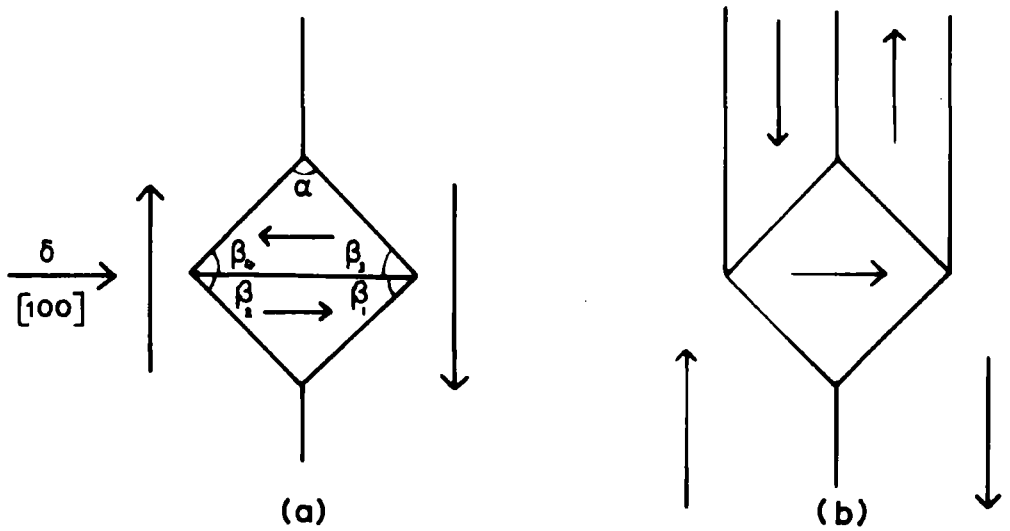

Square domains from which transverse domains grow

FIG. 40

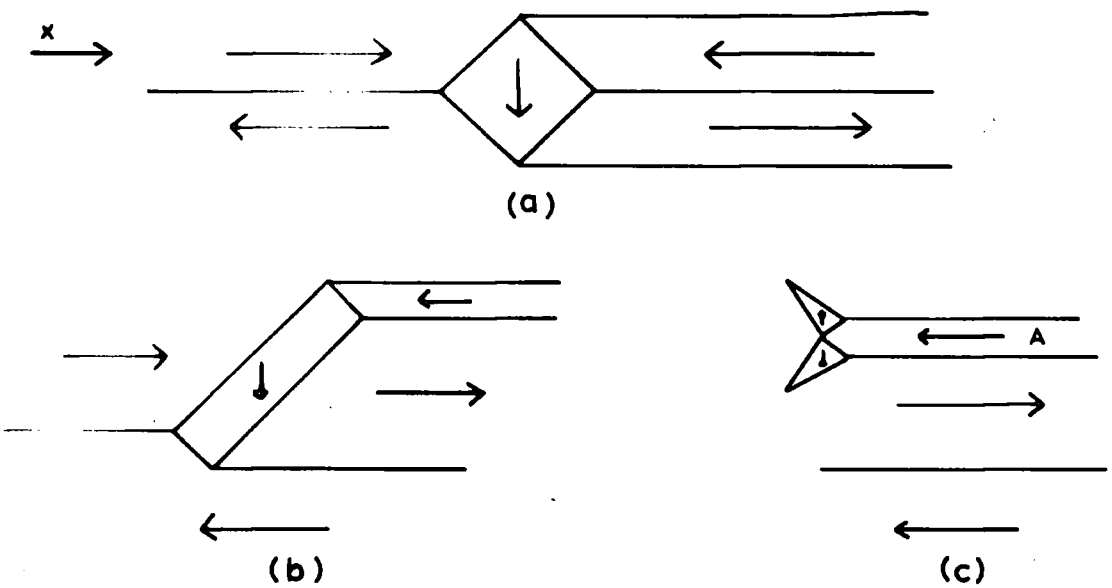

Tensional force in X direction increasing from (a) to (c) The process shows the formation of domains of reverse magnetization A

FIG. 41

of the magnetization is rotated through 90° in a stress range of about 6 kgms/mm^2. The stress at which this change-over was initiated seemed somewhat variable, ranging from 0.5 kgms/mm^2 to 7 kgms/mm^2. Although by far the majority of cases lay between 0.5 kgms/mm^2 and 3 kgms/mm^2. Presumably this is due to random stresses in the specimen as it was not possible to relate this variation to the type of transverse magnetization growth.

Nature of growth of transverse magnetization

If the zero stress pattern consisted of a fir tree structure, with no spikes on the main domain surfaces, the transverse growth took place by means of square domains on the main walls, with the diagonal along the length of the wall. Although the fir trees were magnetized in favourable directions they did not grow in size (see Plate 7.). The square domains appeared to grow at random along the walls presumably from points of high stress. Usually the square domains consisted of two triangular domains, magnetized in opposite direction (Fig. 40a), although in a few cases more complicated structures (Fig. 40b) were observed. In all cases there is a continuity of magnetization across the domain walls, although at first this did not seem to be so. Measurements of the angles of the 'square' showed them to vary between 80° and 99° and it

was noted that generally opposite angles were supplementary.

On small grains, of about 0.5 cm diameter, in the polycrystalline material, there was usually only one such square domain, which grew with increasing stress until it occupied the whole of the grain. There were more transverse domains on the single crystal specimens so that the intermediate stage, equal areas magnetized in the [010] and [001] directions, was very complicated consisting of many small domains bounded by 90° walls.

As the stress was increased further the area of magnetization in the initial direction became less, until it was confined to small square domains sited on the main Bloch Walls. The way these areas decreased with increasing stress was rather interesting. The transverse domain became elongated and finally broke off from the main wall forming a spike on a domain of reverse magnetization (Fig. 41).

In those cases where the surface was exactly a (100) plane, the only transversely magnetized areas were small spikes formed either at non-magnetic inclusions or on domains of reverse magnetization. Growth usually took place from both types of spike, the process being the reverse to that described above.

4.3.4. Theoretical Considerations

It is important to know whether the square domains are only surface structures or whether they penetrate to a reasonable depth. It is possible to infer this from the angles β_1 and β_2 (see Fig. 40) of the square, assuming that no free poles form on the domain walls. If the surface is exactly a (100) plane then the condition that there are no free poles on the wall is given by

$$\beta_1 = \beta_2 = 90^\circ$$

no matter to what depth the domains penetrate.

However if the surface makes an angle δ with the [010] direction, the surface angles β_1 and β_2 are related to ψ the angle between the domain wall and the [011] direction by

$$\tan \beta_1 = \frac{1}{\cos \delta} \frac{1}{\left[1 - \frac{\sqrt{2} \tan \delta}{\tan \psi}\right]}$$

and

$$\tan \beta_2 = \frac{1}{\cos \delta} \frac{1}{\left[1 + \frac{\sqrt{2} \tan \delta}{\tan \psi}\right]}$$

The table below shows the variation of β_1 and β_2 with ψ for $\delta = 1^\circ$.

ψ°	70°	60	50	40	30	20	10	5
β_1	$44^\circ 58'$	$44^\circ 36'$	$44^\circ 26'$	$44^\circ 11'$	$43^\circ 48'$	$43^\circ 7'$	$41^\circ 11'$	$37^\circ 57'$
β_2	$45^\circ 16'$	$45^\circ 26'$	$45^\circ 37'$	$45^\circ 52'$	$46^\circ 16'$	$47^\circ 1'$	$49^\circ 19'$	$54^\circ 32'$

As $\beta_3 = \beta_1$ and $\beta_2 = \beta_4$ it can be seen that in the above range

$$\beta_3 + \beta_1 + \beta_2 + \beta_4 \cong 180^\circ.$$

The graph in Fig. 39 shows the variation of surface magnetization with stress. This can now be modified so as to express the ratio of the volumes of magnetization against stress. For most of the structures ψ is less than 45° which represents a depth of domain less than 0.01 mms. This is negligible compared with the thickness of the specimen 0.32 mms. As far as can be deduced, the ratio of the volume magnetization against stress can be represented by the dotted line in Fig. 39. The change over takes place in, at the most, a 2-3 kgm/mm^2 range.

The energies of the zero stress structure and the final stress structure will now be considered. The zero stress structure is shown in Fig. 5. The final structure has the same form as this only the main domains are magnetized along the [010] and[0$\bar{1}$0] directions.

The energy of the initial structure under the effect of a compressive stress σ dynes/cm^2 in the [001] direction can be written as the sum of the magnetoelastic and wall energies thus

$$E_{TOT} / \text{unit surface area} = \frac{1}{D}\left[\gamma + \frac{D^2}{4L}\left(c_{11}\lambda_{100}^2 - 3\sigma\lambda_{100}\right)\right] + \frac{3}{2}\sigma\lambda_{100} \qquad (4.5)$$

minimising this with respect to D gives the following expression for the domain spacing

$$D = \sqrt{\frac{4\gamma L}{c_{11}\lambda_{100}^2 - 3\sigma\lambda_{100}}} \qquad (4.6)$$

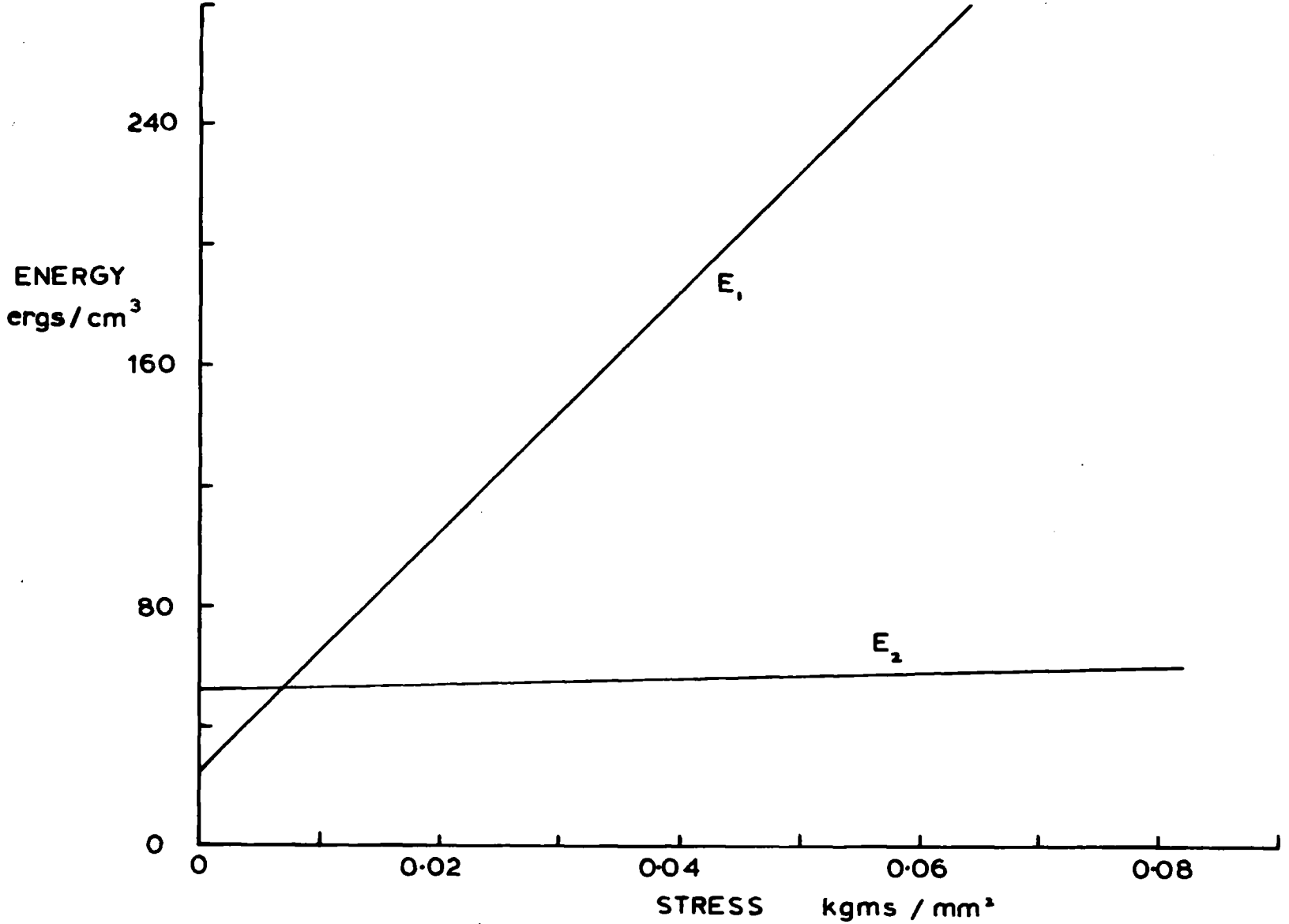

The effect of stress on the energies of domain systems 1 and 2
L = 4 cms. and Y = 1 cm.

FIG. 42

The energy of the first system can now be written, substituting equation (4.6) into equation (4.5)

$$E_1 = \sqrt{\frac{(c_{11}\lambda_{100}^2 - 3\sigma\lambda_{100})\gamma}{L}} + \frac{3}{2}\sigma\lambda_{100}$$

Similarly the energy of the second structure per unit surface area can be written

$$E_2 = \sqrt{\frac{(c_{11}\lambda_{100}^2 + 3\sigma\lambda_{100})\gamma}{Y}}$$

By taking γ constant and putting Y = 1 cm and L = 4 cms curves are obtained as in Fig. 42 for the variation of the energies of the two systems with stress. The second system can be seen to become more favourable than the first at 0.0075 kgms/mm^2. If L = 4 mms and Y = 1 mm this would be increased to 0.024 kgms/mm^2. When considering such small variations of stress, the assumption that the wall energy remains constant is perfectly valid.

Change over values can be calculated for surfaces a few degrees off a (100) plane, under the effect of the compressive force, by adding a magnetostatic energy term to equation (4.5).

The resulting energies for a unit surface area become

$$E_1' = \sqrt{\frac{(c_{11}\lambda_{100}^2 + 4\times 1\cdot 7 1^2 \sin^2\delta_1 L - 3\sigma\lambda_{100})\gamma}{L}} + \frac{3}{2}\sigma\lambda_{100}$$

and

$$E_2' = \sqrt{\frac{(c_{11}\lambda_{100}^2 + 4\times 1\cdot 7 1^2 \sin^2\delta_2 Y + 3\sigma\lambda_{100})\gamma}{Y}}$$

Taking L = 4 cm and Y = 1 cm.

$\delta_1 = 0 \quad \delta_2 = 2^\circ \quad E_1 = E_2$ at 0.04 kgms/mm^2

$\delta_1 = \delta_2 = 0 \quad E_1 = E_2$ 0.01 kgms/mm^2

$\delta_1 = 0 \quad \delta_2 = 1^\circ \quad E_2 = E_1$ 0.02 kgms/mm^2.

Whatever the conditions considered, the energies of the two systems become equal at stresses the order of 100 times smaller than the observed change over stress.

There are two main reasons for this. Kersten (1930) has shown that in cooling a ferromagnetic through its Curie temperature stresses are set up of magnitude $\lambda_s Y$. Upon taking Y as Y_{100}, as the magnetization vectors lie along the easy directions, a stress of 0.65 kgms/mm^2 is obtained. Therefore stresses greater than this must be applied to change the direction of magnetization even if the specimens have been perfectly annealed.

Secondly the equating of the energies of the two systems does not take into account the energy of the intermediate system. This has been observed to be a fairly complicated structure with large areas of Bloch wall. Besides the energy needed to create this domain wall there is also energy needed to move it from one position to another. The system is so complex that it seems impossible to work out any rigorous model of what happens without a detailed knowledge of the stress and structure inhomogeneities in the specimen.

4.4. The stress applied along the [010] direction on a surface 3^{o} off a (100) plane.

4.4.1. Experimental details and Results

Specimens of polycrystalline cube textured silicon iron sheet, 4 cms x 1 cms x 0.032 cms were compressed along the [010] direction. Grains orientated with the direction of magnetization, the [010] direction, in the surface and with the other surface easy direction, the [001] direction, making an angle of about 3^{o} with the surface, were observed. Plate 8 shows the change in structure under stress. At a stress of about 1 kgms/mm^2 the original domain structure disappeared. This was followed by a transitional range of between 1 kgm/mm^2 and 3 kgms/mm^2 in which no domain structure was apparent.

After this a domain structure appeared. It consisted of very small fir tree like structures joined end to end, so as to fom a continuous line. At low stresses these 'lines' seemed rather randomly orientated but as the stress increased the spacing of the lines decreased and they rotated so as to lie along the [001] direction, at right angles to the compressive force. Upon the application of a vertical field colloid was deposited over alternate lines.

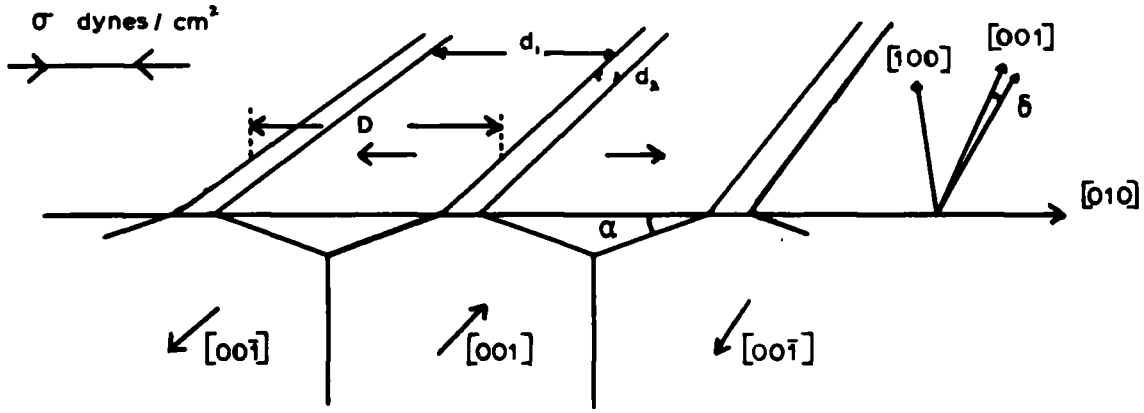

Block diagram of the stress pattern formed on surfaces with δ 2°- 4°

FIG. 43

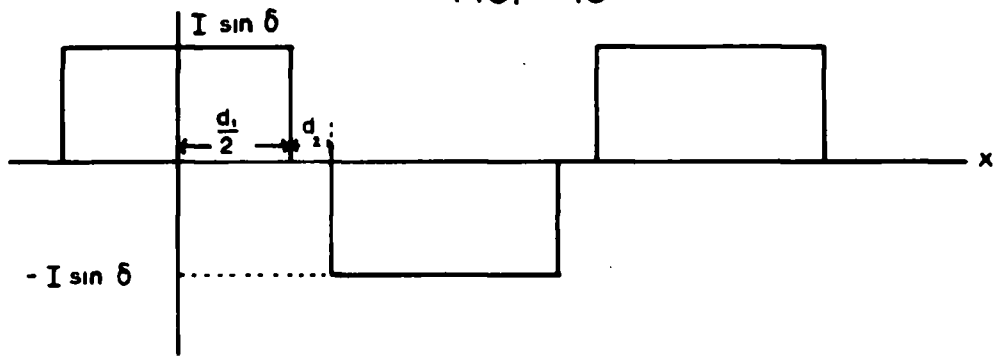

Free pole distribution for the system shown in Fig. 43

(a)

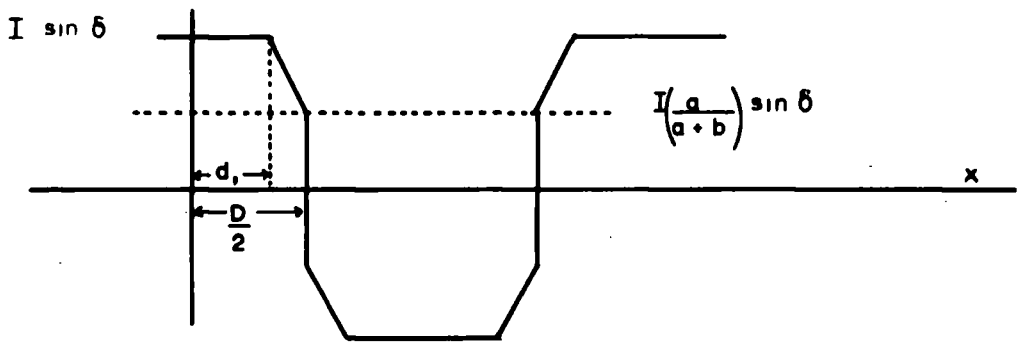

Proposed model for the evaluation of magnetostatic energy

(b)

FIG. 46

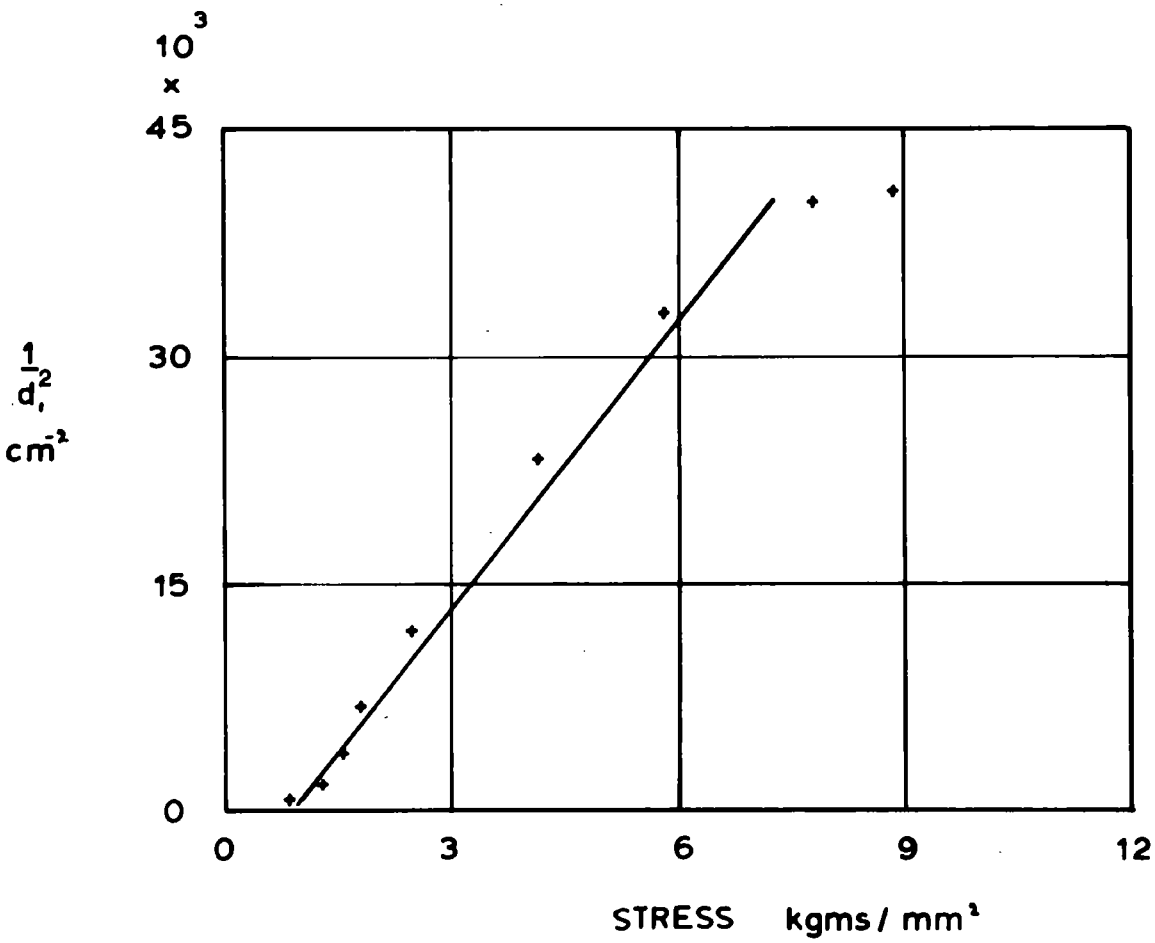

Variation of domain spacing d_1 with stress

FIG. 44

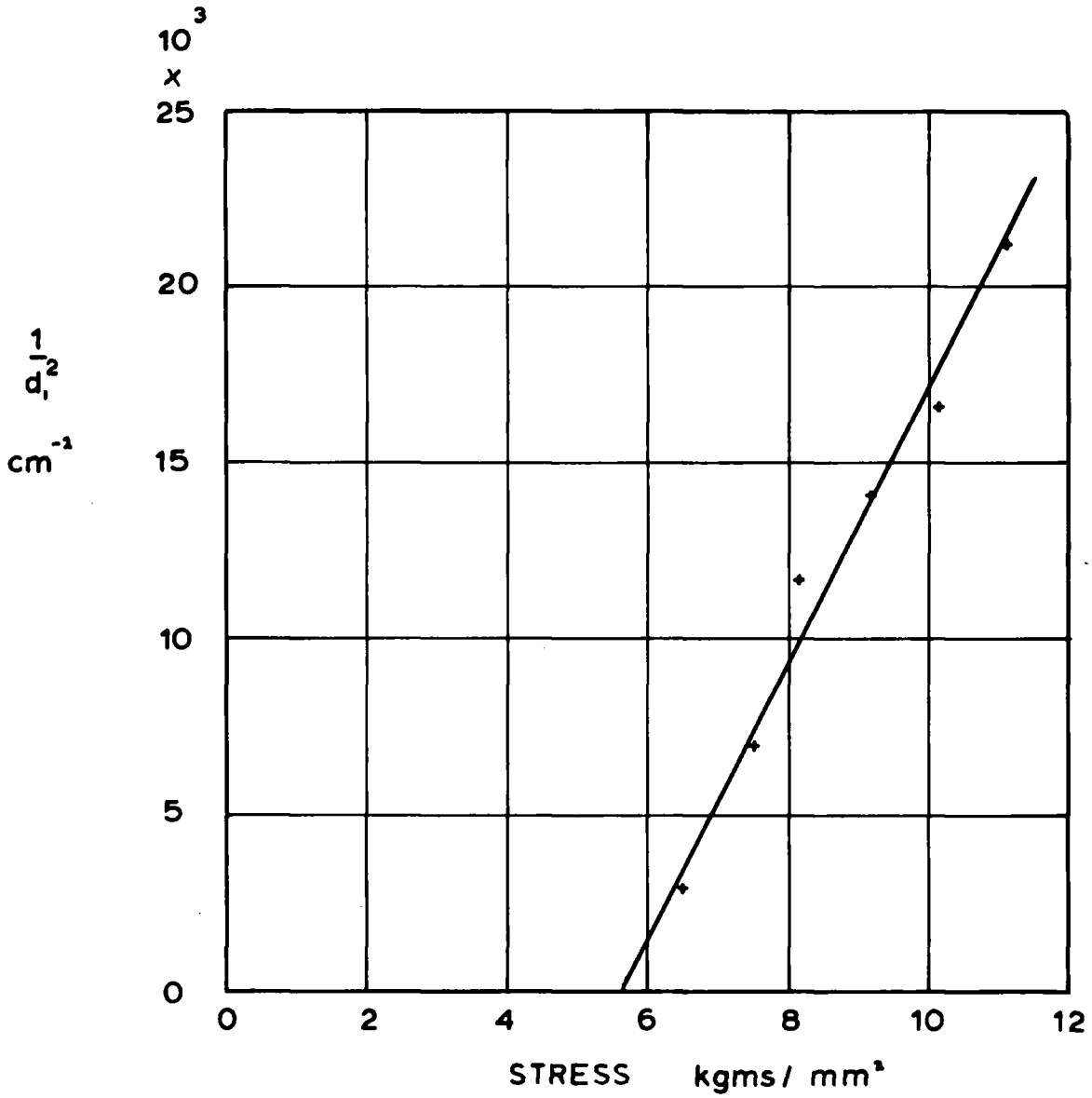

Change in stress pattern spacing d_1 with stress

FIG. 45

Therefore the structure was identical to that observed by Bozorth, Williams and Shockley (1949) on (100) surfaces with the [001] direction making an angle of between 1.9° and 3.9° to the surface. A block diagram of the structure is shown in Fig. 43.

The main domains are magnetized along the [001] direction which has been made more favourable than the [010] direction by the compressive force. The vertical component of magnetization I sin δ is closed by surface closure domains magnetized in the [010] direction. These do not cover the whole of the surface leaving narrow strips of the underlying structure which are observed as lines of fir trees. As the stress is increased the closure domains become more unfavourable and their volume is reduced by a decrease in the domain spacing. The variation of domain spacing d_1 was measured and Figs. 44, 45. show $^1/d_1{}^2$ plotted against the stress σ for two typical specimens, one with $\delta = 3^{\circ}$ and the other $\delta = 4^{\circ}$.

At stresses above 12 kgms/mm^2 the domain spacing d_1 remained constant but the width d_2 of the [001] domain at the surface increased so reducing the volume of the closure domains even further.

4.4.2. Theoretical Considerations

At a first approximation it is assumed that the [001] domains are bounded by straight lines at the surface, as shown in Fig. 43. In order that no free poles are formed on the closure domain walls the angle α is given by

$$\tan \alpha = \sin \delta$$

As $\delta \sim 3^{\circ}$, to a good approximation α equals δ.

The effect of stress on the system will now be considered. The total energy of the system consists of the sum of the magnetostatic, magnetoelastic, and wall energies.

Magnetostatic Energy

The method of evaluating the magnetostatic energies has been described in section 1.2.4. The pole density can be represented by the square wave shown in Fig. 46a. A fourier analysis of this gives the following expression for the pole density

$$\rho = \frac{4I}{\pi} \sin\delta \sum_{n}^{\infty} \frac{1}{n} \sin\left(\frac{n\pi}{2}\right) \cos\left(\frac{n\pi d_2}{2D}\right) \cos\left(\frac{n\pi x}{D}\right)$$

and the magnetic potential

$$\phi = \frac{4I \sin\delta}{\pi} \sum_{1}^{\infty} \frac{1}{n} A \sin\left(\frac{n\pi}{2}\right) \cos\left(\frac{n\pi d_2}{2D}\right) \cos\left(\frac{n\pi x}{D}\right) \exp\left(\frac{n\pi z}{D}\right)$$

A can be evaluated from the boundary conditions. The magnetostatic energy density $E_{m.s}$ can be shown to be

$$E_{m.s.} = \frac{8I^2 \sin^2\delta D}{\pi^2} \sum_{n \text{ odd integers}} \frac{1}{n^3} \cos^2\left(\frac{n\pi d_2}{2D}\right)$$

Taking the first term only, n=1, as the higher terms rapidly diminish

$$E_{m.s.} = \frac{8I^2 \sin^2\delta D}{\pi^2} \cos^2\left(\frac{\pi d_2}{2D}\right)$$

Magnetoelastic Energy

The volume of the closure domains/unit surface area

$$= \frac{d_1^2}{2D} \tan\delta$$

The energy of these domains consists of the stress energy $^3/_2\sigma\lambda_{100}$, where σ is in dynes/cm^2, and the magnetostrictive energy $\frac{1}{2}C_{11}\lambda_{100}^2$.

Therefore Total magnetoelastic energy =

$$\frac{d_1^2 \tan\delta}{2D}\left(\frac{3}{2}\sigma\lambda_{100} + \frac{1}{2}c_{11}\lambda_{100}^2\right)$$

Wall Energy

The wall energy of the closure domains/unit surface area $= \frac{d_1}{\cos\delta} \times \frac{\gamma}{D}$, while that of the main domain walls $= \frac{t\gamma}{D}$, t being the thickness of the specimen. Writing D = $d_1 + d_2$, the total energy of the system becomes

$$E_{TOT} = \left(\frac{2d_1}{\cos\delta} + t\right)\frac{\gamma}{d_1+d_2} + \frac{16I^2\sin^2\delta(d_1+d_2)}{\pi^2}\cos^2\left(\frac{\pi d_2}{2(d_1+d_2)}\right)$$

$$+ \frac{d_1^2\tan\delta}{2(d_1+d_2)}\left(\frac{3}{2}\sigma\lambda_{100} + \frac{1}{2}c_{11}\lambda_{100}^2\right)$$

Minimising the total energy with respect to d_1 leads to a rather complex expression

$$\frac{2d_2\gamma}{\cos\delta(d_1+d_2)^2} - \frac{t\gamma}{(d_1+d_2)^2} + \frac{16I^2\sin^2\delta}{\pi^2}\cos^2\left(\frac{\pi d_2}{2(d_1+d_2)}\right)$$

$$+ \frac{16I^2\sin^2\delta\, d_2}{\pi(d_1+d_2)}\cos\left(\frac{\pi d_2}{2(d_1+d_2)}\right)\sin\left(\frac{\pi d_2}{2(d_1+d_2)}\right) + \frac{\tan\delta}{4}\left(3\sigma\lambda_{100} + c_{11}\lambda_{100}^2\right)\frac{d_1^2+2d_1d_2}{(d_1+d_2)^2} = 0$$

Taking $d_2 = nd_1$ and assuming that both n and γ are constant in the stress range under consideration, an expression of the form

$$\frac{1}{d_1^2} = m\sigma + C$$

is obtained, where $m = \frac{3}{4}\lambda_{100}\frac{(1+2n)}{t\gamma}\tan\delta$

In the stress range 0 - 10 kgms/mm^2, the wall energy will increase by a factor of 1.2, while n will increase from about 0.02 to 0.2, This means that (1+2n) will increase by about 1.4 times. It therefore seems reasonable to consider that the resulting relationahip of $1/d_1^2$ against σ should be approximately linear. The experimental relationships are shown in Fig. 44 and Fig. 45. The gradient obtained from the specimen with $\delta = 3^o$ is 3.9×10^{-5} while a theoretical value taking n = 0.1, $\gamma = 1.3$ ergs/cm^2 and t = 0.032 cms is 3.0×10^{-5}. The gradient obtained from the specimen with $\delta = 4^o$ is 6.4×10^{-5} which compares with a theoretical value of 4.7×10^{-5}. Considering that the grain orientation was determined to an accuracy of $\pm\frac{1}{2}^o$, the agreement is quite

good, although in both cases the theoretical value is about 25% low. The experimental values of the intercepts at $^1/d_1{}^2 = 0$ are 0.07 kgms/mm^2 and 5.5 kgms/mm^2 compared with a theoretical value between -1 kgm/mm^2 and 0.

The case when d_1 remains constant and d_2 increases, that is above σ = 12 kgms/mm^2, cannot be simply calculated using this model as the approximation of straight line intersections of closure domains at the surface looses its validity.

4.5. The effect of stress on fir tree structures

4.5.1. Introduction

The first work on (001) surfaces with the [010] direction inclined at a small angle δ, to the surface, was carried out by Bozorth, Williams and Shockley (1949). They found small closure domains along the main 180° domain walls. These they called fir tree structures and their variation with δ was examined.

δ less than $\frac{1}{2}^\circ$ no fir trees formed.

δ 0.5° - 0.65° Fir trees form and grow to $^D/2$ (D being the main domain spacing)

δ 0.65° - 1.30° Fir trees fill more of pattern until they eliminate the main domain wall at the surface.

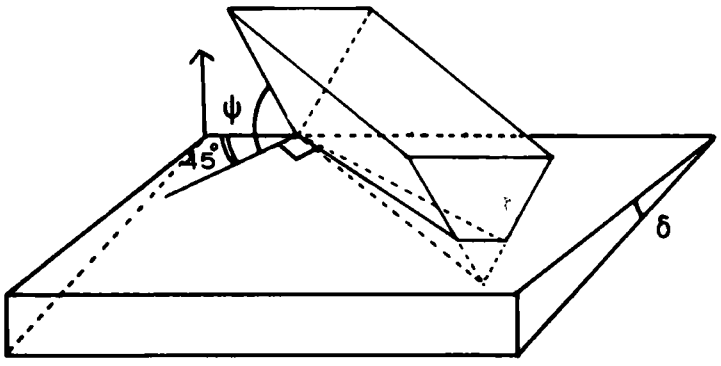

Block diagram of a fir tree structure. Spacek (1957)
The side walls of the fir tree each make an angle ψ with the [110] direction

FIG. 47

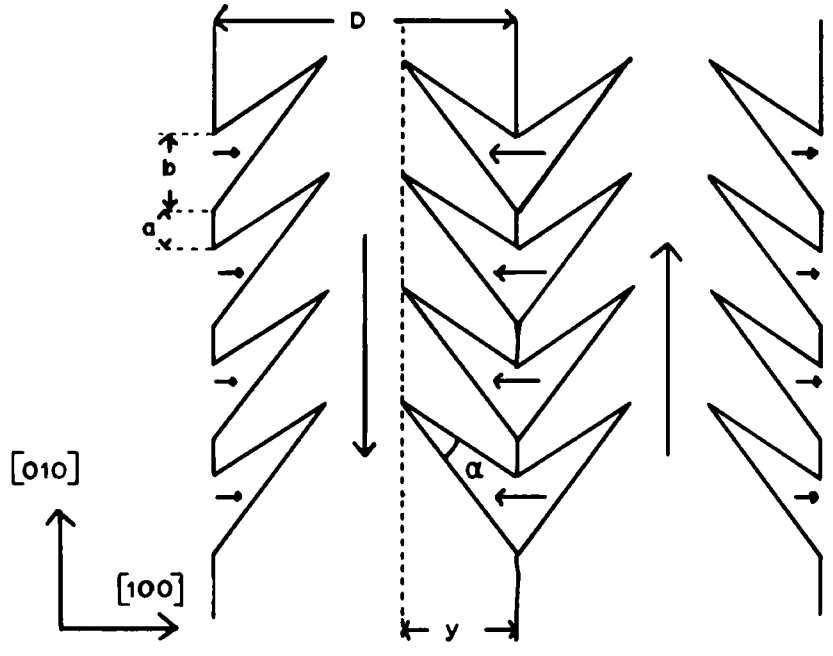

Plan view of fir tree structure

FIG. 48

δ 1.3° - 3.9° Fir tree branches increase in length until all but a narrow strip of underlying domain is visible at the surface.

They suggested that the fir trees were elliptical cones, and calculated theoretical values of their width and separation on the assumption that the branches neutralise the flux of the underlying domains. Due to their elliptical shape free poles were assumed to be formed on the under surface of the closure domains as well as on the surface of the specimen. They estimated the size of the magnetostatic energy so produced by replacing the fir tree system by parallel strips, of width D and pole density $\pm$ I sin δ, running along the [110] direction. The resulting magnetostatic energy equals

$$\frac{1{\cdot}70\, I^2 \sin^2\delta}{[1 + \mu^*(1+\mu^*)/2]^{1/2}}$$

Recently a more rigorous model for the fir tree structure has been proposed by Spacek (1957) (1958). The normals to the fir tree walls lie in a (110) plane therefore no free poles are formed on them. The angle between the (001) plane and the wall is specified by the angle ψ. The proposed structure is shown in Fig. 47. A plan view of a fir tree system is shown in Fig. 48.

In evaluating the variation of α, the angle at the spike of the fir tree, with δ, Spacek assumed that the width of the fir trees equaled $D/2$ and that a = b. The

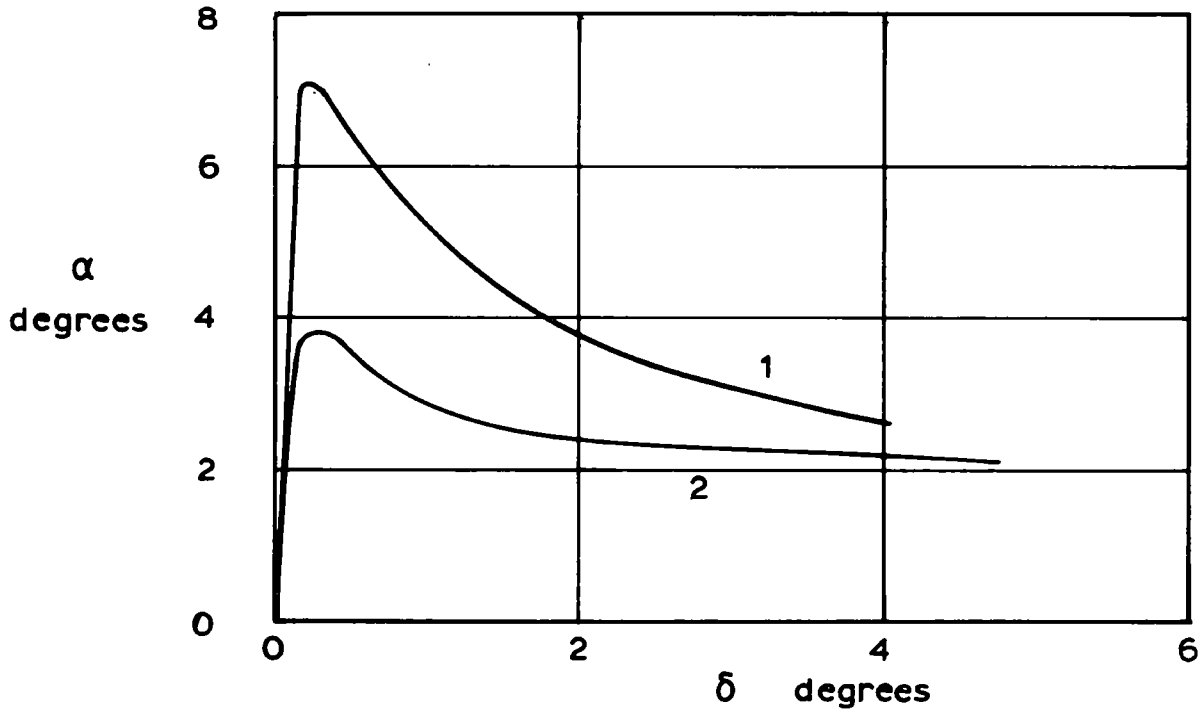

Variation of the angle at the fir tree tip α with the deviation of [100] direction from the surface δ for D = 0·06 cms : y = D/2 : a = b

1. Spacek (1957)
2. Recalculation of Spacek's results using a different wall energy expression.

FIG. 49

model used by Spacek for calculating the magnetostatic energy of the system consisted of strips of width $\frac{D\alpha}{\sqrt{2}}$, in a [110] direction, with magnetic pole densities I sin δ, 0, -I sin δ, 0. This gave a value of the magnetostatic energy which was proportional to $D\alpha$. Of the rest of the energy expressions, the magnetoelastic energy was independent of α. The wall energy expression consisted of a term for the area of the Bloch wall multiplied by one for the variation of wall energy with orientation. Upon minimising the total energy, magnetostatic, magnetoelastic and wall, with respect to α he obtained.

$$\alpha^4 - 0.14\alpha^3 + \left(\sin^2\delta + 0.754D\sqrt{\frac{\alpha^2}{2} + \sin^2\delta}\right)\alpha^2 - 0.11\sin^2\delta = 0 \quad (4.7)$$

The variation of α with δ for a specific value of D (0.06 cm) is shown in Fig. 49. Although no systematic experimental values of α as a function of δ have been measured, Bozorth, Williams and Shockley did show that for $\delta = 1^\circ$ $\alpha = 7^\circ$, which agrees quite well with Spacek's work.

Kaczer pointed out that the variation of Bloch wall energy with ψ, and consequently α, used by Spacek was incorrect, and that the relationship obtained by him (see Fig. 4) should be used. Transforming the γ, ψ relationship in terms of γ and α using

$$\tan\frac{\alpha}{2} = \frac{1}{\sqrt{2}}\ \frac{\tan\delta}{\tan\psi}$$

and not equation (20) (Czech J. Phys. 7 719 1957) a series of curves for various values of δ are obtained. Upon fitting the curves with a parabola of the form

$$\gamma - A = K(\alpha - m)^2$$

the equation relating α and δ (the equivalent to eq. 4.7) becomes

$$\alpha^4 - \alpha^3 m + \alpha^2\left[\sin^2\delta + \frac{2\sqrt{2}\times 0.735\times 10^5 D\sin^2\delta}{K}\sqrt{\frac{\alpha^2}{2} + \sin^2\delta}\right] - \frac{\sin^2\delta}{K}\left[A + Km^2\right] = 0$$

Multiplying through by 10^4, calling $10m = G$ and $B = \sin^2\delta \times 10^4$, the above equation becomes

$$\alpha^4 10^4 - \alpha^3 G 10^3 + \alpha^2\left[B + C\sqrt{\frac{\alpha^2 10^4}{2} + 10^4\sin^2\delta}\right] - B\left[\frac{A}{K} + m^2\right] = 0 \qquad (4.8)$$

The values of the constants, using the correct wall energy values, are shown in the table below.

δ	G	$6 \times 10^{-2}\ C/D$	B	A/K
20	1.22	12.4	.339	.267
40	1.64	54.9	1.26	.322
1^o	2.44	289	3.04	.724
2^o	3.35	659	12.17	.369
4^o	4.71	2747	48.7	.350

The result obtained by solving equation (4.8) graphically for various values of δ, again taking D = 0.06 cms, is shown in fig. 49. The results can be seen to be much lower than those given by Spacek. At $\delta = 1^{o}$, $\alpha = 3^{o}$ which is roughly half the experimental value.

4.5.2. Proposed Magnetostatic Model

The model used by Spacek for calculating the magnetostatic energy gives a result proportional to α. As he has assumed a=b a change in α will only alter the scale of the fir tree pattern along the main wall, and not the relative amounts of free pole and zero pole along unit length of wall. Under these circumstances it is difficult to imagine how a change in α will alter the magnetostatic energy. Besides the rather curious result obtained by this method, it is extremely limited in its applications. The variation of magnetostatic energy with other parameters, the separation of fir trees b, and the width of fir tree y, cannot be evaluated.

As the rigorous solution of the magnetostatic energy involves a rather complicated two dimensional integration, the following model (see Fig. 46b) is proposed for the simplification of the problem. If the pole density is to be represented by a square wave, then it seems logical that the period should remain 2D. However as this

represents in one dimension, x direction, what happens in the y direction too, it seems logical to assume that the effective pole strength at the main domain wall is $I \sin \delta\left(\frac{a}{a+b}\right)$, while that between y and $\frac{D}{2}$ (centre of the domain) remains at $I \sin \delta$. In the limit, when $a \to 0$ and $y = D/2$ the model used is a triangular wave.

Consider the general case with a, y and b not particularised. Upon representing the wave with a Fourier expansion, the following pole density expression can be obtained

$$\rho = \frac{4I \sin\delta}{\pi} \sum_{1}^{\infty} \frac{1}{n} \left\{ \frac{a}{a+b} \sin\frac{\pi n}{2} + \frac{1}{n} \frac{b \cos\left(\frac{2\pi n d_1}{d}\right)}{(a+b)\left(\frac{\pi}{2} - \frac{2\pi d_1}{d}\right)} \right\} \cos\frac{2\pi n x}{d}$$

The potential Φ is given by

$$\Phi = \frac{4I \sin\delta}{\pi} \sum_{n}^{\infty} \frac{d}{m^2} \left\{ \frac{a}{a+b} \sin\frac{\pi n}{2} + \frac{b \cos\left(\frac{2\pi m d_1}{d}\right)}{n(a+b)\left(\frac{\pi}{2} - \frac{2\pi d_1}{d}\right)} \right\} \cos\frac{2\pi m x}{d} \cdot \exp\left(\frac{-2\pi m z}{d}\right)$$

From these the magnetostatic energy per unit surface area E_{ms} can be obtained.

$$E_{m.s} = \frac{1}{2} \int \frac{4I \sin\delta}{\pi} \sum_{1}^{\infty} \frac{d}{m^2} \{\} \cos\frac{2\pi m x}{d} \cdot \frac{4I \sin\delta}{\pi} \sum_{1}^{\infty} \frac{1}{n} \{\} \cos\frac{2\pi n x}{d} \, dx$$

$$= \frac{8I^2 d \sin^2\delta}{\pi^2} \sum_{n=1}^{\infty} \sum_{m=1}^{\infty} \frac{1}{nm^2} \{\}^2 \int \cos\frac{2\pi n x}{d} \cos\frac{2\pi m x}{d} \, dx$$

Where $$\{\} = \frac{a}{a+b} \sin\frac{\pi n}{2} + \frac{b}{n} \frac{\cos\left(\frac{2\pi n d_1}{d}\right)}{(a+b)\left(\frac{\pi}{2} - \frac{2\pi d_1}{d}\right)}$$

The integral can be evaluated between 0 and $^{kd}/_{2}$, the same energy density being obtained for any integral value of k.

The energy density =

$$\frac{8I^2\sin^2\delta d}{2\pi^2}\sum_{n=1}^{n=\infty}\frac{1}{n^3}\left[\frac{a}{a+b}\sin\frac{\pi n}{2}+\frac{1}{n}\frac{b}{(a+b)\left(\frac{\pi}{2}-\frac{2\pi d_1}{d}\right)}\cos\frac{2\pi n d_1}{d}\right]^2$$

As the expression decreases rapidly (the second term n=3 is $^{1}/_{27}$th the magnitude of the first term) with increasing n, it is a reasonable approximation to consider the first term only. Taking 2D = d: $d_1 = {}^{D}/_{2}-y$: and b = 2yα, the following energy density expression can be obtained

$$E_{m.s} = \frac{8I^2\sin^2\delta D}{\pi^2}\left[\frac{a}{a+2y\alpha}+\frac{2D\alpha}{\pi(a+2y\alpha)}\sin\frac{\pi y}{D}\right]^2$$

When the effective permeability μ^+ is taken into account a correction factor $\frac{2}{1+\mu}$+ multiplies $E_{m.s.}$.

And

$$E_{m.s} = \frac{16I^2\sin^2\delta D}{(1+\mu^+)\pi^2(a+2y\alpha)^2}\left[a+\frac{2D\alpha}{\pi}\sin\frac{\pi y}{D}\right]^2 \qquad (4.9)$$

In the limit, when the fir trees disappear $y\to 0$ and

$$E_{m.s} = \frac{16I^2\sin^2\delta D}{\pi^2(1+\mu^+)}$$

which is the value, taking only the first term in the series, given by Kittel (1949) for parallel strips of width D and pole density $\pm$ I sin δ.

4.5.3. Application to stress free case

4.5.3.1. The relationship between α and δ

The relationship between α and δ can be evaluated by substituting the magnetostatic energy given in equation (4.9) for the one used by Spacek. Taking the same conditions as used by Spacek namely

$$y = \frac{D}{2} \text{ and } a = 2ky\alpha$$

Spacek put k=1

$$E_{m.s} = \frac{16I^2\mu^2\delta D(2yk + 2D/\pi)^2}{(1+\mu^2)\pi^2 4y^2(1+k)^2}$$

Therefore the magnetostatic energy per unit surface area is independent of α under these conditions.

Evaluation of the magnetoelastic energy

The volume of a single fir tree branch $= \frac{1}{12\sqrt{2}} D^3 \frac{\sin^2\delta}{\tan\psi}$

The number of fir trees for a unit length of main wall

$$= \frac{1}{\sqrt{2}\frac{D \tan\delta}{\tan\psi} + \frac{k\sqrt{2} D \tan\delta}{\tan\psi}}$$

Therefore the volume of fir tree structures in a surface area $D/2$ is

$$\frac{D^3 \sin^2\delta}{12\sqrt{2} \tan\delta D\sqrt{2}(1+k)}$$

The magnetoelastic energy is independent of ψ, and consequently α, as it is derived from the product of the fir tree volume and the magnetoelastic energy density.

Bloch Wall energy

As both the magnetoelastic and magnetostatic energies are independent of α the equilibrium value of α must be found from the wall energy term alone.

Spacek gives the surface area of a single fir tree branch as

$$\frac{D^2}{2\sqrt{2}} \frac{\tan \delta}{\sin \psi}$$

To this must be added a second order term which takes into account the fact that the fir tree walls lie at 45° to the main domain wall.

The surface area becomes

$$\frac{D^2}{2\sqrt{2}} \frac{\tan \delta}{\sin \psi} + \frac{D^2}{4\sqrt{2}} \tan^3\delta \frac{\cos^2\psi}{\sin^3\psi} \qquad (4.10)$$

The total Bloch wall energy for the fir trees existing in a surface area $D/2$. is

$$\left[\frac{D^2}{2\sqrt{2}} \frac{\tan\delta}{\sin\psi} + \frac{D^2}{4\sqrt{2}} \tan^3\delta \frac{\cos^2\psi}{\sin^3\psi}\right] \frac{\tan\psi}{\sqrt{2}\, D \tan\delta (1+k)}$$

The energy of a 90° Bloch wall has been expressed by Kaczer (1959) as

$$\gamma = \gamma_o \, (1.7274 - 1.2289 \cos \psi + 0.5015 \cos^2\psi)$$

Taking the value of γ_o used by Spacek, the wall energy for a surface area $D/2$ is given by

$$\frac{D}{2\sqrt{2}(1+k)} \left[\frac{1}{\cos\psi} + \frac{1}{2} \tan^2\delta \frac{\cos\psi}{\sin^2\psi}\right] [1.59 - 1.13\cos\psi + 0.461\cos^2\psi]$$

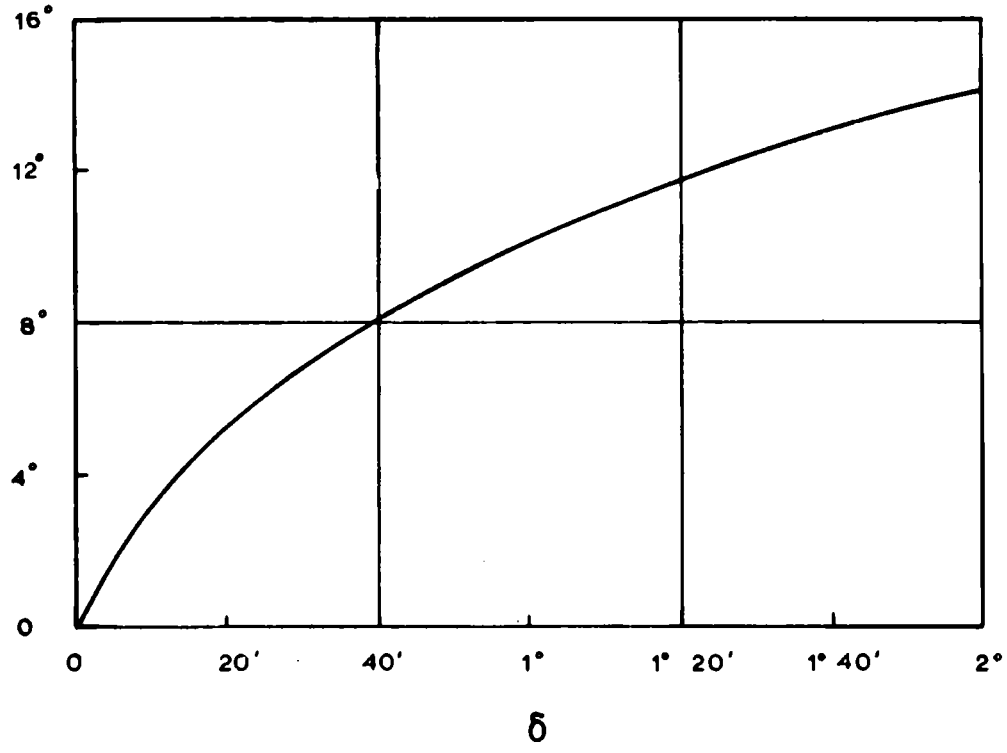

Variation of α with δ for all values of D and n

FIG. 50

Minimising this with respect to ψ, the equation

$$\frac{1.59\sin\psi}{\cos^2\psi} - 0.461\sin\psi - \frac{\tan^2\delta}{2\sin^2\psi}\left[1.59(1+\cos^2\psi) - 1.13\cos\psi + 0.461(3\cos^2\psi - \cos^4\psi)\right] = 0$$

is obtained.

This equation was solved graphically for various values of δ. The values of ψ were converted to α, and the resulting $\alpha\delta$ relationship is shown in Fig. 50. The value of α for $\delta = 1^{\circ}$ is 10° which seems in quite good agreement with available experimental results.

It is important to note that these values of α are independent of D and k, whereas Spacek's theory showed α to be strongly dependent on D and also k. This latter fact invalidates the results of Spacek because as δ varies from 0 to 1.5°, k changes from ∞ to 0, and by putting k = 1 Spacek ignores this large range of variation.

4.5.3.2. Variation of Fir tree spacing a with δ

Unfortunately there are no experimental results showing the effect of inclination of the [010] direction to the surface upon the fir tree angle α, in order to confirm the theoretical results obtained above. As Bozorth, Williams and Shockley (1949) did make measurements of the variation of a with δ, these can provide a basis for the confirmation of theoretical results under

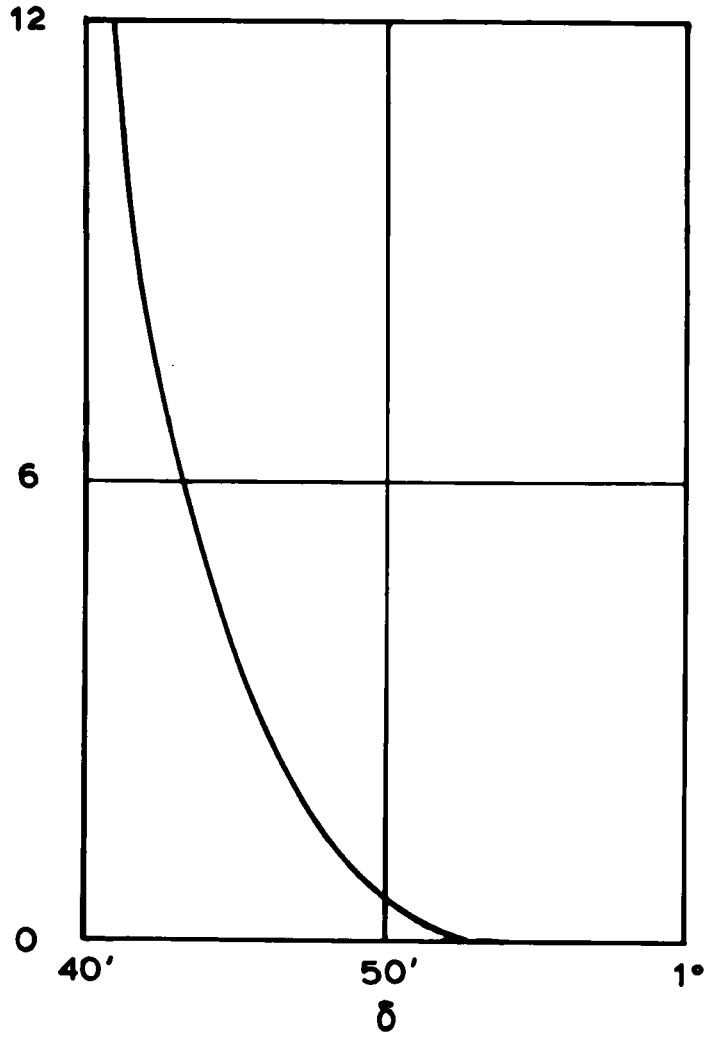

Variation of fir tree spacing a with deviation of surface from (100) plane

FIG. 51

zero stress conditions. Taking $y = D/2$.

The magnetoelastic energy of the fir tree domains for a surface area $D/2$ becomes

$$\frac{1}{24\sqrt{2}} \frac{D^3 \sin^2\delta\, c_{44}\lambda_{100}^2}{[\sqrt{2}D\tan\delta + a\tan\psi]} \qquad (4.11)$$

The wall energy for surface area $D/2$

$$= \frac{D^2}{2\sqrt{2}} \frac{\tan\delta[1.59 - 1.13\cos\psi + 0.461\cos^2\psi]}{\cos\psi[\sqrt{2}D\tan\delta + a\tan\psi]} \qquad (4.12)$$

The magnetostatic energy for a surface area $D/2$

$$= \frac{8I^2\sin^2\delta D^2\left[\pi a + \frac{2\sqrt{2}D\tan\delta}{\tan\psi}\right]^2}{\pi^4(1+\mu^4)\left[a + \frac{\sqrt{2}D\tan\delta}{\tan\psi}\right]^2} \qquad (4.13)$$

$$E_{TOTAL} = E_{m.e} + E_{WALL} + E_{m.s.}$$

Minimising the total energy with respect to a gives the following expression

$$\left[a\tan\psi + \sqrt{2}D\tan\delta\right]\left\{\frac{Dc_{44}\lambda_{100}^2}{24\sqrt{2}}\sin\delta + \frac{1.59 - 1.13\cos\psi + 0.461\cos^2\psi}{2\sqrt{2}\cos\psi}\right\}$$

$$= \frac{16\sqrt{2}D\sin^2\delta I^2\left[\pi a\tan\psi + 2\sqrt{2}D\tan\delta\right]}{\pi^4(1+\mu^4)}$$

By substituting various values of δ into the above equation, and at the same time the value of ψ corresponding to this (as shown in previous section), the value of a/D equivalent to a specific δ can be calculated. The relationship is shown in Fig. 51. It shows that at $\delta = 55'$ $a = 0$ while at $\delta = 41'$ $a \to \infty$. Between these limits a varies very rapidly with δ. The results obtained by

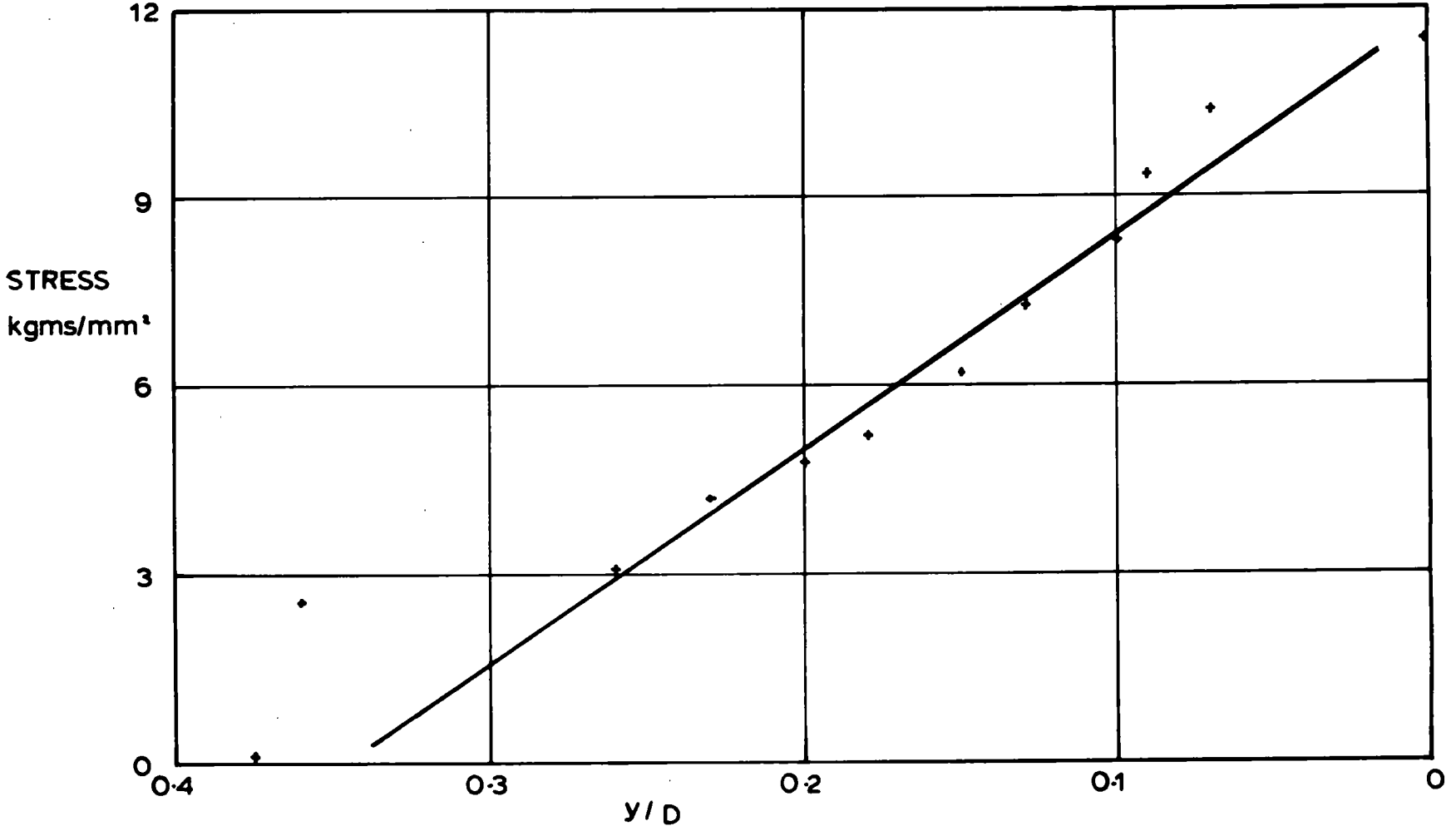

Variation of length of fir tree with stress : $a_0 = 0$: $\alpha = 14°$: $\delta = 1°\ 40'$

FIG. 52

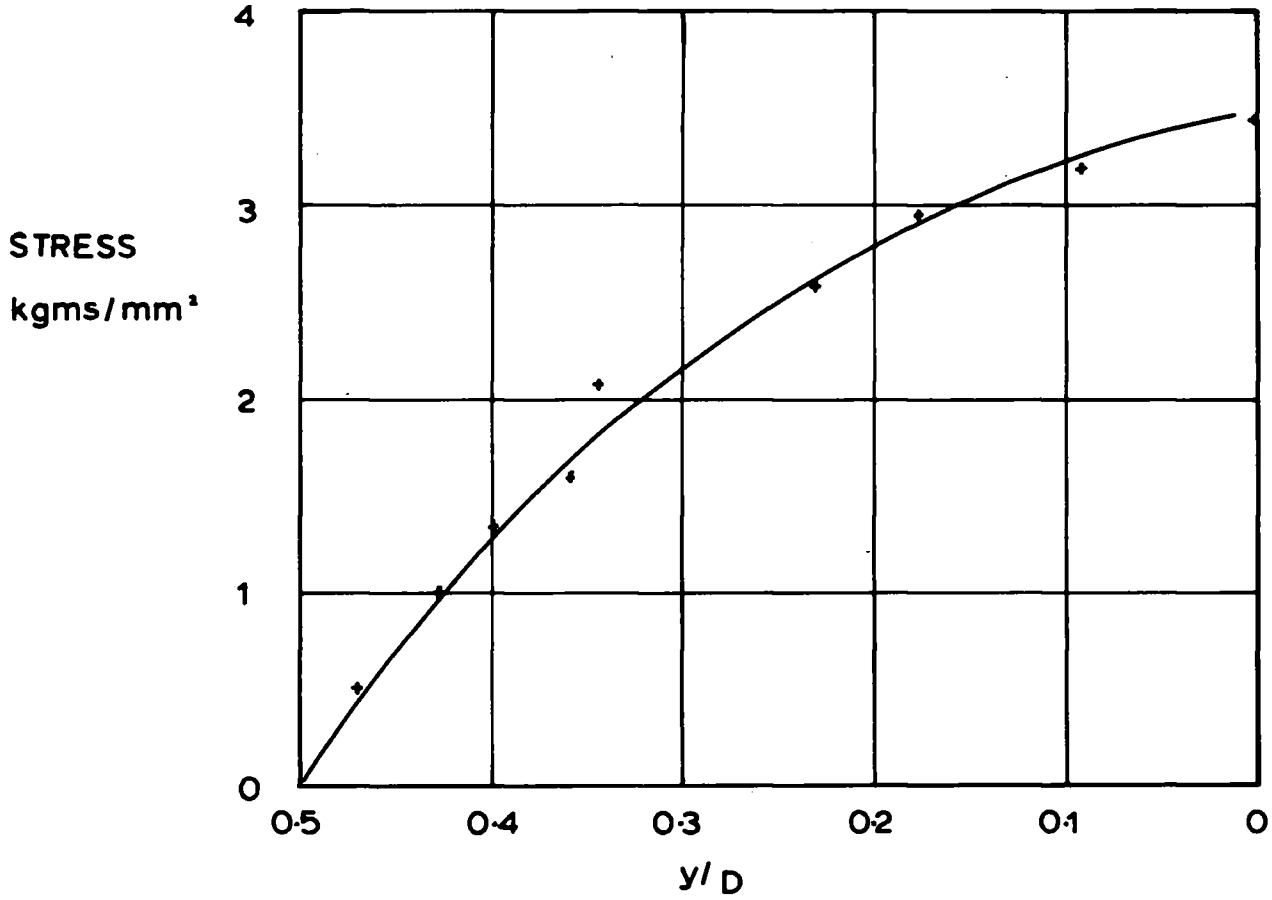

Experimental variation of length of fir trees with stress
$a_o = 2y_o\alpha$: $\alpha \equiv 7°$ indicating $\delta \equiv 40'$.

FIG. 53

Bozorth (1949) show that at $\delta = 1^{o}\ 18'$ $a = 0$, at $\delta = 1^{o}$ $a/D = 1/17$ and in the range δ 0' to 30' there are no fir trees i.e. $a \to \infty$. Also in the range δ 30' to 40' y increases from 0 to $D/2$.

The theoretical values show a reasonable agreement with experimental results.

4.5.4. Stress applied to fir tree structure

4.5.4.1. Experimental results

Specimens of polycrystalline silicon iron were strained by bending, so that in particular grains showing fir tree structure an extensional force σ dynes/cm^2 was applied along the direction of magnetization of the main domains. This contributes an energy $-\frac{3}{2}\sigma\lambda_{100}$ per unit volume to the main domains making them more favourable than the fir tree structure. Therefore a reduction in fir tree size would be expected with increasing stress.

This was observed experimentally. As the stress was increased the length of the branches y decreased until at stresses varying between 4 kgms/mm^2 and 14 kgms/mm^2 they disappeared altogether. Two typical graphs of y against σ are shown in Figs. 52 and 53. Fig. 52 shows the variation for $a_o = 0$ (the subscript represents the zero stress condition) and an experimental value of α of 14^{o}, which corresponds to $\delta = 1^{o}\ 40'$. The second graph Fig. 53 shows the variation for $a_o = 2y_o\alpha$, the value of $\alpha = 7^{o}$

indicating δ to be 40'.

An important result observed was that the number of fir trees per unit length of the main wall remained constant with varying stress. As far as could be measured α also remained constant with stress, although this angle became very difficult to measure when the length of the fir tree tended to zero.

4.5.4.2. Theoretical Considerations

The variation of the fir tree angle α with stress does not depend upon the value of the wall energy γ_{min}, at the minimum position, but depends upon the size of ψ_{min}. It seems likely however, upon considering previous work on the variation of ψ_{min} with stress, that in the range 0 - 15 kgms/mm^2 ψ_{min} will remain effectively constant. It will therefore be assumed that α remains constant.

Converting values of ψ to α in equations (4.11), (4.12) and (4.13) and adding an extra term due to the effect of stress on the main domains, the total energy of the system, for a surface area $D/2$, can be written as

$$\frac{8D^2I^2\sin^2\delta}{\pi^2(1+\mu^2)(a+2y\alpha)^2}\left[a+\frac{2D\alpha}{\pi}\sin\frac{\pi y}{D}\right]^2-\left[\frac{D}{2}-\frac{1}{3}\frac{y^3\alpha\sin\delta}{(a+2y\alpha)}\right]\frac{3}{2}\sigma\lambda_{100}$$
$$+\frac{1}{6}c_{11}\lambda_{100}^2\frac{y^3\alpha\sin\delta}{a+2y\alpha}+\frac{\gamma}{a+2y\alpha}y^2\sqrt{\alpha^2+2\delta^2} \qquad (4.14)$$

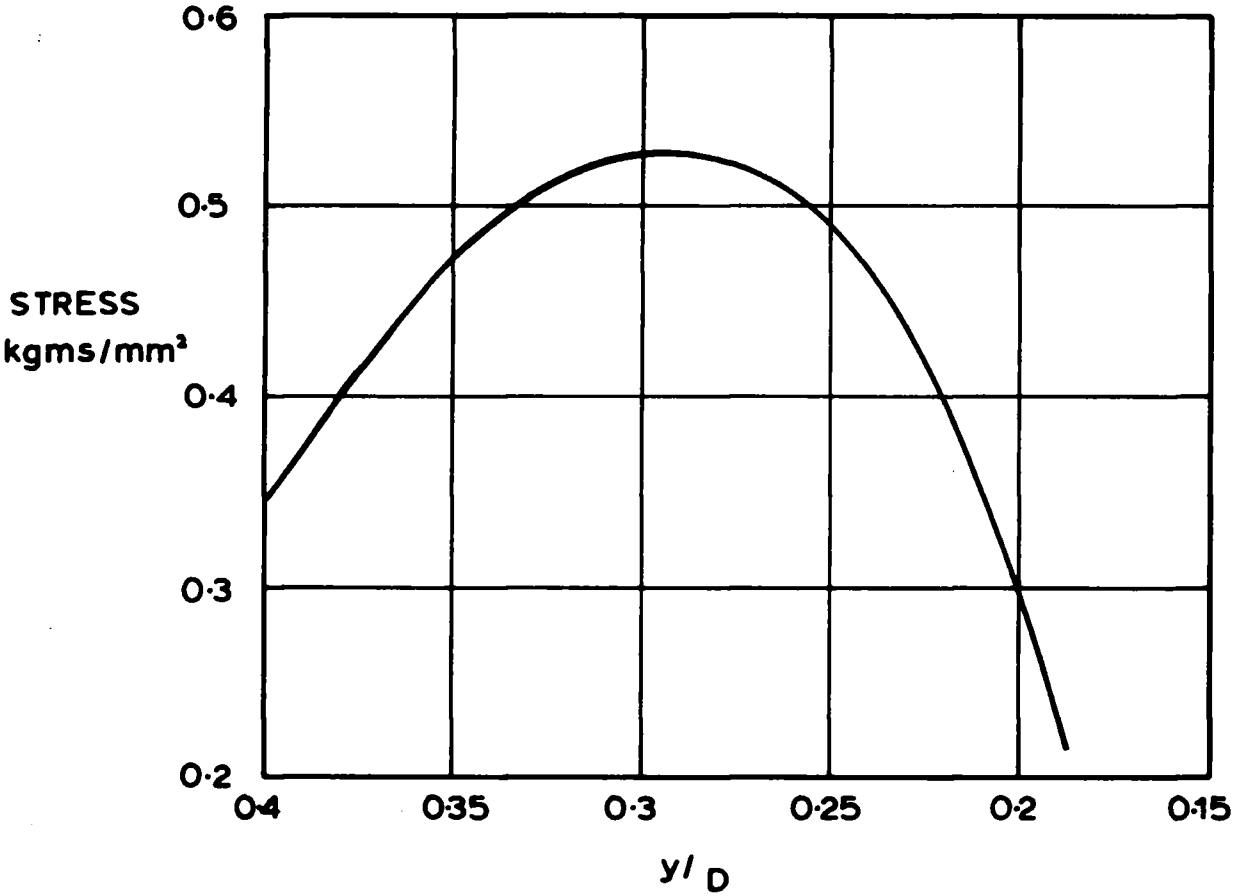

Theoretical relationship between the fir tree length and the applied stress. $\alpha_o = 0$: $y_o = D/2$: $\delta = 51'$

FIG. 54

If the length of the fir tree at zero stress is y_o and the initial separation of the fir trees a_o, then the number of fir trees per unit length of main wall

$$= \frac{1}{2y_o\alpha + a_o}$$

When the length of the fir tree changes to y

$$a = a_o + 2y_o\alpha - 2y\alpha$$

Substituting this into equation (4.14) gives

$$\frac{8D^2I^2\sin^2\delta}{\pi^2(1+\mu^2)(a_o+2y_o\alpha)^2}\left[a_o + 2y_o\alpha - 2y\alpha + \frac{2D\delta}{\pi}\sin\frac{\pi y}{D}\right]^2$$
$$- \left[\frac{D}{2} - \frac{1}{3}\frac{y^3\alpha\sin\delta}{a_o+2y_o\alpha}\right]\frac{3}{2}\sigma\lambda_{100} + \frac{c_o\lambda_{100}^2 y^3\alpha\sin\delta}{6(a_o+2y_o\alpha)} + \frac{\gamma y^2\sqrt{\alpha^2+2\delta^2}}{a_o+2y_o\alpha} \qquad (4.15)$$

This equation can now be minimised with respect to y. Taking $a_o=0$, and $\delta = 1^o$, which corresponds to the first case to be considered, one obtains.

$$4.01\left[1 - 2\left(\frac{y}{D}\right) + \frac{2}{\pi}\sin\frac{\pi y}{D}\right]\left[\cos\frac{\pi y}{D} - 1\right] + \left(\frac{y}{D}\right)^2\left[5.39\sigma + 0.922\right]$$
$$+ 1.84\left(\frac{y}{D}\right) = 0$$

Solving this equation graphically a series of values of (y/D) are obtained corresponding to various values of δ, which are shown in Fig. 54. It can be seen that y/D decreases with increasing stress until a stress of .5 kgms/mm^2 is reached when a reduction of y/D is accompanied by a reduction in stress. Experimentally this would mean that fir trees could not exist with y/D less than .28. At a stress of .5 kgms/mm^2 the fir trees would disappear.

As this does not agree with the experimental values (Fig. 52) the instability below a specific value of y/D could probably be brought into line with theory by a reduction in α with stress. Nevertheless the value of the stress required to cause the fir trees to disappear is experimentally a factor of 10 times larger than the theoretical value.

A family of curves similar to Fig. 54 can be obtained for various zero stress conditions. As δ decreases, the curves still remain the same shape but σ_{max} decreases and $(y/D)_{max}$ increases. For instance, when $a_o = 2y_o\alpha$ ($\delta = 45'$) a value of σ_{max} of 0.08 kgms/mm^2 was obtained. This does not compare very well with the experimental value of 4 kgms/mm^2 (Fig. 53.)

4.5.4.3. Conclusion

The proposed magnetostatic energy model, combined with the fir tree structure proposed by Spacek, gives results which are in quite good agreement with experiment when dealing with the stress free case. However it seems to break down when dealing with the fir trees under stress. This seems to indicate that the model is fairly good in predicting the variation of magnetostatic energy with a, but not so accurate when dealing with the variation of y.

CHAPTER FIVE

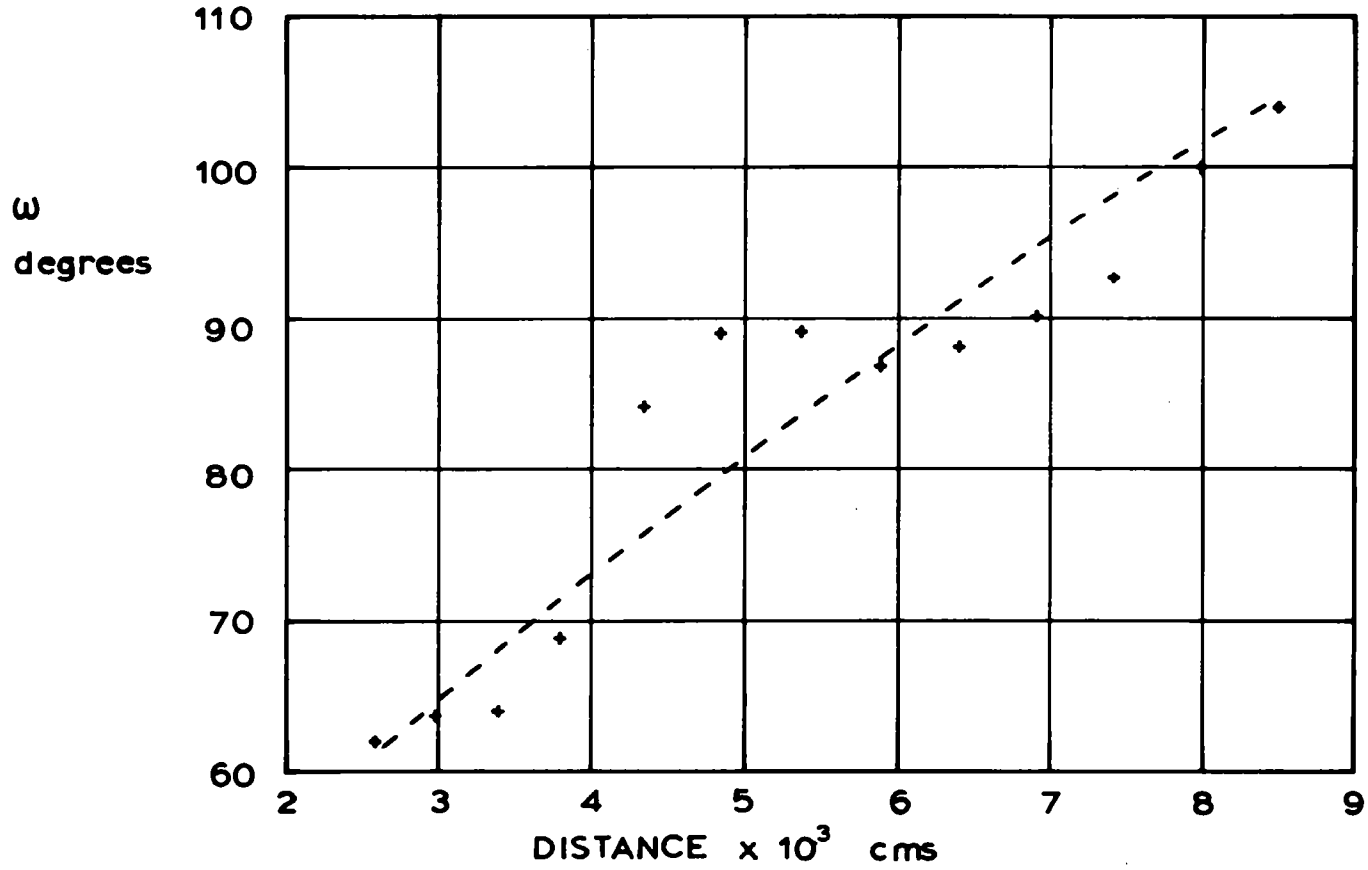

Typical graph of the variation of zig zag angle with distance from a scratch on a (100) surface

FIG. 55

CHAPTER FIVE

THE EFFECT OF SCRATCHES ON (100) AND (110) SURFACES

5.1. Scratches on a (100) Surface

The work of Chikazumi and Suzuki, in which they obtained strain patterns on (100) surfaces of silicon iron by drawing a deep scratch on the surface of the specimen, has been described in section 4.1.1. This work was repeated and identical experimental results were obtained. From the width of the scratch produced, 1.1×10^{-2} cms, and the size of the applied load, 1 kgm, the pressure on the scratch can be calculated to be approximately 100 kgms/mm^2. The distribution of stresses near the scratch is not known, though Chikazumi and Suzuki assumed them to be tensional forces normal to the surface.

A zig-zag structure is observed with the zig-zag walls running along the [001] direction when the scratch lies in a [010] direction (see plate 9). The zig-zags first appear at a distance of about 2.6×10^{-6} cms from the edge of the scratch and disappear at about 9×10^{-3} cms from the scratch. In this range the domain spacing remains constant at 10^{-3} cms, while the zig-zag angle varies from about 60° nearest the scratch to 105° farthest away. A typical variation is shown in Fig. 55.

Assuming that the stress pattern is due to a tensional force, σ dynes/cm^2 normal to the surface, the domain spacing d is given by

$$d = \frac{8\gamma L}{3\lambda_{100}\sigma}^{\frac{1}{2}} \qquad (5.1)$$

Where L is the thickness of the structure.

The zig-zag angle stress relationship, obtained by Chikazumi and Suzuki is shown in Fig. 57.

If L is taken as 0.2 mms, the value used by Chikazumi and Suzuki, a value of σ = 32 kgms/mm^2 can be calculated from equation (5.1), whereas the variation of ω indicates a change of stress along the scratch from 0 kgms/mm^2 to 370 kgms/mm^2. These two results are not entirely incompatible as it may be that L increases with decreasing distance from the scratch so that with σ increasing at the same rate, a constant value of d would result.

What is difficult to imagine is how a compressive force of 100 kgms/mm^2 can change into an extensional force of 370 kgms/mm^2 only 2.6 x 10^{-3} cms away from its point of action. It leaves the variation of ω with σ, obtained by Chikazumi and Suzuki, in some doubt. It will be noticed that in their derivation they ignored the effect of stress on Bloch wall energy.

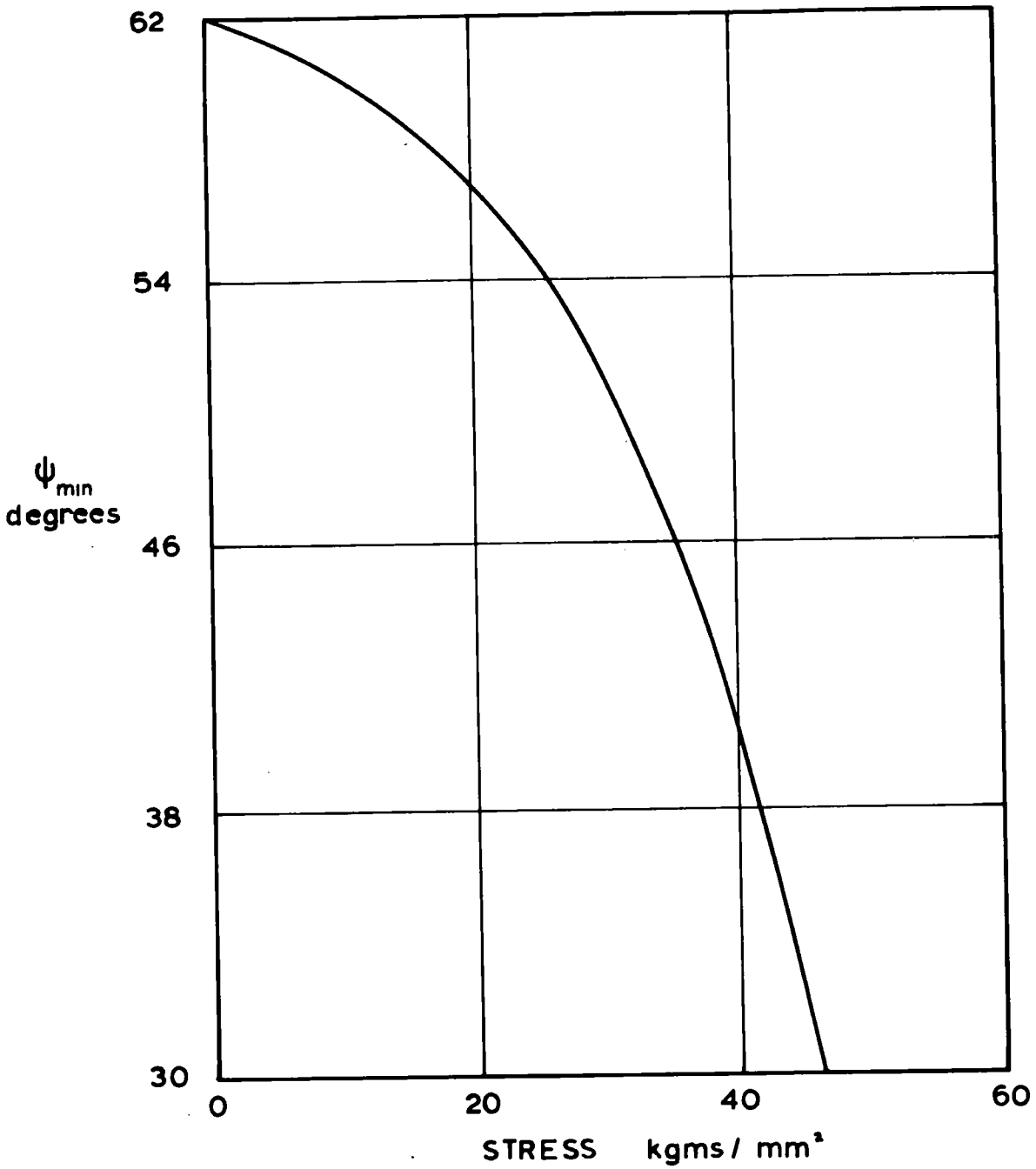

ψ_{min}, (value of ψ corresponding to minimum $\gamma / \sin \psi$) as a function of stress

FIG. 56

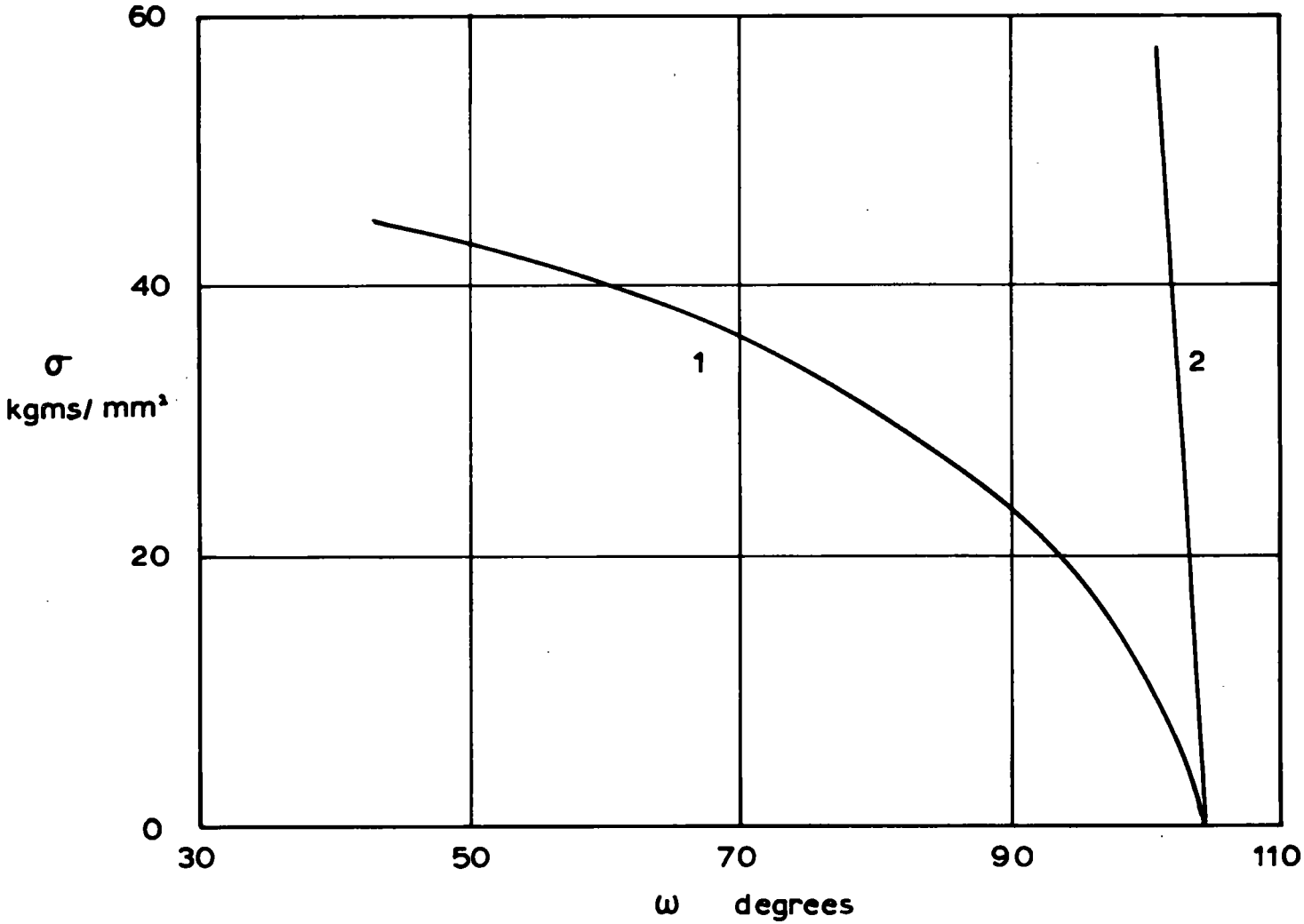

1. Variation of zig-zag angle ω with σ, a tensional stress normal to the surface, allowing for the change of γ with stress
2. Theoretical relationship due to Chikazumi and Suzuki (1955)

FIG. 57

The extent to which this effects the ω,σ relationship will now be considered.

Using the nomenclature as in section 4.1.4.2., the anisotropy energy of the wall, taking into account the effect of the tensional stress σ dynes/cm^2 in a [100] direction, is given by

$$g_o' = \frac{K}{8}\sin^2(\theta+\psi)[3\cos^2(\theta+\psi)+1] - \frac{3}{8}\sigma\lambda_{100}\sin^2(\theta+\psi) \qquad (5.2.)$$

Using this value of g_o' and working out the values of $\gamma/\sin\psi$ for various values of ψ, the value of ψ_{min} for a particular value of σ can be evaluated. The variation is shown in Fig. 56 and ψ can be seen to vary considerably with σ in the range 0 to 60 kgms/mm^2. Therefore in this case this is the main contribution to the variation of ω, with stress, the free pole energy contribution being negligible by comparison.

Converting the angles ψ to ω using

$$\omega = 2.09\ \psi - 25.1$$

the ω,σ variation as shown in Fig. 57 was obtained.

Equation (5.2) tends to zero when

$$\frac{K}{8}\sin^2(\theta+\psi)[3\cos^2(\theta+\psi)+1] = \frac{3}{8}\sigma\lambda_{100}\sin^2(\theta+\psi) \qquad (5.3)$$

Thus for a particular value of ψ the value of σ, σ_{crit}, at which the energy of the wall tends to zero can be evaluated. This corresponds to zero anisotropy, and

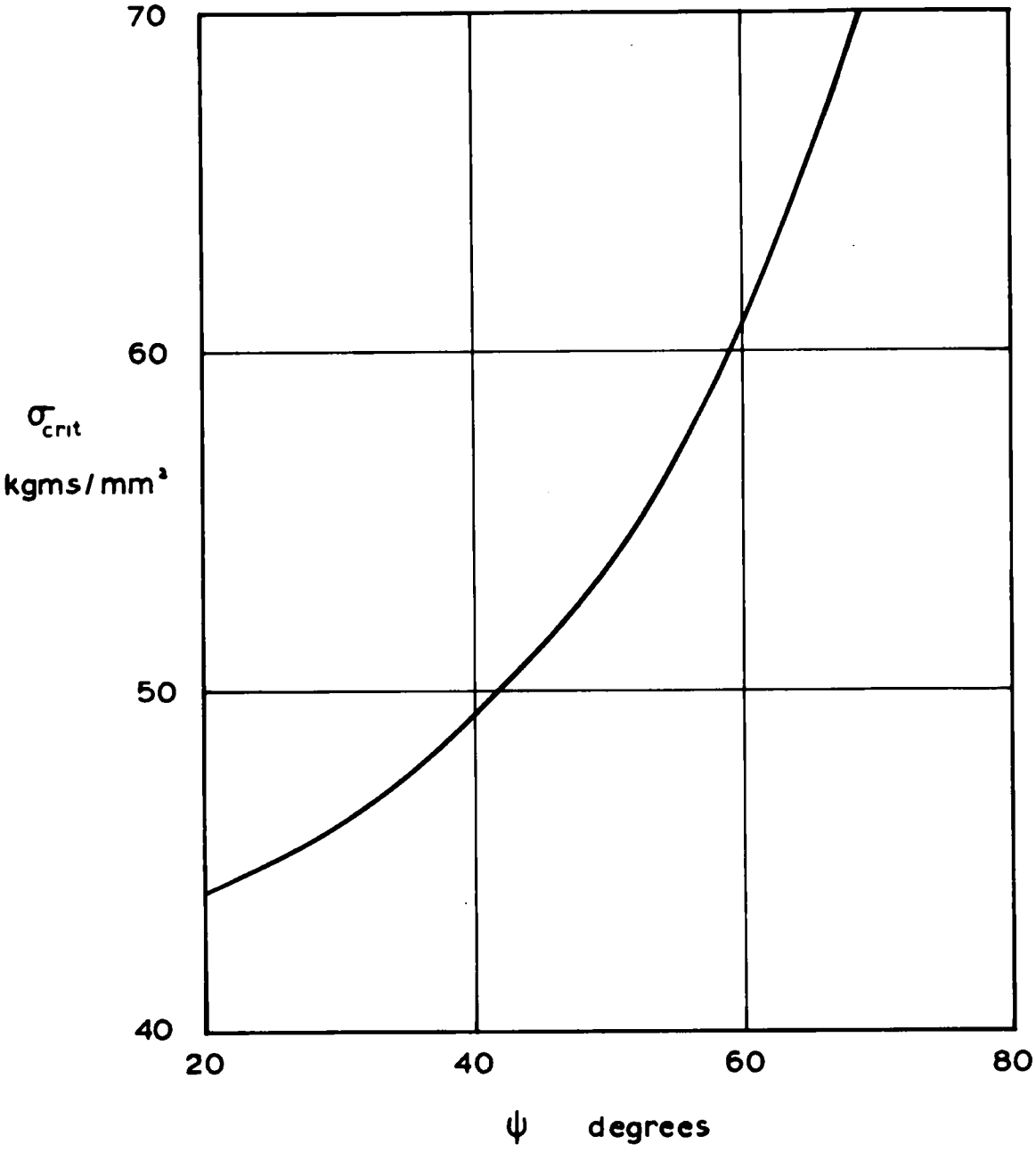

Dependence of cut off stress (value of the tensional stress, normal to the surface, at which the wall becomes infinitely thick) on ψ

FIG. 58

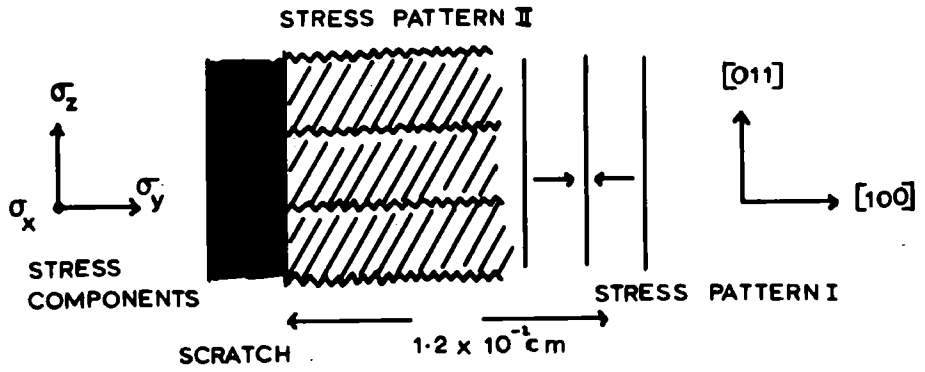

Scratch on a (110) surface

(a)

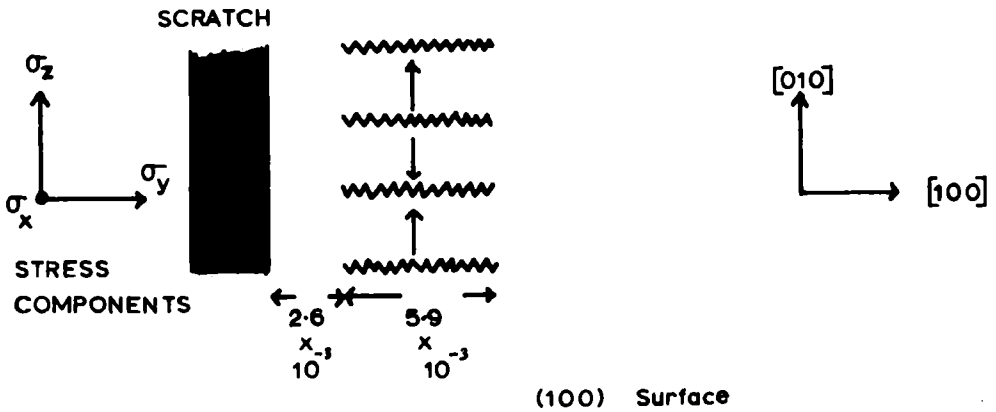

(100) Surface

(b)

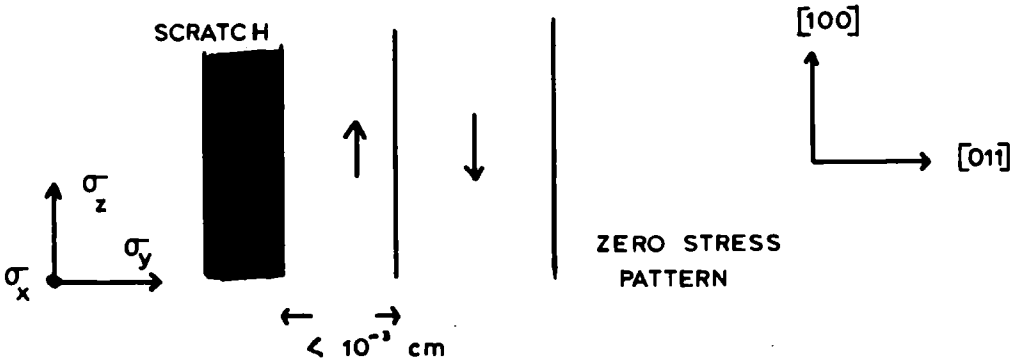

(110) Surface

NOT TO SCALE

(c)

FIG. 59

consequently infinite wall thickness and the disappearance of the zig-zag structure. The variation is shown in Fig. 58. If this is superimposed on the graph in Fig. 57 the value of the cut off angle $\omega_{crit} = 43^{\circ}$ is obtained.

These results are most interesting. They show that the value of σ along the pattern varies from only 10 kgms/mm^2 to 45 kgms/mm^2 which agrees far better with the evaluation of σ from the domain spacing than that obtained by Chikazumi and Suzuki. More important still, they predict a cut off value for ω at 43° while in practice a value of about 50° was obtained (see Fig. 55).

5.2. Scratches on a (110) surface

A scratch was ruled in a [110] direction on a (110) surface of silicon iron using a ball pen loaded with a one kgm weight as was used on a (100) surface.

Plate 10 shows the domain structure observed. It consisted of stress pattern II extending from the edge of the scratch for 1.2×10^{-2} cms. The main walls of this structure were in a [100] direction being spaced 2.0×10^{-3} cms apart. (Fig. 59a). Stress pattern II then merged into stress pattern I which extended for a further 3.5×10^{-3} cms.

The change over from stress pattern I to stress pattern II at surface compression stresses of about

20 kgms/mm^2 was explained (see section 3.1.3.4.) as due to the variation of the main wall energies of the two systems under stress. The effect of a tension stress σ dynes/cm^2 along the normal to the surface, on these energies will now be considered.

The energy of the main wall in pattern I increases under the stress by an amount given by

$$\beta' f_m = + \frac{3}{4}\lambda_{100}\sin^2\phi\,[3\lambda_{100}(c_{11}-c_{12}) + \sigma]$$

The energy of the wall given by this reduced anisotropy has been shown in Fig. 21.

The energy of pattern II also increases, this time the reduced anisotropy energy is

$$\beta' f_m = \frac{9}{4}\lambda_{100}^2(c_{11}-c_{12})\sin^2\phi + 3|\lambda_{111}|\sigma\sin\phi\cos\phi$$

Unfortunately the evaluation of the wall energy, which involves an integration of $\beta' f_m^{\frac{1}{2}}$ is made very complicated by the $\sin\phi\cos\phi$ term and has not been carried out. However it seems likely that it does not increase as rapidly with stress as the pattern I energy because the stress term involves λ_{111} which is much smaller than λ_{100}. It is therefore probable that even under a tensional stress σ, pattern II will become more favourable than pattern I at high values of stress.

From the zig-zag spacing on the (100) surface the size of the normal extensive force σ_x can be found to be 30 kgms/mm^2. This cannot be the only stress in the system as the zig-zag walls lie normal to the scratch and not parallel to it. This implies the existence of a small compressive force σ_y normal to the scratch, see Fig. 59. The size of this will not affect the stress energy of the system as the magnetization direction of both the closure domains and the main domains are normal to it.

Assume that the strains produced by the scratches are the same on the (100) surface and the (110) surface. This seems reasonable because near the scratch the specimen has been deformed beyond the yield point.

In all examples let the stress normal to the surface be given by σ_x, that parallel to the scratch by σ_z, and that normal to the scratch by σ_y. Therefore σ_z and σ_y lie in the surface.

In the (110) system, the extensive force σ_x' is related to the tensional force σ_x, normal to the (100) surface, by

$$\frac{\sigma_x'}{Y_{110}} = \frac{\sigma_x}{Y_{100}}$$

$$\sigma_x' = \frac{30 \times 2.06}{1.23} \text{ kgms/mm}^2$$

To simplify the calculations, it will be assumed that stress pattern I exists over the area occupied by stress pattern II. This will not alter the size of the domain spacings.

Consider the energy of the system under the two forces σ_x' and σ_y.

The volume of the closure domains/unit surface area

$$= \frac{d}{2\sqrt{2}}$$

The energy of these domains/unit surface area for compressive stress σ_y

$$= \frac{3}{2} \sigma_y \lambda_{100} \frac{d}{2\sqrt{2}} .$$

Similarly the energy of the main domains

$$= -\frac{3}{4} \sigma_x' \lambda_{100} \left(t - \frac{d}{2\sqrt{2}} \right)$$

The domain wall energy/unit surface area

$$= \left(\frac{t}{d} - \frac{1}{\sqrt{2}} + \sqrt{6} \right) \gamma$$

Neglecting the magnetostatic energy which has been shown before to be negligible in this case, and the effect of stress on domain wall energy, the equilibrium domain spacing d is given by

$$\frac{t\gamma}{d^2} = \frac{3}{4} \frac{\lambda_{100}}{\sqrt{2}} \left[\sigma_y + \frac{\sigma_x'}{2} \right] \qquad (5.4)$$

At a specific distance from the scratch, where σ_x = 30 kgms/mm^2 on a (100) surface, on a (110) surface d = 2.0 x 10^{-3} cms. Assuming the thickness t of the strained layer to be the same in both cases i.e. 0.02 cms

and allowing for the fact that the observed spacing on stress pattern II is $\sqrt{2}d$, a value of

$$\sigma_y = -16 \text{ kgms/mm}^2$$

can be obtained from equation (5.4).

This is obviously an unreasonable result for although this extensive stress, normal to the scratch, is needed to explain the structure on a (110) surface, it would mean that on a (110) surface the zig-zag walls should lie parallel to the scratch.

Even though the tensional force normal to the surface explains the zig-zag structure on a (100) surface very well, it seems necessary to consider other stress distributions to interpret the stress patterns produced on all surfaces.

5.3. Stress patterns due to compressive surface stresses

Application of external stresses to a (100) surface has shown that zig-zag structures can be produced by compressive forces acting along the surface easy directions.

Therefore it will be assumed that the scratch produces compressive forces σ_y and σ_z in the surface with no force normal to the surface. For a (100) surface the domain spacing d will depend upon σ_z, which has been shown previously to be 30 kgms/mm^2. For the zig-zags to exist normal to the scratch $\sigma_y > \sigma_z$.

A (110) Surface

Using the same structure as was considered when dealing with a tensional stress normal to the surface (see previous section) the energy of the system can be written

$$E_{TOT} = \left(t/d - \frac{1}{\sqrt{2}} + \sqrt{6}\right)\gamma + \frac{3}{2}\sigma_y \lambda_{100} \frac{d}{2\sqrt{2}} + \frac{3}{4}\lambda_{100}\sigma_z\left(t - \frac{d}{2\sqrt{2}}\right)$$

Minimising this with respect to d, the equilibrium spacing as a function of stress is given by

$$\frac{t\gamma}{d^2} = \frac{3\lambda_{100}}{4\sqrt{2}}\left(\sigma_y - \frac{\sigma_z}{2}\right) \qquad (5.5)$$

Substituting into equation 5.5 the values used before gives

$$\sigma_y = 36 \text{ kgms/mm}^2$$

As the normal to the scratch on a (110) and (100) surface is a [010] direction, the above stress obeys the requirements of a (100) surface also as

$$\sigma_y > \sigma_z$$

This stress distribution can now be applied to a similar scratch in a [001] direction on a (110) surface. Plate 11 shows the stress pattern obtained. At the distance from the scratch considered above, 6×10^{-3} cms, there is no stress pattern. Instead the zero stress structure, with magnetization along the 001 surface easy direction, exists.

In this case the stress normal to the scratch is given by

$$\frac{36 \times 2.06}{1.23} \text{ kgms/mm}^2.$$

If a stress pattern existed, the main domains would be magnetized in a [010] direction, and the stress energy associated with this direction of magnetization is

$$\frac{3}{2} \sigma_y \lambda_{\underline{100}}$$
$$= 45.2 \lambda_{100}$$

The energy associated with magnetization in the surface easy direction

$$\frac{3}{2} \lambda_{100} \sigma_z$$
$$= 45 \lambda_{100}.$$

A stress pattern would not be expected to exist as the surface easy direction remains easier than the other possible magnetization directions. This agrees with the experimental observations.

5.4. Suggestion for the variation of ω with distance from the scratch

The proposed system of surface stresses seems to agree quite well with experimental results at a fixed distance 6×10^{-3} cms from the scratch. No suggestion has been made as to the variation of these stresses with distance from the scratch. This is because it is impos-

sible to infer this from the surface structure as the variation of the thickness of the strained layer with distance is not known.

The variation of siz-zag angle with different surface forces $\sigma_y = \sigma_z$ is shown in Fig. 35. If σ_y equals 36 kgms/mm^2 at all points along the zig-zag structure then w should remain constant.

Consider how the zig-zag angle alters for values of σ_y ranging from 60 kgms/mm^2 to 270 kgms/mm^2 with σ_z constant at 30 kgms/mm^2.

The anisotropy energy term in the expression for the wall energy can be written

$$g_o' = \frac{K}{8}\sin^2(\theta+\psi)\left[3\cos^2(\theta+\psi)+1\right] + \frac{3}{4}\sigma_{zy}\left[\frac{1}{2}\sin^2(\theta+\psi)\gamma_2^2 + \cos^2(\theta+\psi)\gamma_3^2\right]$$

The table below shows the values of γ_2 and γ_3, the stress direction cosines for various values of σ_y.

σ_y kgms/mm^2	γ_2	γ_3	σ_{yz} kgms/mm^2
60	63° 26'	26° 34'	67.08
90	71° 34'	18° 26'	94.89
150	78° 42'	11° 18'	153.1
200	81° 29'	8° 31'	202.8
270	83° 40'	6° 20'	273.0

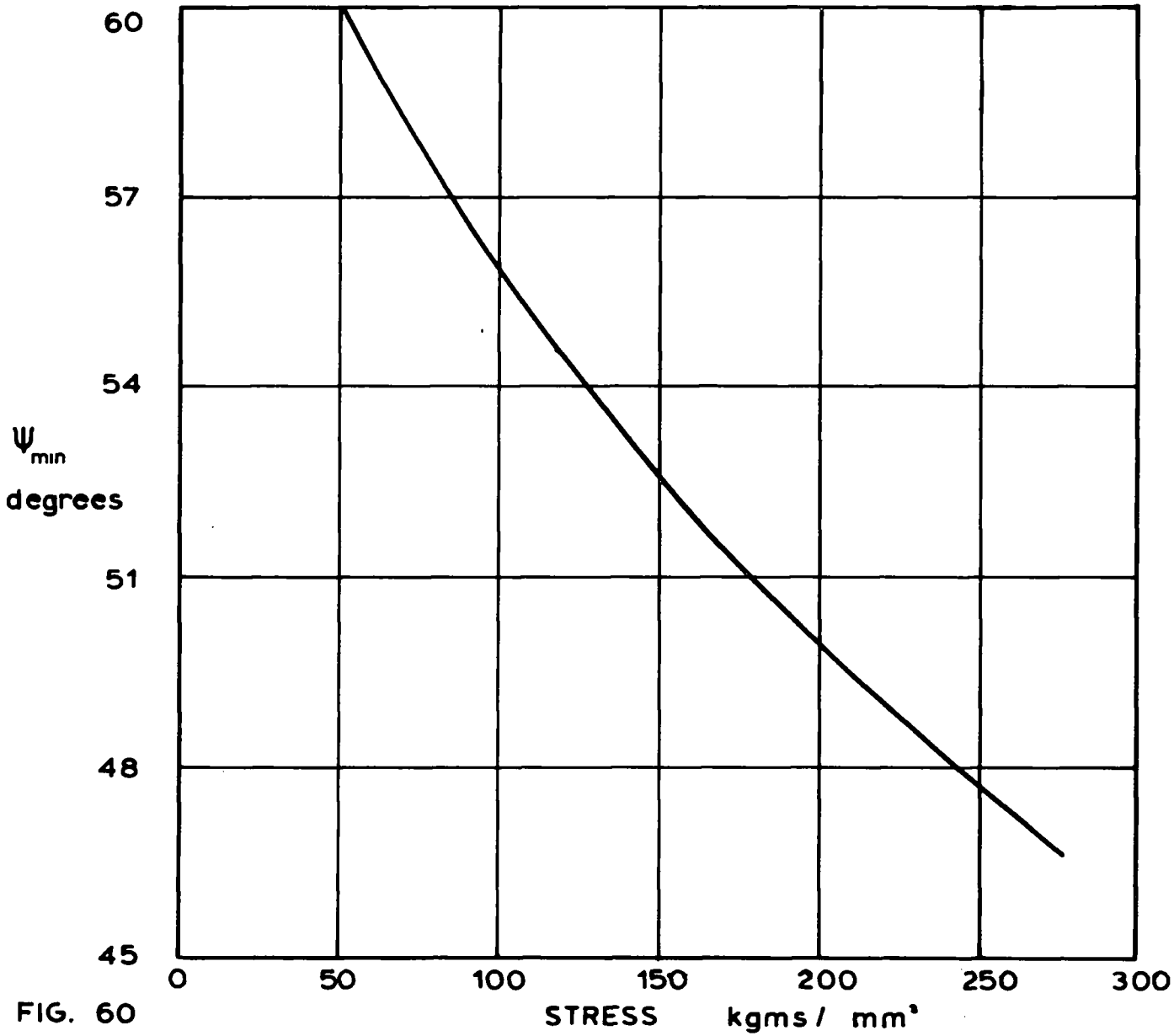

FIG. 60

Variation of ψ_{min} with σ_2. The other surface stress is constant at 30kgm/mm²

Fig. 60 shows the variation of ψ_{min} with σ_z. It is therefore possible that the decrease in ω, and consequently ψ, with decrease in distance from the scratch can be explained by the increase in σ_y. The value of ω, not allowing for the effect of free pole formation on the walls for σ_y = 300 kgms/mm^2 is 71°.

However this treatment does not predict a cut off value of ω. This is only one way of dealing with the problem of a variation of ω with constant zig-zag spacing. One could consider σ_z increasing with L increasing at the same rate or the variation of a compressive force normal to the surface σ_x, so that $\sigma_y - \sigma_x$ remained constant while σ_z increased. The actual stress variation is probably a combination of all three.

5.5. Stress Patterns on the Scratches

The scratched surfaces were electropolished for 7 minutes. This was enough to remove the damanged layer caused by the load but left the surrounding stress pattern very much as before.

No domain patterns were observed on scratches on the (100) plane. The structure on the scratch in a [100] direction on a (110) surface is shown in plate 12. It consists of domains magnetized in the easy direction nearest the surface separated by 180° Bloch walls. The domain spacing is rather variable but the order of 1.5×10^{-3} cms.

A scratch in a [110] direction produces a domain structure consisting of Bloch walls in a [110] direction with a spacing of about 10^{-3} cms, as shown in plate 13. A small vertical magnetic field polarized the magnetic colloid on alternate walls indicating that the structure is stress pattern I with surface closure domains and main [100] domains. Therefore the domain structure changes from stress pattern I to stress pattern II and back to stress pattern I, with distance from the centre of the scratch.

Any explanation of the patterns on a scratch on a (110) surface by a combination of stresses fails to explain the non-appearance of a domain structure on a scratch on a (100) surface.

CHAPTER SIX

CHAPTER SIX

SUMMARY OF RESULTS

The work on the effect of a tensional force in a [110] direction on a (110) surface proved quite satisfactory. The results of Dijkstra and Martius, and also their interpretation were found to be inaccurate and not comprehensive. The accuracy of the experiment was improved by using a bending technique, while a more detailed interpretation of the results was carried out. This involved a theoretical study of the effect of stress on Bloch walls and the proposal of a structure for stress pattern II, both of which agreed well with experimental results. The main gap in this work is the lack of knowledge of the domain structure in the transitional stress range between the zero stress pattern and the stress pattern I. However, interesting information might be obtained of this region if the specimens were examined by the Kerr magneto-optical effect.

The main inconsistencies in this work, and also work on (100) surfaces seemed to be the residual strain in the specimen which is in a supposed stress free state. Even though specimens were prepared using the most strain free methods possible, and then well annealed, measurements seemed to indicate internal stress of up to 10 kgms/mm^2.

A tensional force in a [100] direction on a (110) surface gave rather negative results. Theory predicts an increase, admittedly very small, in the stress range used, in the domain spacing, whereas experiment showed this spacing to be constant. Previous workers indicated that under such circumstances the domain spacing had decreased. This problem could be better resolved by using a specimen with a similar yield point and magnetic anisotropy as iron but with a much higher magnetostriction constant. It would mean that the effect of stress would be much more pronounced than in the case of iron. 50% nickel iron might be useful with its low anisotropy 5×19^3 ergs/cm^2 and λ equal to 25×10^{-6}, although the magnitude of the anisotropy indicates that a magneto-optical method would probably be necessary.

The explanation of the removal of dagger structures from a surface, a few degrees off a (110) plane, by the application of a tensional stress along the [100] direction, as due to the rotation of the minimum energy position of the 180° wall and not the rotation of the magnetization direction into the surface, was supported by experimental evidence.

The application of a compressive stress in a [110] direction on a (100) surface gave experimental verification for the relationship between the inverse square of

the zig-zag spacing and the applied stress. The results of the relationship between zig-zag angle and stress were rather variable due probably to small stress irregularities in the specimen. In these respects a homogeneous crystal, such as an iron whisker, would be useful even though difficulties in manipulation and the application of small stresses would have to be overcome.

A modification of the theory of Chikazumi and Suzuki shows that in this stress range the zig-zag angle should remain effectively constant. However, the same modification, when applied to the variation of zig-zag angle with stress, directed normal to the surface in a [100] direction, predicts a different variation to the above one, with a specific cut off value. Unfortunately an experimental verification was not possible.

The main drawback of the experiments on a (100) surface concerning the change of the magnetization from one surface easy direction to another, by the application of stress, was the complexity of the systems under observation. Results showed that the change over occurred in a very small stress range, perhaps less than 1 kgms/mm^2. More useful information about the mechanism of change over would probably be obtained by using an iron whisker which has a much simplified domain structure.

Fir tree structures were investigated. The papers of Spacek, in which he proposed a new fir tree model, were criticised with respect to the expression for the magnetostatic energy of the system. Using another expression for this, relationships between the size of the fir trees and the orientation of the surface were evaluated for stress free systems. These agreed well with the available experimental results. Unfortunately these are rather incomplete and there is room for systematic work on 1) the variation of the angle of tip with the inclination of the surface to a (100) plane, the domain width, being fixed: 2) the variation of the angle of the tip with the domain width, the inclination of the surface being fixed: 3) the variation of the fir tree spacing with the inclination of the surface to a (100) plane.

The application of a tensional stress along the direction of magnetization in the main domains caused the fir trees to decrease in size, as expected, but not as predicted by theory. This is either due to a fault in the theory or, once again, to inconsistencies in the zero stress state of the specimens.

Stress patterns were also obtained by scratching the specimens. This method is of limited use because of the lack of knowledge of the stress distributions so produced.

ACKNOWLEDGMENTS

The author wishes to thank his supervisor, Dr. W.D. Corner, F.Inst.P., for his help and guidance throughout the period of research.

Thanks are also due to:-

Professor G.D. Rochester, F.R.S. for the facilities granted and to the Physics Department Workshop Staff for technical assistance.

W.C. Roe, B.Sc., my fellow research student, for many stimulating discussions and interesting suggestions.

Those research departments, mentioned specifically in the text, from which single crystal and polycrystalline specimens were obtained.

D.S.I.R. for providing a research scholarship from 1958 to 1961.

J.J.M.

October, 1961.

REFERENCES

Barret, C.S., 1943, Structure of Metals, 35. (McGraw Hill, New York).

Bates, L.F., 1957, Bull. Acad. Sci. U.S.S.R., 21, 1134.

Bates, L.F. and Carey, R., 1960, Proc. Phys. Soc., 76, 754.

Bates, L.F. and Hart, A., 1956, Proc. Phys. Soc., B69, 1200.

Bates, L.F. and Martin, D.H., 1956, Proc. Phys. Soc. B69, 145.

Bates, L.F. and Mee, C.D., 1950, J. Sci. Inst., 27, 317.
1952, Proc. Phys. Soc. A65, 129.

Bates, L.F. and Neale, F.E., 1950, Proc. Phys. Soc., A63, 374.

Becker, R. and Doring, W. 1939, Ferromagnetismus. (Springer, Berlin).

Benford, F.G., 1946, Metals Progress, 46, 94.

Bitter, F., 1931, Phys. Rev., 38, 1903.

Bloch, F., 1932, Z. Phys., 74, 295.

Carey, R., 1960, Proc. Phys. Soc., 76, 567.

Chikazumi, S. and Suzuki, K. 1955, J. Phys. Soc. Japan, 10, 523.

Cole, M., Bucklow, I.A. and Grigson, C.W.B., 1961, Brit. J.A.P., 12, 296.

Craik, D.J., 1956, Proc. Phys. Soc., B69, 647.

Dijkstra, L.J. and Martius, U.M., 1953, Rev. Mod. Phys., 25, 146.

Dijkstra, L.J. and Martius, U.M., 1954, Nondestructive Testing, 7, 13.

Elmore, W.C., 1938, Phys. Rev. 54, 310.

Fallot, M., 1936, Ann. de Phys. 6, 305.

Fletcher, G.C., 1954 , Proc. Phys. Soc., A67, 505.

Fowler, C.A. and Fryer, E.M., 1954, Phys. Rev., 94, 52.

Goodenough, J.B., 1954, Phys. Rev., 95, 917.

Graham, C.D., 1957, A.I.E.E. Conf. on Magnetism, 410.
1958, Report No. 58-RL-1948. G.E. Research Lab.

Heisenberg, W., 1928, Z. Phys., 49, 619.

Holden, A.N. and Holloman, J.H., 1949, Trans. A.I.M.M.E. 185, 179.

Kaczer, J., 1958, Czech. J. Phys. 8, 747.

Kaczer, J., and Gemperle, R., 1959, Czech J. Phys., 9, 311.

Kersten, M., 1930, Z. Phys. 62, 253.

Kirenskii, L.V., Dylgerov, V.D. and Savchenko, M.K., 1957, Bull. Acad. Sci. U.S.S.R., 21, 1157.

Kittel, C., 1949, Rev. Mod. Phys., 21, 541.

Langevin, P., 1905, Ann. Chim. Phys. 5, 70.

Lifshitz, E., 1944, J. Phys. U.S.S.R. 8, 337.

Lilley, B.A., 1950, Phil. Mag. 41, 792.

Martin, D.H., 1957, Proc. Phys. Soc., B70, 77.

Martin, D.H. and Bloor, D., 1959, Proc. Phys. Soc., 73, 695.

Neel, L. 1944(a) J. Phys. Rad. 5, 241.

1944(b) J. Phys. Rad. 5, 265.

1944(c) Cah. de Phys. 25, 1.

Nosov, A.V. and Bykov, D.V., 1956, Working Metals by Electro Sparking, H.M.S.O., London.

Shockley, W., 1948, Phys. Rev., 73, 1246.

Shur, Ia. S. and Zaikova, V.A., 1958, Phys. Metals and Metallography, 6, 158.

Slater, J.C., 1930, Phys. Rev., 35, 509.

1930, Phys. Rev. 36, 57.

Spacek, L., 1957, Czech J. Phys. 7, 714.

1958, Czech J. Phys. 8, 411.

1959, Czech J. Phys. 9, 414.

Stephan, W., 1956, Exp. Tech. der Phys., 4, 153.

1957, Exp. Tech. der Phys., 5, 145.

Stoner, E.C., 1950, Rep. Prog. Phys., 13, 112.

Suda, P., 1956, Czech J. Phys., 6, 300.

Tarasov, L.P., 1939, Phys. Rev., 56, 1231.

Van Vleck, J.H., 1938, Phys. Rev., 52, 1178.

Weiss, P., 1907, J. Phys. Theo. Appl., 6, 661.

Williams H.J., Bozorth, R.M. and Shockley, W., 1949, Phys. Rev. 75, 155.

Yensen, T.D., 1915, A.I.E.E., 34, 2601.

1915. A.I.M.E., 53, 274.

PLATES

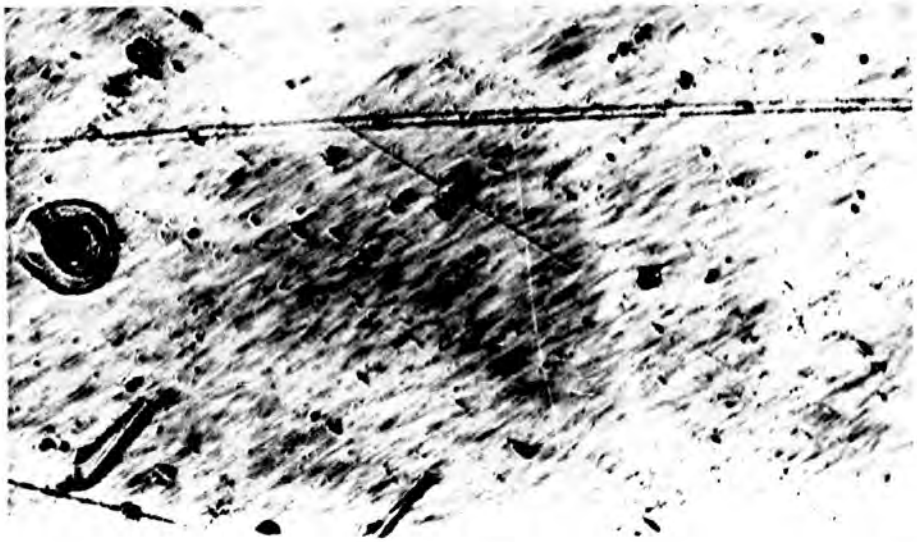

Zero stress pattern. No 180° walls are visible though markings on the surface indicate that the magnetization lies along the [001] direction.

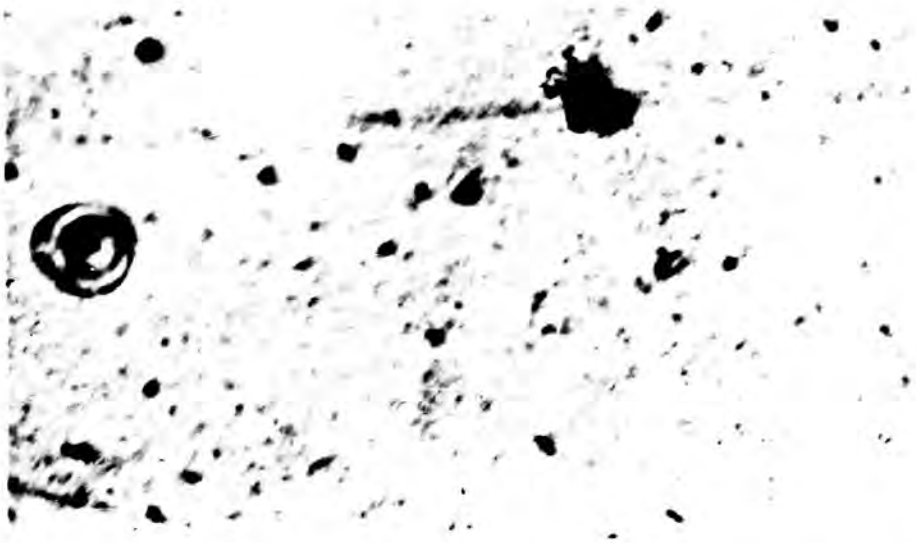

Compressive stress of 0.5 kgms/mm^2 applied along the [001] direction. The photograph shows that there is no visible domain structure.

Scale

0 0·1 mm

PLATE 1

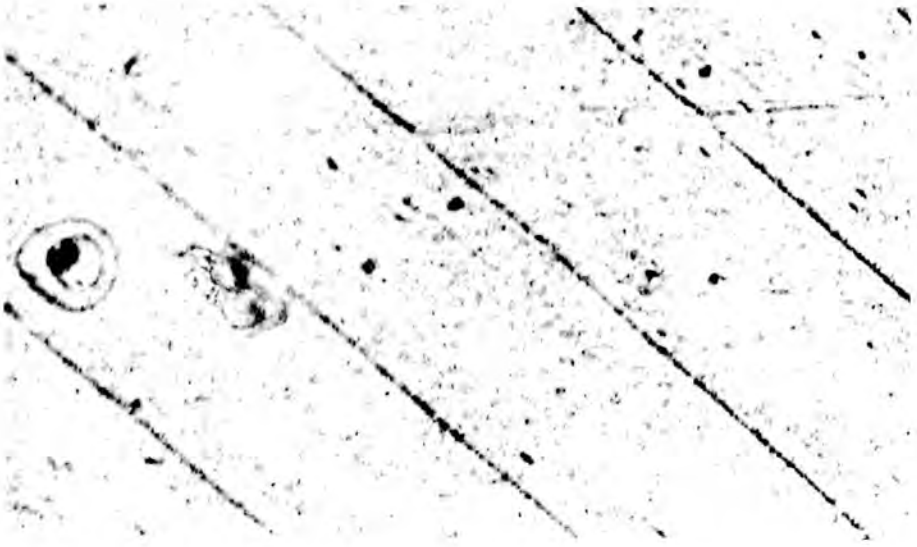

Stress 2.8 kgms/mm^2 in [001] direction. A vertical field of 20 oersteds has been applied. The photograph shows stress pattern I, with the surface closure domains magnetized in the [001] direction.

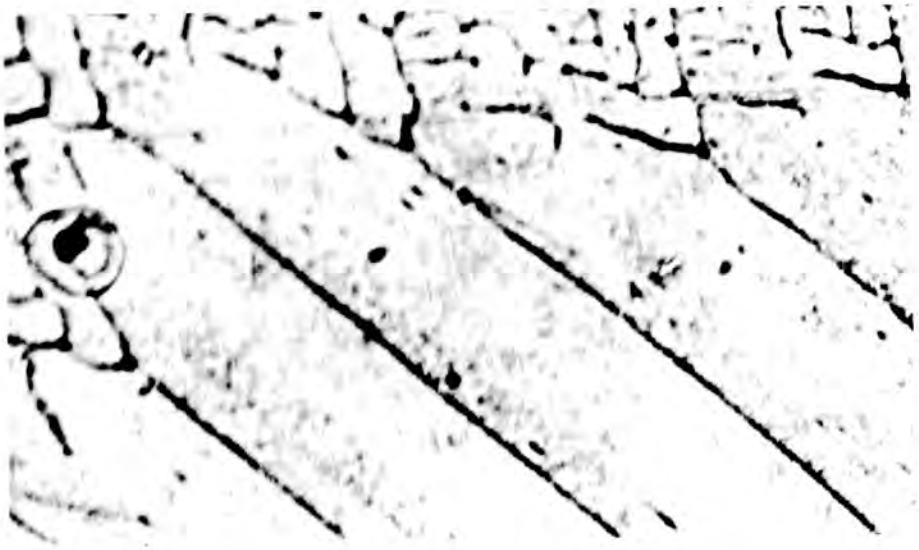

Stress 4.1. kgms/mm^2. Stress pattern II can be seen at the edge of the photograph. It occurs at this low stress because of the presence of a vertical field.

PLATE 1

Stress 6 kgms/mm^2. Increase in area of Pattern II and decrease in Pattern I spacing. Vertical field of 15 oersteds applied.

Stress 6 kgms/mm^2. Vertical field applied in the opposite direction to that in the above photograph. Colloid can be seen to be polarized on alternate walls of Stress Pattern I structure in the two cases.

PLATE 1

Stress 10.3 kgms/mm^2. Vertical field 15 oersteds.

Stress 25.6 kgms/mm^2. Vertical field 15 oersteds. The photograph shows a further decrease in Pattern I spacing.

PLATE 1

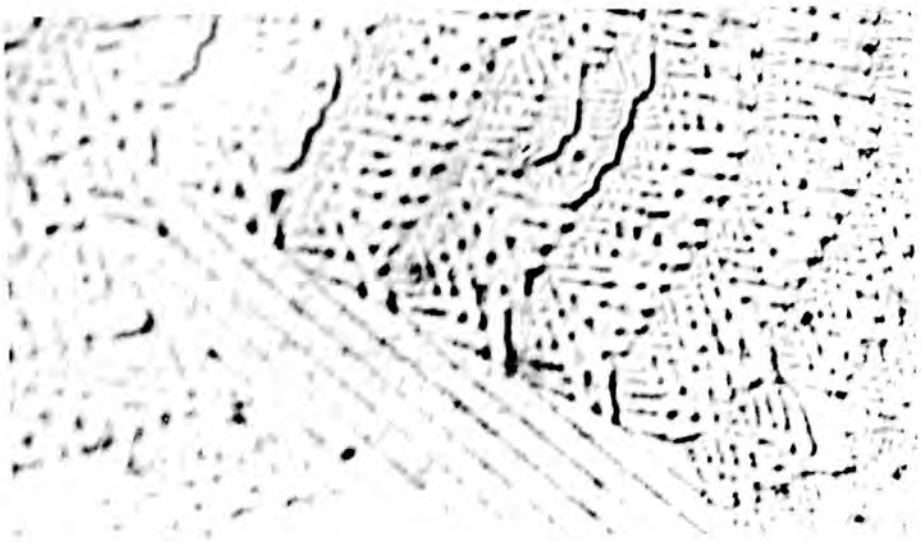

Stress 25.6 kgms/mm^2. No magnetic field.

PLATE 1.

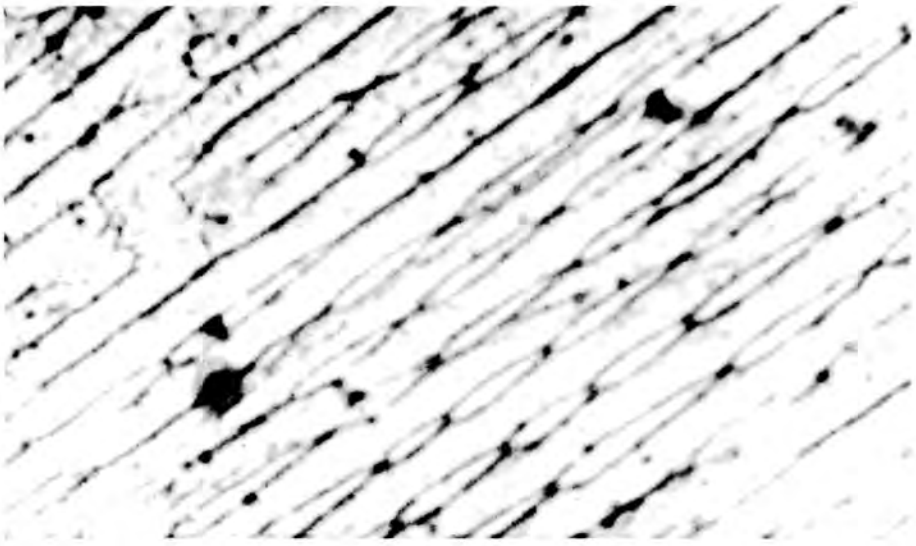

Chain structure at a stress of 36 kgms/mm^2. No magnetic field has been applied.

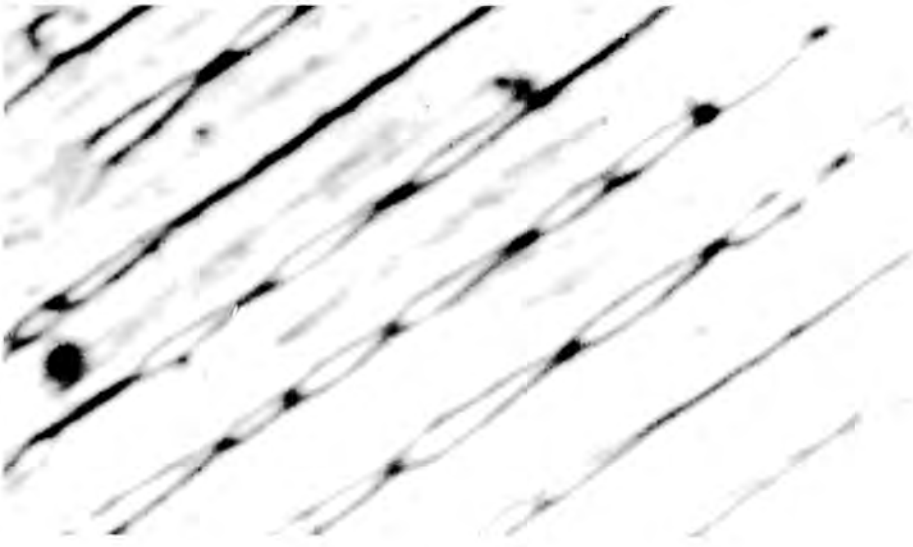

Stress 36 kgms/mm^2. A small vertical field has caused alternate chains to disappear.

Scale

0 0·05 mm

PLATE 2

Stress 27 kgms/mm^2. No magnetic field. Small elliptically shaped domains have started to nucleate along the walls at the surface.

The co-existence of Stress Pattern II and the chain structure is shown above.

PLATE 2

A high magnification photograph, taken of a quenched silicon iron specimen, shows Stress Pattern II in detail. The main 'zig-zag' walls are indicated by arrows. In between them lie the complex closure structure.

Vertical field of 15 oersteds has been applied causing alternate 'zig-zag' walls to disappear and a modification of the closure structure.

PLATE 3

The direction of the vertical field is the reverse of that in the previous photograph.

PLATE 3

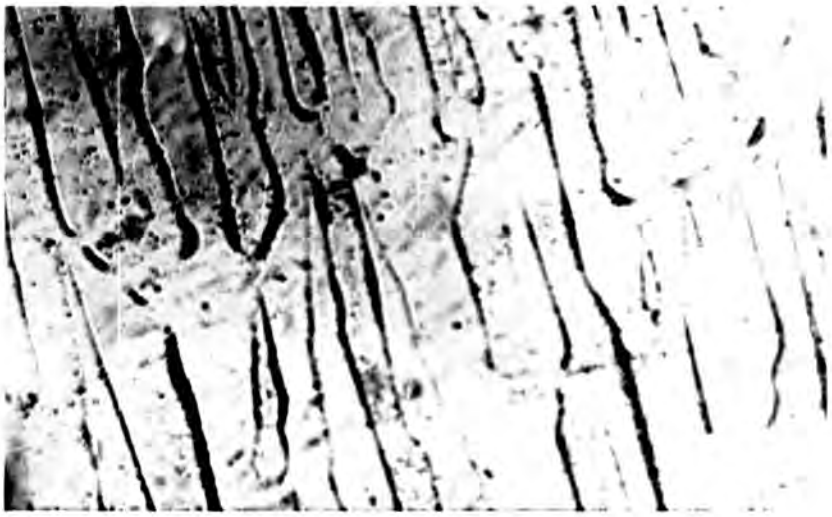

The photograph shows a typical zero stress dagger structure formed when the [001] direction makes an angle of about 3^{o} with the surface. The main 180^{o} Bloch walls are not very coherent.

Tensional stress of 1.55 kgms/mm^2 has been applied along the [001] direction. There is also a small vertical magnetic field.

Scale

0 0·05 0·1 mms

PLATE 4

Stress 4.13 kgms/mm^2. There has been an initial growth in the size of daggers. A small magnetic field, applied in a vertical direction, is present in all the photographs of plate 4.

Stress 10.6 kgms/mm^2. The main 180° walls are more distinct. Daggers are smaller now.

PLATE 4

Stress 20.9 kgms/mm^2. The daggers have almost disappeared. The polarization of magnetic colloid by the vertical field shows that the magnetization has not rotated into a surface direction.

Stress 25. kgms/mm^2. The domain structure now seems to consist of simply 180° Bloch walls.

PLATE 4

Zero stress pattern on surface which is a (100) plane to within $\frac{1}{2}^{o}$. The dark line, indicated with an arrow, is a guide to the stress direction.

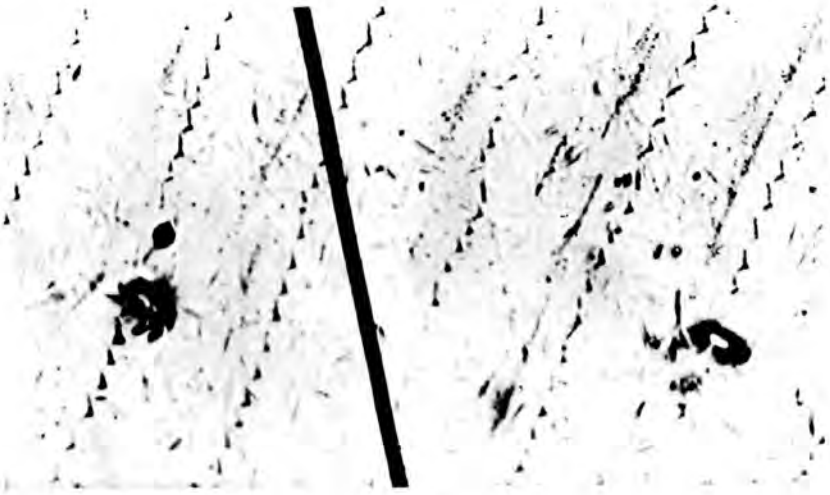

A compressive stress of 3.71 kgms/mm^2 has been applied along the [110] direction. A vertical magnetical field makes alternate zig-zag walls of the closure structure visible.

Scale

0 0·1 mm

PLATE 5

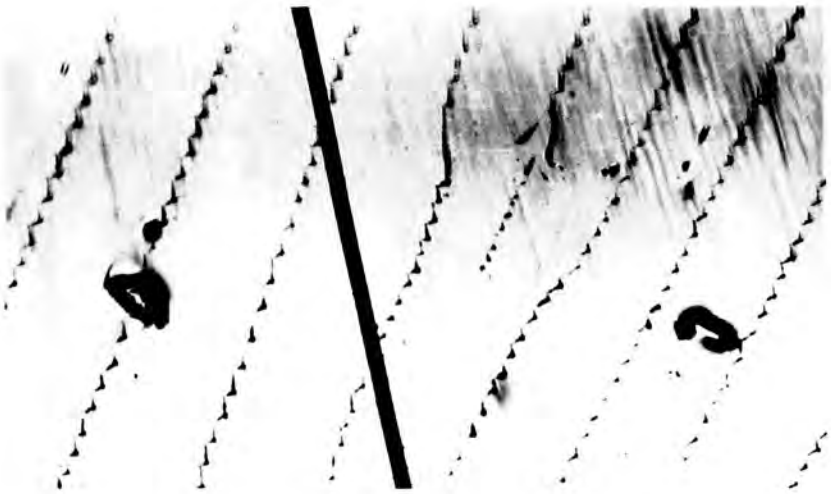

Stress 5.06 kgms/mm^2. A vertical field of 15 oersteds exists.

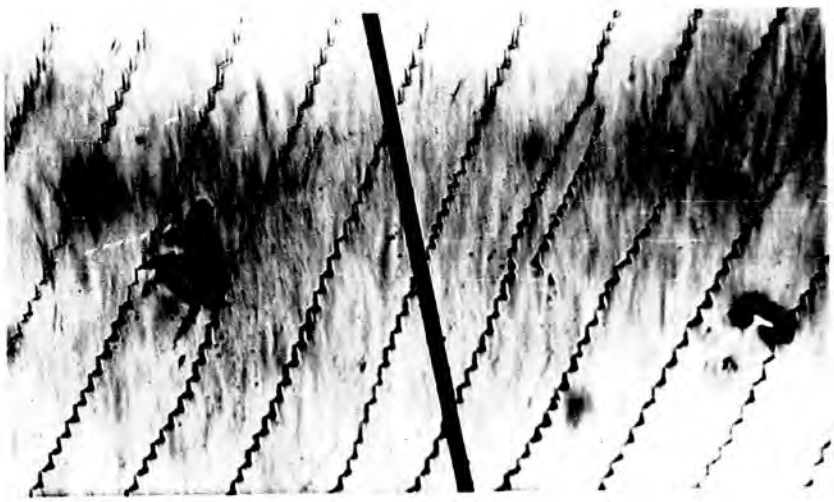

Stress 8.62 kgms/mm^2. The increasing stress causes a reduction in the domain spacing.

PLATE 5

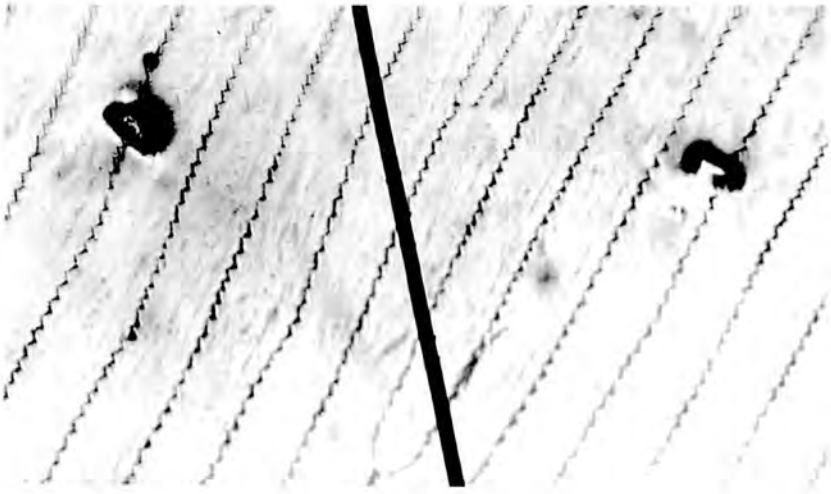

Stress 12.00 kgms/mm^2.

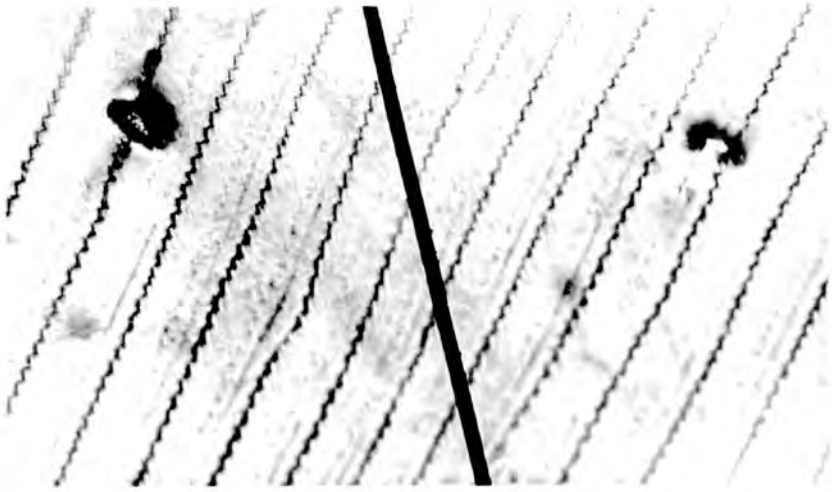

Stress 15.34 kgms/mm^2. Measurements of the variation of ω with stress cannot be made from photographs at this magnification.

PLATE 5

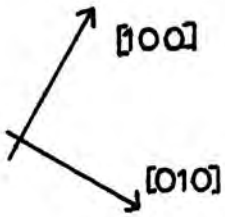

Zero stress photograph. The [100] direction makes an angle of about 3^{o} with the surface.

A Compressive stress of 2.50 kgms/mm^{2} has been applied along the [110] direction. There is a vertical field of 10 oersteds normal to the surface. The presence of arrow-heads and zig-zag walls are shown.

Scale

0 0·1 mm

PLATE 6

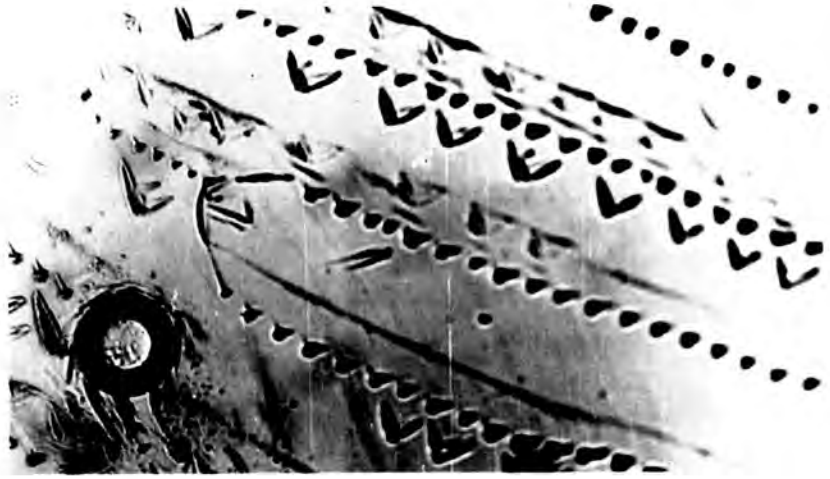

Stress 6.23 kgms/mm^2. Vertical field applied. Colloid deposited over half of each arrowhead.

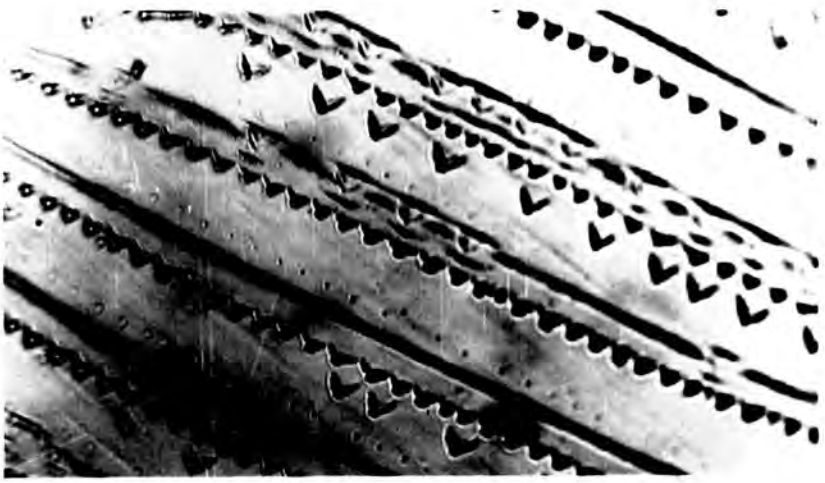

Stress 10.3 kgms/mm^2. Vertical field of 10 oersteds applied. The band and zig-zag structure is clearly shown. There is a reduction in the size of arrowheads.

PLATE 6

Stress 10.3 kgms/mm^2. The vertical field is in the opposite direction to that in the previous photograph. The band structure can be seen to be more distinct where the arrowheads have disappeared.

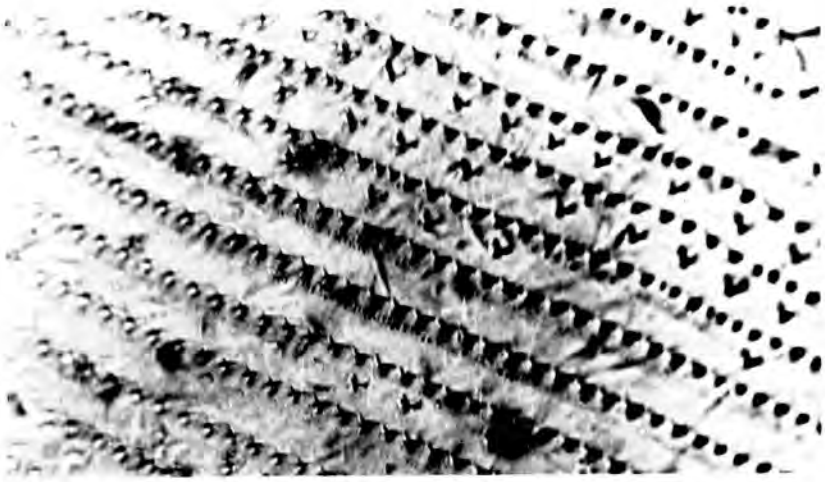

Stress 15.4 kgms/mm^2. No vertical field.

PLATE 6

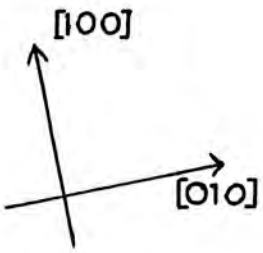

Zero stress. A small square domain can be seen on the left hand side of the photograph. The thick black line is a guide to the direction of stress.

A compressive stress of 1.2 kgms/mm^2 has been applied along the [010] direction. The square domain has grown in size.

Scale

PLATE 7

0 0·1 mm.

Stress 3.2 kgms/mm^2. The square domain has grown further.

Stress 5.7 kgms/mm^2. The grain is now completely magnetized in the [100] direction except for the surface closure domains.

PLATE 7

Zero stress photograph. Domains magnetized along the [010] directions. The [001] direction makes an angle of 4° with the surface.

A compressive stress of 0.7 kgms/mm^2 has been applied along the [010] direction. The direction of stress is indicated by the black line.

Scale

0 0·1 mm

PLATE 8

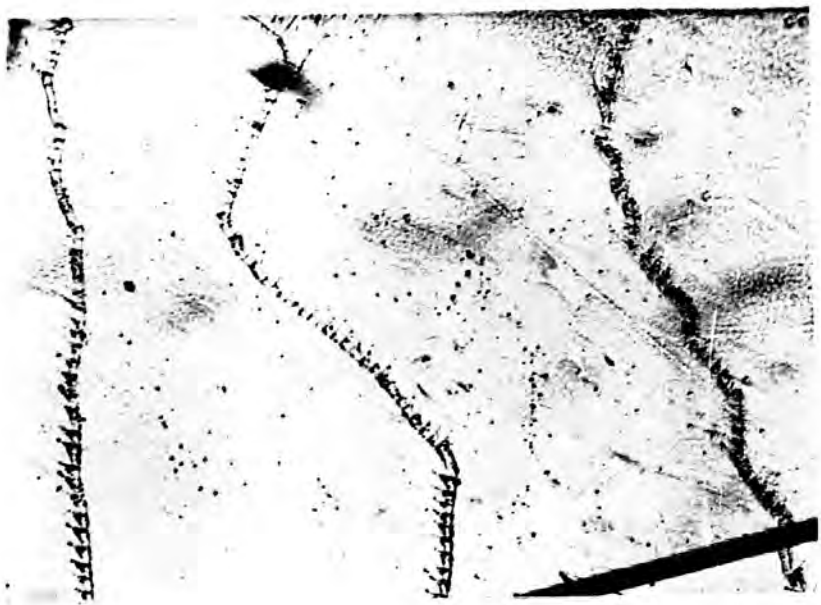

Stress 1.6 kgms/mm^2. No vertical field applied.

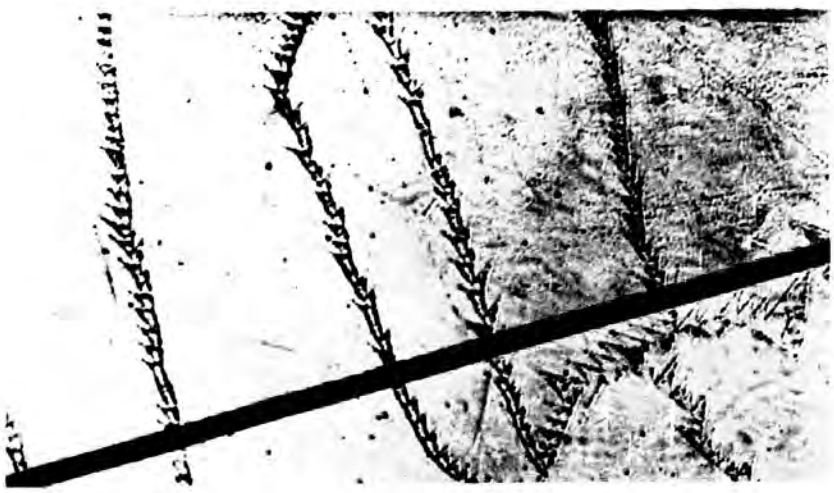

Stress 2.5 kgms/mm^2. The domain spacing is still rather variable.

PLATE 8

Stress 7.9 kgms/mm^2. The domain spacing is much closer than at lower stresses.

PLATE 8

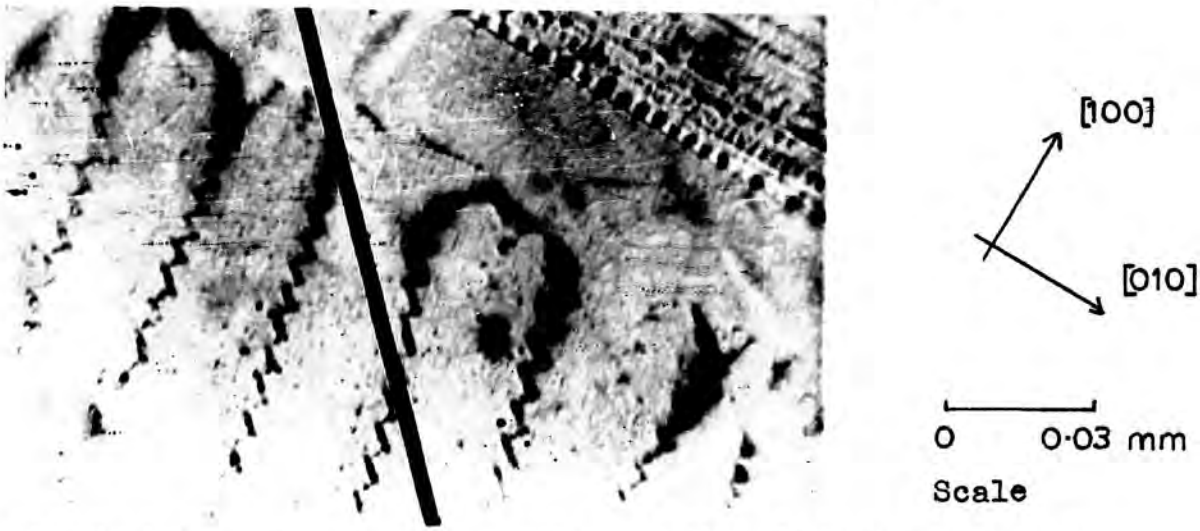

The dark line across the centre of the photograph is not on the surface of the specimen. The zig-zag spacing can be seen to remain constant at all distances from the scratch.

PLATE 9

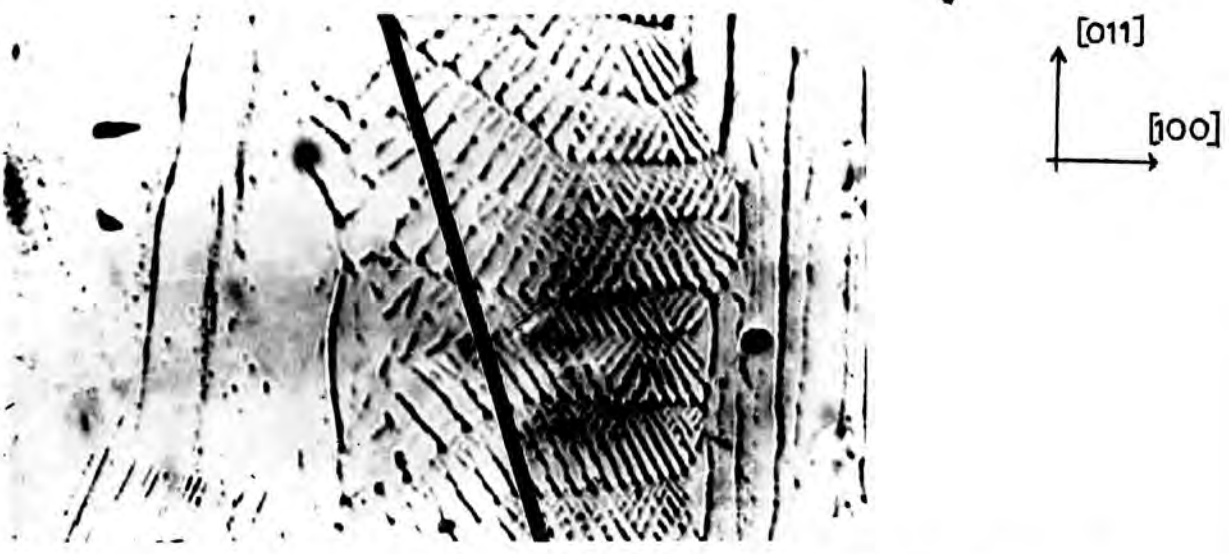

Scratch on a (110) surface. Stress Pattern I(1) changes to Stress Pattern II(2) and back to Stress Pattern I(3) with increasing distance from scratch.

PLATE 10

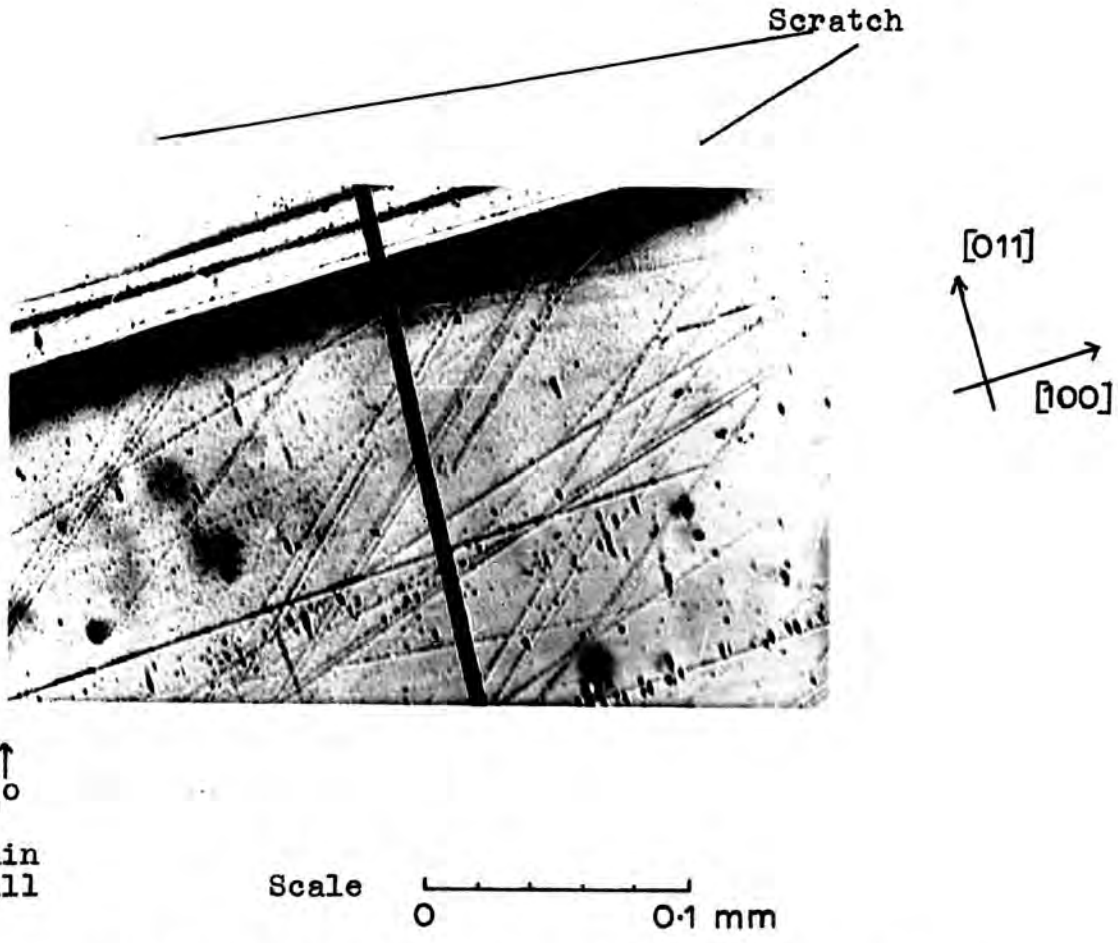

The photograph shows that the domains adjacent to the scratch are magnetized along the [100] surface easy direction. No stress pattern, caused by the scratch, can be seen.

PLATE 11

The dark line normal to the scratch is used for orientation purposes. A vertical field has been applied.

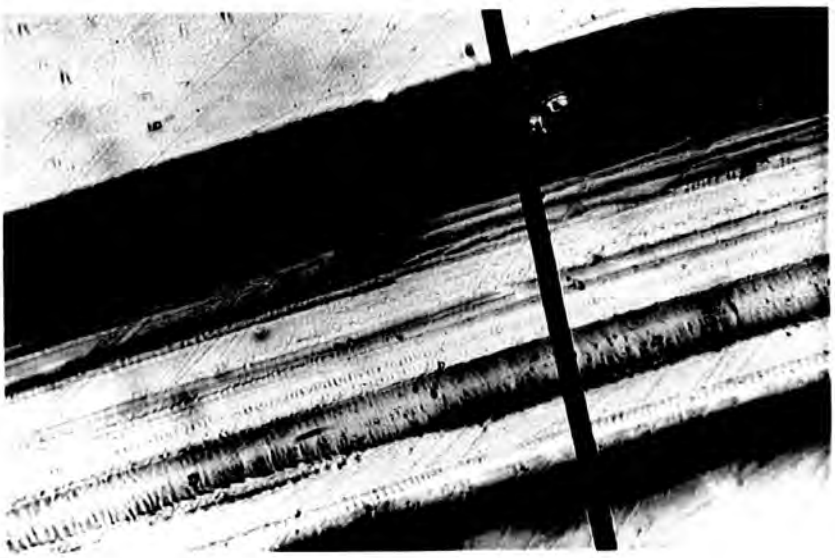

The vertical field has been reversed.

PLATE 12

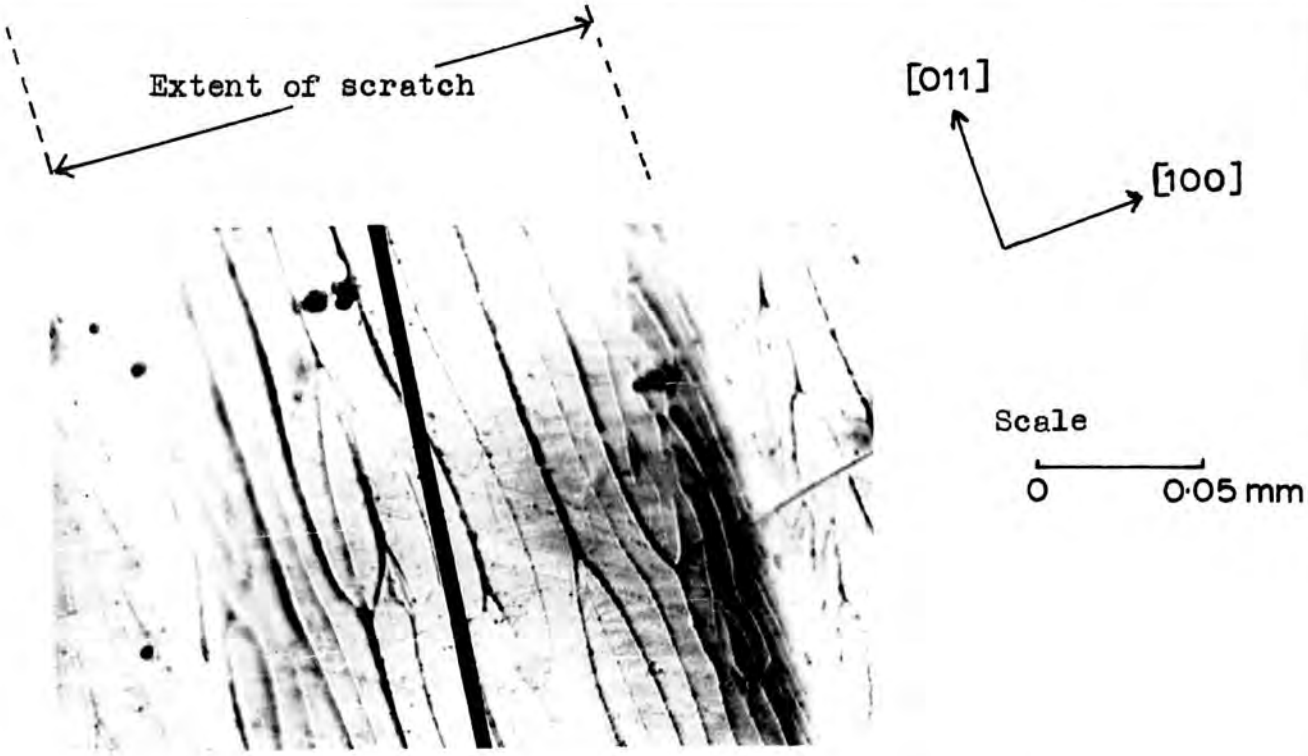

Electropolished scratch on a (110) surface. Dark line runs along length of scratch. A vertical field of 10 oersteds has been applied.

Vertical field has been reversed. Colloid deposited mainly on alternate Bloch Walls.

PLATE 13